

University of Mississippi

eGrove

---

Electronic Theses and Dissertations

Graduate School

---

1-1-2019

## A computational approach to predicting and understanding new psychoactive substances (NPS) for developing a database for state and federal crime laboratories

Caroline Amelia Spencer

Follow this and additional works at: <https://egrove.olemiss.edu/etd>

 Part of the [Chemistry Commons](#)

---

### Recommended Citation

Spencer, Caroline Amelia, "A computational approach to predicting and understanding new psychoactive substances (NPS) for developing a database for state and federal crime laboratories" (2019). *Electronic Theses and Dissertations*. 1787.

<https://egrove.olemiss.edu/etd/1787>

This Dissertation is brought to you for free and open access by the Graduate School at eGrove. It has been accepted for inclusion in Electronic Theses and Dissertations by an authorized administrator of eGrove. For more information, please contact [egrove@olemiss.edu](mailto:egrove@olemiss.edu).

A COMPUTATIONAL APPROACH TO PREDICTING AND UNDERSTANDING NEW  
PSYCHOACTIVE SUBSTANCES (NPS) FOR DEVELOPING A DATABASE FOR STATE  
AND FEDERAL CRIME LABORATORIES

A Dissertation  
presented in partial fulfillment of requirements  
for the degree of Doctor of Philosophy  
in the Department of Chemistry and Biochemistry,  
The University of Mississippi

by

CAROLINE SPENCER

August 2019



## ABSTRACT

The object of this dissertation was to use a computational approach to predict and understand new psychoactive substances (NPS) to develop a database for state and federal crime. The primary scope of the dissertation was to better understand the interactions that take place between new psychoactive substances and their corresponding receptors. Through analysis of the interactions between the amino acids within the receptors and the NPS, an understanding into the pharmacology and toxicology of these drugs can be gained. NPS such as synthetic cannabinoids, fentanyl and its analogs, and kratom have become more problematic for both state and federal crime labs, as they rush to keep up with new compounds that appear on the drug market for recreational use. NPS pose many issues within the criminal justice field. A main issue is the inability of agencies, like the Drug Enforcement Administration (DEA), to keep up with the increasing number of NPS that are used recreationally and have a high potential for abuse. When a new compound surfaces, it can take weeks and sometimes months to identify the compound and understand its properties. This project used the molecular modeling software from Schrödinger, Maestro, to virtually dock NPS of interest to their receptors. Following thorough docking studies of known synthetic cannabinoids, possible new structures of synthetic cannabinoids were designed and studied in the same way. This project focused on the specific structural characteristics of these compounds and how those characteristics influence the binding of the ligand to its receptor. Specific residue interactions taking place within the binding pocket of the receptor were also analyzed. This project sets the foundation of a larger project that will

lead to a database, that can be made available to all state and federal crime laboratories, containing potential NPS that will aid in the rapid identification and pharmacological understanding of previously unidentified compounds.

## DEDICATION

To my family and fiancé.

## ABBREVIATIONS AND SYMBOLS

NPS – New Psychoactive Substances

DEA – Drug Enforcement Administration

UNODC – United Nations Office on Drugs and Crime

$\Delta^9$ -THC –  $\Delta^9$ -tetrahydrocannabinol

EMCDDA – European Monitoring Centre for Drugs and Drug Addiction

CB1 – Cannabinoid Receptor 1

CB2 – Cannabinoid Receptor 2

GPCR – G-protein Coupled Receptor

GTP – Guanosine Triphosphate

GDP- Guanosine Diphosphate

CNS- Central Nervous System

PNS – Peripheral Nervous System

G – Gibbs Free Energy

H – Enthalpy

S – Entropy

OPRL1 – opioid receptor like 1

pH – hydrogen ion concentration

pKa – strength of an acid

Ka – acid dissociation constant

NMR – Nuclear Magnetic Resonance

ppm – parts per million

m/z – mass-to-charge

amu – atomic mass units

3D – Three Dimensional

2D – Two Dimensional

SP – Standard Precision

MM-GBSA – Molecular Mechanics-Generalized Born Surface Area

NIST – National Institute of Standards and Technologies

Å – Angstrom, unit of length

Ki – binding affinity

kcal/mol – kilocalorie per mole

nM – nanomolar

fmol/mL – femtomole / milliliter

ALA – Alanine

ARG – Arginine

ASN – Asparagine

ASP – Aspartic acid

CYS – Cysteine

GLN – Glutamine

GLU – Glutamic acid

GLY – Glycine



HIS – Histidine

ILE – Isoleucine

LEU – Leucine

LYS – Lysine

MET – Methionine

PHE – Phenylalanine

PRO – Proline

SER- Serine

THR – Threonine

TRP – Tryptophan

TYR – Tyrosine

VAL – Valine

## ACKNOWLEDGEMENTS

I cannot express enough gratitude for Dr. Murrell Godfrey and the Godfrey research group. My fellow graduate students; Brandon Stamper, Sarah Glenn and Ann-Elodie Robert, have been an essential support system throughout the years. Dr. Godfrey has been a wonderful advisor over the last five years, as well as a mentor and someone I have looked up to for the last nine years through my undergraduate and graduate degree. Without his guidance, support, and confidence in me, I might not have even considered graduate school and for that I will forever be grateful.

I would also like to thank Dr. Robert Doerksen and Dr. Pankaj Pandey for collaborating on this project. Dr. Pandey was essential in training me to use the software necessary to complete this project.

## TABLE OF CONTENTS

|  |      |
|--|------|
| ABSTRACT.....  | ii   |
| DEDICATION.....  | iv   |
| ABBREIVATIONS AND SYMBOLS.....   | v    |
| ACKNOWLEDGEMENTS.....  | viii |
| LIST OF TABLES.....  | x    |
| LIST OF FIGURES.....   | xii  |
| CHAPTER 1: INTRODUCTION.....   | 1    |
| CHAPTER 2: THE COMPUTATIONAL STUDY OF SYNTHETIC CANNABINOIDS FROM<br>THE JWH FAMILY.....                                   | 18   |
| CHAPTER 3: THE COMPUTATIONAL STUDY OF KNOWN AND NOVEL<br>HALOGENATED DERIVATIVES OF THE SYNTHETIC CANNABINOID JWH-018..... | 44   |
| CHAPTER 4: THE COMPUTATIONAL STUDY OF KNOWN AND NOVEL HOMOLOGS<br>OF SYNTHETIC CANNABINOIDS IN THE CP FAMILY.....          | 73   |
| CHAPTER 5:THE COMPUATIONAL STUDY OF KNOWN AND NOVEL FENTANYL<br>ANALOGS AND THE MU-OPIOID RECEPTOR.....                    | 108  |
| CHAPTER 6: THE COMPUTATIONAL STUDY OF KRATOM ALKALOIDS AND THE<br>MU-OPIOID RECEPTOR.....                                  | 135  |
| CHAPTER 7: CONCLUSIONS AND FUTURE WORK.....  | 147  |
| REFERENCES.....  | 152  |
| CURRICULUM VITAE.....  | 158  |

## LIST OF TABLES

|  |     |
|--|-----|
| Table 1. Summary of experimental binding affinities, docking scores, glide Emodel values and binding free energy estimations. ....           | 51  |
| Table 2. Number and identification of interacting residues within 5 Å for JWH-018 and its halogenated derivatives.....                       | 53  |
| Table 3. Residues interacting with the ligands CB1 receptor within the binding pocket within a distance of 5 Å. ....                         | 54  |
| Table 4. Summary of results showing experimental binding affinities, docking scores, glide Emodel values and binding energy estimations..... | 81  |
| Table 5. Number and identification of residues interacting with each homolog.....  | 84  |
| Table 6. Residues interacting with the ligands and the CB1 receptor within the binding pocket within a distance of 5 Å.....                  | 86  |
| Table 7. Summary of experimental binding affinities, docking scores, glide Emodel values, and binding free energy estimations.....           | 115 |
| Table 8. Number and identification of interacting residues within 5 Å. ....  | 116 |
| Table 9. Residues interacting with the analogs within a distance of 5 Å. ....  | 117 |
| Table 10. Summary of experimental binding affinities, docking scores, glide Emodel values, and binding free energy estimations.....          | 123 |
| Table 11. Number and identification of interacting residues within 5 Å.....  | 125 |
| Table 12. Residues interacting with the analogs within a distance of 5 Å. ....   | 126 |
| Table 13. Results from the docking of the alkaloids to the mu-opioid receptor. ....  | 141 |

Table 14. Number and identification of interacting residues within 5 Å for the kratom alkaloids  
alkaloids.....143

Table 15. Residues interacting with the kratom alkaloids within a distance of 5 Å. ....144

## LIST OF FIGURES

|  |    |
|--|----|
| Figure 1. The global emergence of NPS as of December 2018.....   | 2  |
| Figure 2. NPS divided by psychoactive effect group as of December 2018.....  | 2  |
| Figure 3. Process of GPCR activation by an agonist.....  | 5  |
| Figure 4. Structure types of Proteins.....   | 7  |
| Figure 5. <sup>1</sup> H NMR of ethanol.....   | 14 |
| Figure 6. <sup>13</sup> C NMR of ethanol.....  | 15 |
| Figure 7. Basic components of a mass spectrometer.....   | 16 |
| Figure 8. Validated 3D homology model of the active-state CB1 receptor developed by the Doerksen Lab (P Pandey, K K Roy, R J Doerksen, unpublished).....   | 21 |
| Figure 9. Diagram showing the design of the novel synthetic cannabinoids based on structural similarities between the parent compounds JWH-175, JWH-073, JWH-018, JWH-122, JWH-210, and JWH-182..... | 22 |
| Figure 10. Docking scores vs length of alkyl chain graph for the JWH-073 and MGCS-175-073 groups.....  | 26 |
| Figure 11. Interacting residues observed within 5 Å for the MGCS-175-073 ligand group.....   | 27 |
| Figure 12. Interacting residues observed within 5 Å for the JWH-073 ligand group.....  | 28 |
| Figure 13. 3D interactions diagram of JWH-073 (green), JWH-073-1 (cyan), JWH-073-2 (pink), JWH-073-3 (purple), JWH-073-4 (yellow), and JWH-073-5 (orange).....                                       | 30 |

|   |    |
|---|----|
| Figure 14. 3D interaction diagram of MGCS-175-073 (purple), MGCS-175-073-1 (green), MGCS-175-073-2 (orange), MGCS-175-073-3 (pink), MGCS-175-073-4 (cyan), and MGCS-175-073-5 (yellow)..... | 31 |
| Figure 15. 3D interaction diagram of MGCS-175-073-2 (orange) and MGCS-175-073-4 (cyan).....   | 32 |
| Figure 16. 3D interaction diagram of MGCS-175-073-3 (pink) and MGCS-175-073-5 (yellow).....   | 33 |
| Figure 17. Docking scores vs length of alkyl chain for the JWH-175 and JWH-018 groups.....  | 34 |
| Figure 18. Interacting residues observed within 5 Å for the JWH-175 ligand group.....   | 35 |
| Figure 19. Interacting residues observed within 5 Å for the JWH-018 ligand group.....   | 36 |
| Figure 20. 3D interaction diagram of JWH-175 (pink), JWH-175-1 (yellow), JWH-175-2 (green), JWH-175-3 (cyan), JWH-175-4 (orange), and JWH-175-5 (purple).....                               | 38 |
| Figure 21. 3D interaction diagram of JWH-175 (pink), JWH-175-1 (yellow), JWH-175-2 (green), JWH-175-3 (cyan), and JWH-175-5 (purple).....   | 39 |
| Figure 22. 3D interaction diagram of JWH-018 (yellow), JWH-122 (orange), JWH-210 (cyan), JWH-182 (pink), JWH-018-4 (purple), and JWH-018-5 (green).....                                     | 40 |
| Figure 23. 3D interaction diagram of JWH-122 (orange) and JWH-210 (cyan).....   | 41 |
| Figure 24. Spectral data of the novel synthetic cannabinoid MGCS-175-073; A) <sup>1</sup> H NMR, B) <sup>13</sup> C NMR, C) Mass Parent Peak.....   | 42 |
| Figure 25. Chemical structure of JWH-018, naphthalene-1-yl(1-pentyl-1 <i>H</i> -indol-3-yl)methanone.....   | 45 |

|   |    |
|---|----|
| Figure 26. Validated 3D homology model of the active-state CB1 receptor, developed by the Doerksen Lab, with a bound $\Delta^9$ -THC ligand (P Pandey, K K Roy, R J Doerksen, unpublished)..... | 47 |
| Figure 27. Structures of known and novel halogenated derivatives of JWH-018.....  | 48 |
| Figure 28. 3D interaction diagram of JWH-018 (green) and all the halogenated derivatives; JWH-018 F (cyan), JWH-018 Cl (pink), JWH-018 Br (yellow), and JWH-018 I (purple).....                 | 57 |
| Figure 29. 3D interaction diagram of JWH-018 and the PHE177 and TRP279 residues of the CB1 receptor (shown as cartoon). Interacting residues are shown in grey.....                             | 58 |
| Figure 30. 3D interaction diagram of JWH-018 showing the distance from TRP279 (2.2 Å) and SER383 (5.8 Å).....   | 59 |
| Figure 31. 3D interaction diagram of halogenated derivatives; JWH-018 F (cyan), JWH-018 Cl (pink), JWH-018 Br (yellow), and JWH-018 I (purple).....   | 60 |
| Figure 32. 3D interaction diagram with JWH-018 (green), JWH-018 F (cyan), and JWH-018 Cl (pink).....  | 61 |
| Figure 33. 3D interaction diagram of JWH-018 F (cyan) and JWH-018 Cl (pink) and the interacting residues TRP279, TRP356, PHE200, and SER383 (grey).....   | 62 |
| Figure 34. 3D interaction diagram with JWH-018 (green), JWH-018 Br (yellow), and JWH-018 I (purple).....  | 63 |
| Figure 35. 3D interaction diagram of JWH-018 Br (yellow) and JWH-018 I (purple).....  | 64 |



|  |    |
|--|----|
| Figure 36. 3D interaction diagram of JWH-018 Br (yellow) and JWH-018 I (purple) with the interacting residues TRP279, TRP356, PHE200, and SER383.....  | 65 |
| Figure 37. Spectral data of JWH-018; A) <sup>1</sup> H NMR, B) <sup>13</sup> C NMR and C)Mass Parent Peak.....   | 66 |
| Figure 38. Spectral data of JWH-018 F; A) <sup>1</sup> H NMR, B) <sup>13</sup> C NMR, and C)Mass Parent Peak.....  | 67 |
| Figure 39. Spectral data of JWH-018 Cl; A) <sup>1</sup> H NMR, B) <sup>13</sup> C NMR , and C)Mass Parent Peak.....  | 68 |
| Figure 40. Spectral data of JWH-018 Br; A) <sup>1</sup> H NMR, B) <sup>13</sup> C NMR , and C)Mass Parent Peak.....  | 69 |
| Figure 41. Spectral data of JWH-018 I; A) <sup>1</sup> H NMR, B) <sup>13</sup> C NMR, and C)Mass Parent Peak.....  | 70 |
| Figure 42. Chemical Structure of CP-47,497.....  | 74 |
| Figure 43. Validated 3D homology model of the active-state CB1 receptor, developed by the Doerksen Lab, with a bound $\Delta^9$ -THC ligand. (P Pandey, K K Roy, R J Doerksen, unpublished)..... | 75 |
| Figure 44. Chemical structures of CP-47,497, CP-55,244 and CP-55,940.....  | 76 |
| Figure 45. Structures of the CP-47,497 homologs. (C7)-CP-47,497* is the parent structure.....  | 77 |
| Figure 46. Structures of the CP-55,244 homologs. (C7)-CP-55,244* is the parent structure.....  | 77 |
| Figure 47. Structures of the CP-55,490 homologs. (C7)-CP-55,490* is the parent structure.....  | 78 |
| Figure 48. 3D interaction diagram of CP-47,497 (green) and its homologs (C6)-CP-47,497 (pink), (C8)-CP-47,497 (cyan), and (C9)-CP-47,497 (yellow).....   | 88 |
| Figure 49. 3D interaction diagram of CP-47,497 (green) and (C8)-CP-47,497 (cyan).....  | 89 |

|   |    |
|---|----|
| Figure 50. 3D interaction diagram of CP-47,497 (green) and (C8)-CP-47,497 (cyan) and the residues TRP 279 and PHE 278. PHE 278 only interacted with (C8)-CP-47,497 (cyan) through a hydrogen bond.....                | 90 |
| Figure 51. 3D interaction diagram of CP-47,497 (green) and (C8)-CP-47,497 (cyan) and the residue PHE278. PHE278 only interacted with (C8)-CP-47,497 (cyan) through a hydrogen bond within a distance of 1.9 Å.....    | 91 |
| Figure 52. 3D interaction diagram of CP-47,497 (green) and (C6)-CP-47,497 (pink).....   | 92 |
| Figure 53. 3D interaction diagram of CP-47,497 (green) and (C8)-CP-47,497 (cyan) and the hydrophobic residue PHE381. PHE381 was only observed with the (C8)-CP-47,497 (cyan).....                                     | 93 |
| Figure 54. 3D interaction diagram of CP-47,497 (green) its homologs (C6)-CP-47,497 (pink), (C8)-CP-47,497 (cyan), and (C9)-CP-47,497 (yellow) shown with the hydrophobic residues PHE381 and PHE102.....              | 94 |
| Figure 55. 3D interaction diagram of CP-55,244 (pink) and its homologs (C6)-CP-55,244 (cyan), (C8)-CP-55,244 (yellow), and (C9)-CP-55,244 (green).....  | 95 |
| Figure 56. 3D interaction diagram of CP-55,244 (pink) and (C8)-CP-55,244 (yellow).....  | 96 |
| Figure 57. 3D interaction diagram of CP-55,244 (pink) and (C8)-CP-55,244 (yellow) and the residues TRP279, PHE279 and VAL196. VAL196 only interacted with (C8)-CP-55,244 (yellow) through a hydrogen bond.....        | 97 |
| Figure 58. 3D interaction diagram of CP-55,244 (pink) and (C8)-CP-55,244 (yellow) and the residue VAL196. VAL196 only interacted with (C8)-CP-55,244 (yellow) through a hydrogen bond within a distance of 1.9 Å..... | 98 |

|   |     |
|---|-----|
| Figure 59. 3D interaction diagram of CP-55,244 (pink) and (C6)-CP-55,244 (cyan) and the hydrophobic residues ILE175 and LEU387. ILE175 and LEU387 were only observed with CP-55,244 (pink).....                           | 99  |
| Figure 60. 3D interaction diagram of CP-55,244 (pink), (C6)-CP-55,244 (cyan) and (C8)-CP-55,244 (yellow) the hydrophobic residue ILE175. ILE175 was only observed with CP-55,244 (pink) and (C8)-CP-55,244 (yellow).....  | 100 |
| Figure 61. 3D interaction diagram with CP-55,490 (purple), (C6)-CP-55,490 (green), (C8)-CP-55,490 (orange), and (C9)-CP-55,490 (yellow).....  | 101 |
| Figure 62. 3D interaction diagram with CP-55,490 (purple) and (C8)-CP-55,490 (orange).....  | 102 |
| Figure 63. 3D interaction diagram with CP-55,490 (purple) and (C8)-CP-55,490 (orange) with the residues TRP279 and LYS192. LYS192 was only observed interacting with (C8)-CP-55,490 (orange) through a hydrogen bond..... | 103 |
| Figure 64. Spectral data for CP-47,497; A) <sup>1</sup> H NMR, B) <sup>13</sup> C NMR, C) Mass Parent Peak.....   | 104 |
| Figure 65. Spectral data for CP-55,244; A) <sup>1</sup> H NMR, B) <sup>13</sup> C NMR, C) Mass Parent Peak.....   | 105 |
| Figure 66. Spectral data for CP-55,490; A) <sup>1</sup> H NMR, B) <sup>13</sup> C NMR, C) Mass Parent Peak.....   | 105 |
| Figure 67. Structures of N-methyl fentanyl, N-ethyl fentanyl, N-propyl fentanyl, and fentanyl.....  | 110 |
| Figure 68. Structures of the designed carfentanyl analogs and the parent structure of carfentanyl.....  | 110 |
| Figure 69. 3D interaction diagram of N-methyl fentanyl (green), N-ethyl fentanyl (cyan), N-propyl fentanyl (pink), and fentanyl (grey).....   | 118 |

|  |     |
|--|-----|
| Figure 70. 3D interaction diagram of N-methyl fentanyl (green) and fentanyl (grey).....  | 119 |
| Figure 71. 3D interaction diagram of N-methyl fentanyl (green), N-ethyl fentanyl (cyan), N-propyl fentanyl (pink), and fentanyl (grey) with the ASP147 residue.....  | 120 |
| Figure 72. 3D interaction diagram of N-methyl fentanyl (green), N-ethyl fentanyl (cyan), and fentanyl (grey) with the ASP147 residue and the TRP293 residue.....   | 121 |
| Figure 73. 3D interaction diagram of fentanyl (grey) with the residues TRP293, TYR326 and ASP147.....  | 122 |
| Figure 74. 3D diagram of the ligands carfentanyl (methyl) (yellow), carfentanyl (ethyl) (green), carfentanyl (aldehyde) (cyan), carfentanyl (ketone) (pink), carfentanyl (carboxylic acid) (orange), and carfentanyl (grey)..... | 127 |
| Figure 75. 3D interaction diagram of carfentanyl (grey) and carfentanyl (ethyl) (green).....   | 128 |
| Figure 76. 3D interaction diagram of carfentanyl (grey) and carfentanyl (ethyl) (green) with interacting residues ASP147, TRP293, and TYR326.....  | 129 |
| Figure 77. 3D interaction diagram of carfentanyl (ethyl) (green), carfentanyl (ketone) (pink), carfentanyl (carboxylic acid) (orange), and carfentanyl (grey) with interacting residues TRP 293 and ASP147.....                  | 130 |
| Figure 78. 3D diagram of carfentanyl (aldehyde) (cyan) and carfentanyl (grey) with the interacting residues ASP147, TRP293, TYR326 and HIS297.....   | 131 |
| Figure 79. Spectral data for N-ethyl fentanyl; A) <sup>1</sup> H NMR, B) <sup>13</sup> C NMR, C) Mass Parent Peak.....   | 132 |

Figure 80. Spectral data for N-propyl fentanyl; A)  $^1\text{H}$  NMR, B)  $^{13}\text{C}$  NMR, C) Mass Parent  
Peak.....133  
Figure 81. Structures of the kratom alkaloids.....137

# CHAPTER 1

## INTRODUCTION

### **1.1 New Psychoactive Substances (NPS)**

The objective of this dissertation is to gain a better understanding of the pharmacology and toxicology of specific drugs of abuse through the use of molecular modeling and docking studies. This project will focus on new psychoactive substances (NPS) including synthetic cannabinoids, fentanyl and its analogs, and the plant based NPS known as kratom. NPS emerged on the drug scene in the recent years and have been labeled as “legal highs”. However, there is very little information on what influences the adverse effects associated with these substances.<sup>1</sup> There is also a large misconception that since some of these drugs are sold legally and that they are safer than the drug they were designed to mimic.<sup>2</sup> In reality the drugs sold are not regulated and they can vary from one package to the another because of the large quantity of analogs.<sup>2</sup> The growth of NPS are still increasing as more and more drugs are developed to stay ahead of the law. Across the United States there is a reported 301-423 substances that are considered NPS (Figure 1). There are many groups of drugs classified as NPS, including sedatives, opioids, hallucinogens, stimulants and synthetic cannabinoids (Figure 2). One of the main issues with NPS in the criminal justice field is the inability to predict new structures related to known NPS, or analogs, before they appear on the street for recreational use.

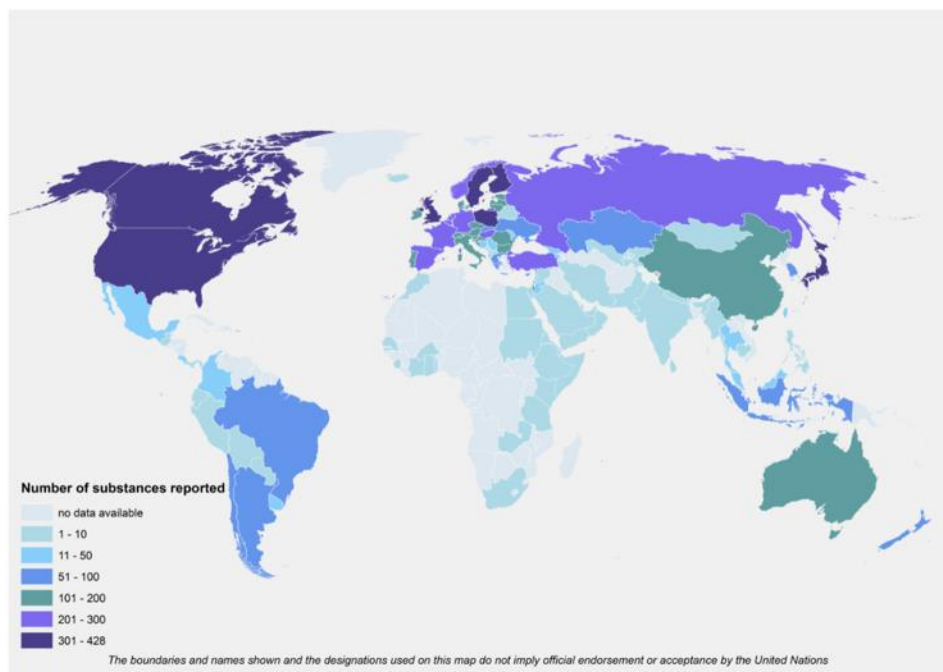


**Figure 1.** The global emergence of NPS as of December 2018. Courtesy of the UNODC Early Warning Advisory, 2019. <sup>1</sup>

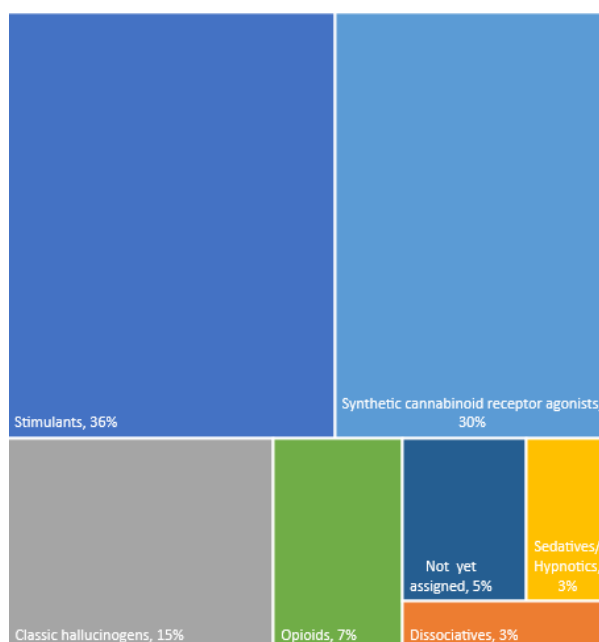


**Figure 2.** NPS divided by psychoactive effect group as of December 2018. Courtesy of the UNODC Early Warning Advisory, 2019. <sup>1</sup>

Through the studies in chapters 2-6, the specific interactions that take place between NPS and their corresponding receptors were thoroughly analyzed to better understand the binding differences that may contribute to adverse effects. Identifying the specific structural characteristics associated with the essential interactions within the binding pocket were used to help design potential new compounds which could be intended for recreational use. Once new compounds have been designed, their toxicological and pharmacological properties can be studied, and mass spectral data can be calculated with the overall goal of developing a database. State and federal labs can access the database to rapidly identify and characterize new compounds.

## **1.2 Synthetic Cannabinoids**

Synthetic cannabinoids came onto the drug scene as an alternative to marijuana. Synthetic Cannabinoids first made their major appearance in the 1990's with Dr. John W. Huffman's creation of a large number of compounds that were considered to be structural derivatives of  $\Delta^9$ -tetrahydrocannabinol ( $\Delta^9$ -THC).<sup>3</sup> Many other classes of synthetic cannabinoids soon followed, such as HU and CP which were synthesized by Dr. Mechoulam and the Pfizer Corporation respectively.<sup>3</sup> Initially, the products were widely available, easily attainable, and legal. Brand names such as 'Spice' and 'K2' sold herbal packets advertised as incense packs to be used in aromatherapy. In 2009, Europol's European Monitoring Centre for Drugs and Drug Addiction (EMCDDA) discovered, like marijuana, many of these packets were being used as hallucinogenic inhalants.<sup>3</sup>

Synthetic cannabinoids have been determined to act similarly to  $\Delta^9$ -THC in marijuana and produce psychoactive effects.  $\Delta^9$ -THC is known to interact with the cannabinoid receptors CB1 and CB2. These receptors are a part of the endocannabinoid system. Cannabinoid receptor 1



(CB1) is located in the central and peripheral nervous systems and is responsible for the psychoactive effects brought on by  $\Delta^9$ -THC.<sup>4</sup> Even though there are similarities between  $\Delta^9$ -THC and synthetic cannabinoids, many synthetic cannabinoids have been determined to be full agonists for the CB1 receptor whereas  $\Delta^9$ -THC is only a partial agonist.<sup>4</sup> Agonists are able to bind to the receptor and produce the maximum biological response. Partial agonists bind to the receptor's active site as well, but the maximum biological response of the receptor is not produced. Little is known about these compounds and their effects on humans. More information is needed on how these compounds interact with the cannabinoid receptors and their resulting effects.

### **1.2.1 Endocannabinoid System**

The human body naturally produces endocannabinoids that are similar to cannabis structures.<sup>5</sup> These naturally occurring endocannabinoids are a part of what is known as the endocannabinoid system. The endocannabinoid system includes both the cannabinoid 1 (CB1) and cannabinoid (CB2) receptors. Originally it was believed that the cannabinoid receptors only existed in the brain and nerves, but they were later found in other parts of the body including the skin, heart, and the immune system. The endocannabinoid system plays a role in various processes throughout the body including appetite control, metabolism, the immune system, etc.<sup>5</sup>

Both the CB1 and the CB2 receptors are known as G-protein coupled receptors (GPCRs). GPCRs are membrane bound receptors, located in the membrane of the cell. It is estimated that one-third to one-half of all drugs commercially available bind to a type of GPCR.<sup>6</sup> All GPCRs consist of seven segments that are formed from the folding of the receptor. The receptor has extracellular loops outside of the cell membrane, intercellular loops inside the cell and then transmembrane portions that exist inside the cell membrane itself.<sup>6</sup> These receptors are known as

“G-protein coupled” because of their interaction with the G protein within the membrane. G proteins are responsible for binding guanosine triphosphate (GTP) and guanosine diphosphate (GDP). When the receptor is activated, and a conformational change occurs, the G protein that is bound to it also activates. The G proteins bound to GPCRs are heterotrimeric, with alpha, beta, and gamma subunits.<sup>7</sup> The activation of the G protein allows these subunits to send messages into the cell through the process of signal transduction (Figure 3).<sup>6</sup>

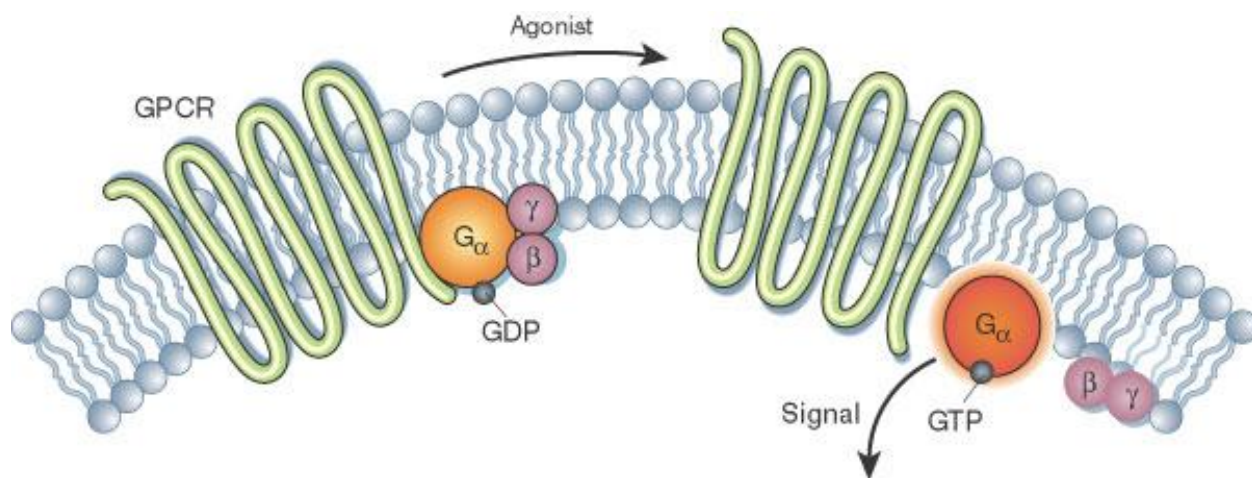


**Figure 3.** Process of GPCR activation by an agonist. This image has been reproduced with permission of the Springer Nature under copyright license number 4632820585277.<sup>6</sup>

The synthetic cannabinoids analyzed in this study were all agonists for the CB1 receptor located in the endocannabinoid system. The CB1 receptor is a GPCR that contains 472 amino acids and is encoded by the *CNR1* gene.<sup>8</sup> The CB1 receptor is found predominately in the brain and throughout the central nervous system (CNS). However, it has also been noted in the peripheral nervous system (PNS).<sup>8</sup> The CB1 receptor is speculated to play a role in many physiological processes including appetite, memory, depression, anxiety, addiction, and more.

Because of its location in the PNS it can also play a role in pain, metabolism, inflammation, energy and many other physiological and pathological processes.<sup>8</sup>

### **1.2.2 General Structural Characteristics of Proteins**

Proteins are essential to most biological processes and their function is dictated by their structure. Proteins are made up of amino acids which each consist of an amino group, a carboxyl group, a side chain and a hydrogen. The sequence of amino acids in a protein is responsible for its properties such as the fold of the protein or its surface properties. The amino acids in a protein are linked through peptide, or amide, bonds. Peptide bonds are covalent bonds that occur between the carbonyl carbon of one amino acid and the nitrogen of the adjacent amino acid. Proteins have various structures or conformations.<sup>9</sup> The primary structure is the sequence of amino acids. The secondary structures include two different types of formations, the alpha-helix and the beta-sheet. In the alpha-helix structure of proteins the backbone of the structure forms hydrogen between the carbonyl oxygens and the NH hydrogens as turns are made in the structure and the side chains are pointed outwards. Beta-sheet secondary structures occur when the CO group and NH group of an amino acids can form hydrogen bonds to adjacent strands of either sides.<sup>9</sup> The next level of structure of a protein is the tertiary structure, which refers to the overall three-dimensional conformation or fold of the molecule. The conformation of most importance is that which occurs when the protein is biologically active. The final level of structure is the quaternary structure, in which multiple chains of proteins are bound together to form one unit.<sup>9</sup>

(Figure 4)

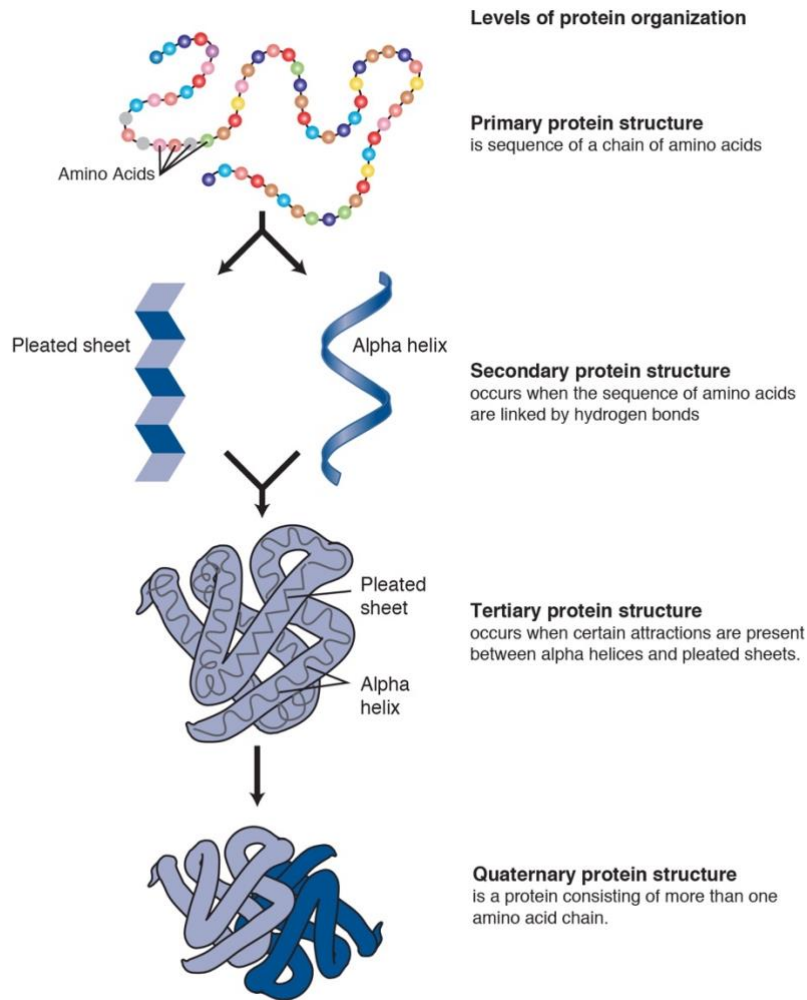


**Figure 4.** Structure types of proteins. Courtesy: National Human Genome Research Institute<sup>10</sup>

### 1.3 Fentanyl and Kratom

The second set of NPS analyzed in this study was the synthetic opioids, specifically fentanyl and its analogs. Fentanyl was first discovered in 1960 but reports of overdoses were not reported until around 1972 as various methods of administration were becoming readily available.<sup>11</sup> Fentanyl has been found to be 80-100 times stronger, or more potent, than morphine and 25-40 times more potent than heroin. Fentanyl analogs in the illegal drug market were not

reported until around the 1980s.<sup>12</sup> One of the most potent analogs is carfentanyl. Carfentanyl has been found to be up to 100 times more potent than fentanyl. From 1999 to 2011, the number of fatal opioid analgesic overdoses quadrupled and, for the year 2015, the death toll in the United States totaled 33,091.<sup>13</sup> One reason for this spike in overdose deaths is the now common practice by drug dealers of lacing heroin with fentanyl in order to increase the high of the abuser and keep them coming back for more. Fentanyl and its analogs act on the opioid receptor system with the most prominent receptor being the mu-opioid receptor. The mu-opioid receptor and fentanyl and its analogs were the focus of this study.

The last set of NPS analyzed in this study belongs to the plant-based NPS group. Kratom, or *Mitragyna speciosa*, is a plant found in countries of Southeast Asia. The alkaloids found within the leaf of the plant are what is currently marketed and sold as the drug kratom. Up to 44 alkaloid compounds have been isolated from the leaves of the *Mitragyna speciosa* plant. Two of the alkaloids, mitragynine and 7-hydroxymitragynine, are known to be some of the most potent.<sup>14</sup> These two alkaloids have the potential to be even more potent than morphine. These alkaloids have been found to act upon the mu-, kappa-, and delta-opioid receptors.<sup>15</sup> The work in this dissertation will focus on the kratom alkaloids and their binding to the mu-opioid receptor. The popularity of the drug has significantly increased because of its euphoric effects and its potential to help with opioid withdrawal.<sup>16</sup> The increase in popularity in this drug can also be related to the ease at which one is able to obtain it, as it is legal and sold largely online and even in some convenience stores. Due to this increase and the addictive effects of kratom, the DEA has noted kratom as a “drug of concern”. Some cities, however, are taking action and banning kratom from being sold within the city limits as reports of kratom use and overdoses associated with kratom are increasing.

### **1.3.1 Mu-opioid receptor**

Like the cannabinoid receptors, the opioid receptors are also a part of the GPCR family. There are four types of opioid receptors: mu, kappa, delta and opioid receptor like 1 (OPRL1). This study focuses on the binding of NPS to the mu-opioid receptor. The opioid system plays a key role in pain behavior and antinociception. Opioid receptors are found throughout the CNS and the nociceptive neural circuitry.<sup>17</sup> The mu-opioid receptor was first identified in 1973 and most opioids used for pain interact with the mu-opioid receptor. However, opioids that act on this receptor have also been known to be mood enhancers and cause euphoria. Similarly to the CB1 receptor, the mu-opioid receptor binds to a G protein. When the receptor is activated by an agonist, the G protein subunits are released and are able to act on various signal transduction pathways.<sup>17</sup>

## **1.4 Molecular Docking**

Molecular docking is used in the research to virtually dock known and novel NPS to their receptors. The steps include ligand selection, ligand design, ligand preparation, protein preparation, receptor grid generation, ligand docking, and binding energy estimations.

The ligand preparation involved generating possible states at a target pH of  $7.0 \pm 2.0$  using Epik, which predicts pKa values and determines chemically sensible structures.<sup>18</sup>

### **1.4.1 pH**

The pH expresses the acidity of a solution based on its hydrogen-ion concentration. It is determined by finding the negative logarithm of the hydrogen-ion concentration.<sup>19</sup> The pH scale ranges from 0-14, with 7 being neutral and anything lower than that is considered acidic and anything higher is basic.

### 1.4.2 pKa

A pKa value determines the strength of an acid based on the acid dissociation constant (Ka). The acid dissociation constant is the ability of compound to donate a proton to a base. The pKa is found by taking the negative logarithm of the Ka. A lower pKa values indicates a stronger acid.<sup>20</sup>

After docking was completed binding free estimations were done for the best possible poses.

### 1.4.3 Binding Free Energy

Gibbs free energy (G) is defined as the energy required to be used for work. The energy is determined using the enthalpy, temperature and entropy. Enthalpy (H) is defined as the measure of energy in a system that is equal to the heat of the system. Entropy (S) is the measure of energy that is not available which measures the disorder of a system.<sup>21</sup> The free energy of a reaction can be determined by taking the sum of the free energy of the products minus the sum of the free energy of the reactants. The binding free energy in this research was estimated using the following equation:  $\Delta G_{\text{bind}} = E_{\text{complex (minimized)}} - (E_{\text{ligand (minimized)}} + E_{\text{receptor (minimized)}})$ .<sup>22</sup> The binding free energy estimations done in the Maestro software are not expected to be the same as the experimental binding affinities (Ki), but should be similar in rank compared to the experimental values. Binding affinity is defined as the strength of interaction between the ligand and the receptor.<sup>23</sup>

After the ligands have been docked and calculations have been performed, through the 2D ligand interactions diagram it is possible to analyze the residues interacting with the ligand at a specific distance. The type of interactions observed are hydrophobic, polar,  $\pi$ - $\pi$  stacking,  $\pi$ -cation, hydrogen bonds and salt bridges.

#### **1.4.4 Hydrophobic Residues**

Hydrophobic residues are amino acids that have a side chain made up of mostly carbons and hydrogens. The side chains of these residues are nonpolar and therefore do not interact with water molecules. Nonpolar bonds are formed when electrons between atoms are equally shared.<sup>24</sup>

#### **1.4.5 Polar Residues**

Polar amino acid residues are found to have an -OH or -NH<sub>2</sub> group and, due to the electronegative atoms on their side chains, they are able to form hydrogen bonds.<sup>25</sup> A polar molecule occurs when the electrons between atoms are unequally distributed causing a dipole moment due to one end of the molecule being slightly positive and the other slightly negative.<sup>26</sup>

#### **1.4.6 Aromatic ( $\pi$ - $\pi$ ) stacking**

$\pi$ - $\pi$  stacking is a type of attractive force that can occur between two neighboring aromatic rings.<sup>27</sup> Aromatic rings contain a benzene ring, a ring of six carbons with alternating double and single bonds, or another similar ring structure.  $\pi$ - $\pi$  stacking occurs due to the positive electrostatic potential of one ring interacting with the negative electrostatic potential of another ring.<sup>28</sup>

#### **1.4.7 $\pi$ -Cation Interactions**

$\pi$ -cation interactions are caused by an electrostatic interaction between a cation and the negatively charged face of an aromatic ring.<sup>29</sup>

#### **1.4.8 Hydrogen Bonding**

Hydrogen bonding is the attraction of hydrogen bond to an electronegative atom, like nitrogen, oxygen or fluorine, and another electronegative atom. This attraction occurs due to the dipole-dipole interactions. Dipole-dipole interactions take place when the positive end of a polar molecule is attracted to the negative end of another.<sup>30</sup>



### **1.4.9 Salt Bridges**

A salt bridge is a type of non-covalent interaction that occurs between two ionized sites. This type of interaction consists of both a hydrogen bond and an electrostatic interaction. Salt bridges are the strongest type of non-covalent interaction.<sup>31</sup>

## **1.5 Spectral Simulation**

Following the analysis of the known and designed novel NPS, spectral data was calculated. The type of potential spectra calculated in this research were  $^1\text{H}$  NMR,  $^{13}\text{C}$  NMR and mass parent peaks displaying isotopic distribution.

### **1.5.1 Nuclear Magnetic Resonance (NMR) Spectroscopy**

NMR spectroscopy is a nondestructive analytical technique predominately used for determining the structure of an organic compound. Spectroscopy refers to the study of light and matter interacting. The theory behind NMR is based on the idea that atomic nuclei are positively charged, spin on an axis, and create a magnetic field.<sup>32</sup> The orientation of these magnetic fields is random. When an external magnetic field is applied they can either align with the direction of the external magnetic field or against it. The applied radiation is absorbed by the nuclei which is what causes the spins to flip and become in resonance with the external magnetic field. Nuclei will absorb the radiation at difference wavelengths. The signals detected and used to produce the NMR spectra are determined by the chemical shifts and the splitting of the signals. The position of the signal on the spectra is determined by the chemical shift, while the pattern is dependent on the splitting.<sup>32</sup> The chemical shift is the measurement of the change on the spin of the nucleus caused by the external magnetic field.<sup>33</sup> There are two types of NMR utilized in this research,  $^1\text{H}$  NMR and  $^{13}\text{C}$  NMR. In  $^1\text{H}$  NMR spin-spin coupling, or splitting, occurs when protons on

neighboring carbons interact and cause the resonances to split into more than one peak. The splitting is shown on the spectra as multiple peaks including doublets, triplets and quartets or singlets if they have not been split. For example, a doublet is caused by one proton on an adjacent carbon splitting the proton into two, a triplet is caused by two protons on an adjacent carbon splitting the proton into three peaks and so on.<sup>32</sup>  $^{13}\text{C}$  NMR is not as sensitive as  $^1\text{H}$  NMR, but  $^{13}\text{C}$  NMR spectra can display the carbon framework of the compound.  $^{13}\text{C}$  NMR deals with  $^{13}\text{C}$  isotope which has a low natural abundance and since it is unlikely that two  $^{13}\text{C}$  will be next to each other spin-spin coupling is not seen. But  $^1\text{H}$ - $^{13}\text{C}$  coupling can be observed between  $^{13}\text{C}$  and the hydrogens they are bound to. However, this method is not typically used, and a technique called broadband decoupling is used instead. This technique turns off the  $^1\text{H}$ - $^{13}\text{C}$  coupling and therefore all signals are seen as singlets.<sup>34</sup> ChemDoodle was used to determine a  $^1\text{H}$  NMR and  $^{13}\text{C}$  NMR spectra of the simple compound ethanol and display what can be determined from NMR spectra. (Figure 5-6)

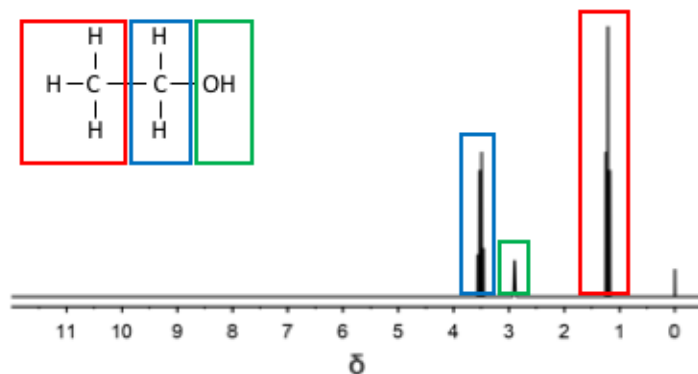


**Figure 5.**  $^1\text{H}$  NMR spectra of ethanol generated by ChemDoodle. The methane,  $-\text{CH}_3$  (red), group signal is displayed at around 1-1.5 ppm and will be a triplet because of the spin-spin coupling that occurs with the  $\text{CH}_2$  group (blue). The singlet (green) at 2.8-3.0 ppm is caused by the H of the  $-\text{OH}$ . It is a singlet because no coupling occurs. At around 3.5 ppm, the  $\text{CH}_2$  group gives a signal. This quartet occurs from the spin-spin coupling with the three hydrogens on the neighboring  $\text{CH}_3$  group.

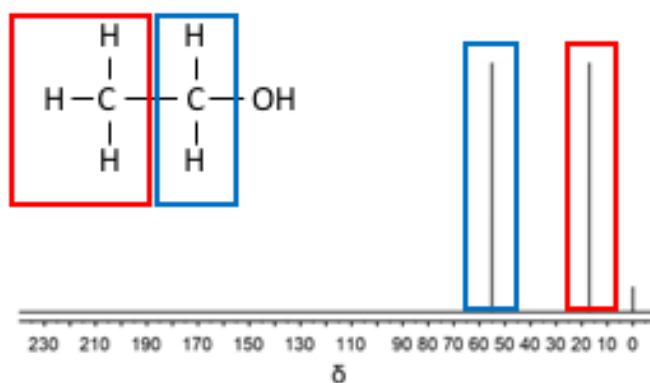


**Figure 6.**  $^{13}\text{C}$  NMR of ethanol generated by ChemDoodle. Because only two carbons are present in this compound, only two singlets are observed. The carbon of the  $\text{CH}_3$  (red) signal is observed around the 15-20 ppm range, while the carbon of the  $\text{CH}_2$  (blue) signal is observed around the 55 ppm range.

The software used in this research to calculate spectral data was ChemDoodle. The ChemDoodle software uses an algorithm to identify the key functional groups in the structure and estimate the chemical shifts. A separate algorithm is then used to examine the chemical environment around each nucleus. The algorithm is a breadth-first algorithm that is able to analyze one nuclei by exploring the neighboring nuclei. The splitting is determined through the J constants and the spins of adjacent nuclei. The J constant is a measure of the interaction between a pair of protons.<sup>35</sup>

## 1.5.2 Mass Spectrometry

Mass spectrometry is used for a variety of applications including forensic science, environmental sciences, chemistry, biology, toxicology, proteomics and much more. This analytical technique measures the mass-to-charge ratio of ionized analytes in the gas-phase, based on how the ions respond to electric and/or magnetic fields applied to the ions. Mass-to-charge ( $m/z$ ) is based off of the mass, or atomic mass units (amu), and  $z$  which is a multiplier of the unit of charge. Mass-to-charge is a unitless measurement. The information gathered for mass spectrometers is useful in identifying unknown samples, quantitation and examining various chemical and physical properties of a molecule.<sup>36</sup>

There are a variety of mass spectrometers, but every mass spectrometer contains the same three components: an ionization source, a mass analyzer, and a detector (Figure 7).<sup>37</sup> Ionization sources are used to convert the analyte of interest into ions in the gas phase. This step allows for the fragmentation of some of the analyte to occur. A mass analyzer is then used to separate the ions by their mass-to-charge. The ion detector is then used to detect and measure the separated ions.<sup>37</sup>

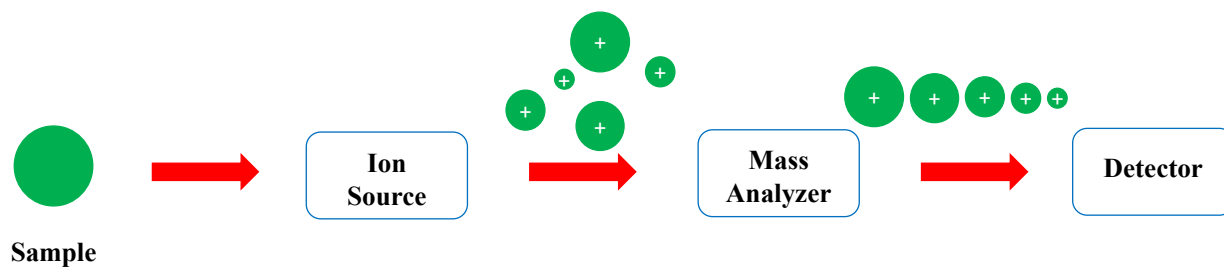


**Figure 7.** Basic components of a mass spectrometer.

There are many different types of mass spectrometry instruments. The type and amount of information obtained from the spectra will vary based on the type of mass spectrometer instrument used and even what other type of instrument it is coupled with for analysis. In this research the software ChemDoodle was used just to predict the mass parent peak. The mass parent peak is the peak that corresponds to the molecular weight of the compound being analyzed. The parent molecule becomes an ion through the ionization source which causes the loss of an electron of the molecule and formation of a positive ion, the molecular ion.<sup>37</sup> The molecular ion peak will most likely not be the most intense peak, but it should be the heaviest. The lower  $m/z$  peaks are from the fragmentation of the molecular ion, so it is not possible for them to have a higher  $m/z$  than the parent peak. The spectra produced by ChemDoodle also displays the isotopic distribution. Most elements have more than one isotope. An isotope is a form of the element that has a different number of neutrons and therefore a different mass.

CHAPTER 2  
THE COMPUTATIONAL STUDY OF KNOWN AND NOVEL SYNTHETIC  
CANNABINOIDS FROM THE JWH FAMILY

## 2.1 Introduction

Synthetic cannabinoids are man-made chemicals that are meant to mimic the effects of marijuana, specifically  $\Delta^9$ -THC, the main psychoactive ingredient in marijuana. Although these drugs have been seen as an “alternative to marijuana” the health effects of the substances are known to be very severe. Symptoms associated with the use of synthetic cannabinoids include altered perception, psychosis, anxiety, paranoia, hallucinations, rapid heart rate, violent behavior, and seizures. Due to the high number of synthetic cannabinoids available the symptoms are unpredictable and can even be fatal.<sup>38</sup>

Synthetic cannabinoids are divided into families based on the structure and who designed the compound. The families include JWH-XXX, CP-XX,XXX, AM-XXX, HU-XXX, WIN-XXX and more. The JWH-XXX family of synthetic cannabinoids included over 400 structures of cannabinoids designed by John W. Huffman and his research group at Clemson University. Huffman’s compound JWH-018 was one of the first synthetic cannabinoids marketed and sold as “Spice”. The JWH compound started an evolution of new designer drugs appearing in the market because of how easy and cheap they were to make and how simple it was to design new structures just by making a simple structural change to the compound.<sup>39</sup>

One of the most prominent structural classes within the JWH-XXX family of synthetic cannabinoids is known as the “naphthoylindoles”. This class of JWH-XXX synthetic

cannabinoids consist of a common base structure of a naphthalene group linked to an indole group. These groups are linked by a carbonyl group, like JWH-018. Very similar in base structure are the “naphthylmethylindoles”. This class also consists of a naphthalene and indole group but is linked by a methyl group instead of a carbonyl, like JWH-175. Being some of the first synthetic cannabinoids, JWH-XXX compounds have been studied extensively, especially by Huffman and his research lab. In 2003, Huffman et al. studied the importance of aromatic stacking in the “indole” classes of their synthetic cannabinoids.<sup>40</sup> This study indicated that, even though previous research had shown hydrogen bonding as an essential interaction between these synthetic cannabinoids and the CB1 receptor, they had new evidence showing that this class of synthetic cannabinoids interact mainly through aromatic, or  $\pi$ - $\pi$  stacking.

The objective of this study was to investigate the binding properties of known synthetic cannabinoids in the naphthoylindoles structural class to an active-state CB1 receptor model through molecular docking. This study thoroughly examined the correlation between aromatic stacking and the binding of the synthetic cannabinoid ligands. To better understand the influence of the various structural characteristics of the synthetic cannabinoids, potential new structures were designed and examined using the same methods. Once the newly designed structures were analyzed, spectral data was calculated for each structure to begin the development of a database of known and novel NPS.

## **2.2 Materials and Methods**

Schrödinger’s molecular modeling software, Maestro, was used to examine the binding of a set of JWH-XXX synthetic cannabinoids to an active-state CB1 receptor model. This study focused on the naphthoylindole class of JWH-XXX synthetic cannabinoids. The three-



dimensional (3D) homology model used in this study was designed and validated by the Doerksen lab at The University of Mississippi, Department of Biomedical Sciences. Since the development of this model a crystal structure has been published. The crystal structure was published by Hua et al. in 2017.<sup>41</sup> The Doerksen lab has examined the crystal structure and compared it to the homology model and found only slight differences in the two structures. The main difference to note is the LYS192 residue. In the crystal structure the side chain is outside the binding pocket, while in the Doerksen model the side chain is pointing towards the binding pocket. It was decided that the study would continue with use of the 3D homology model of the active-state CB1 receptor developed by the Doerksen lab since both structures are comparable.

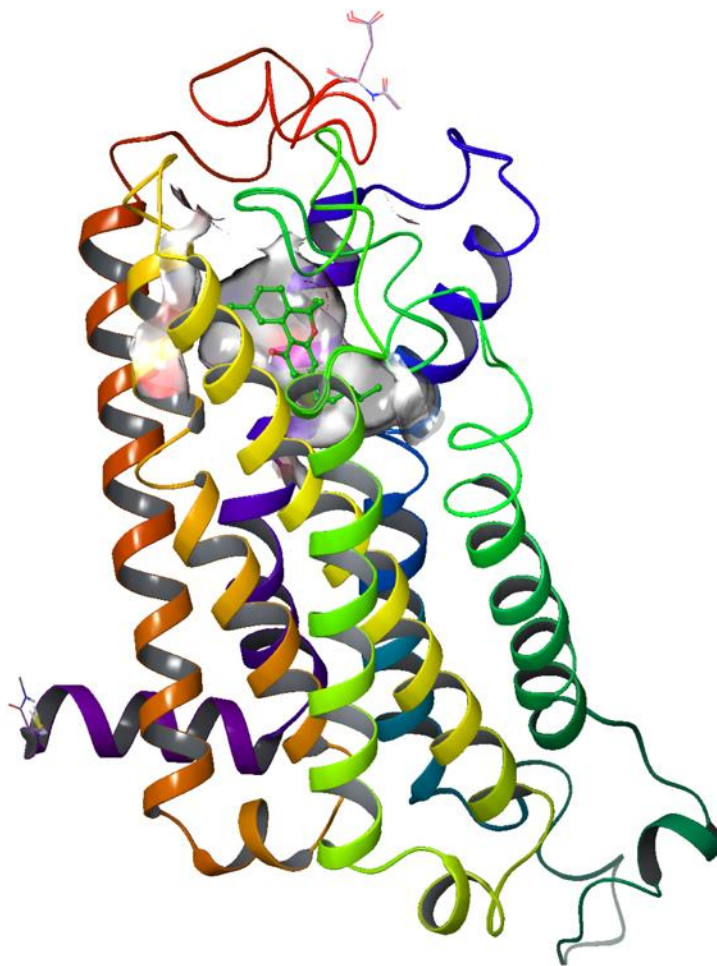


**Figure 8.** Validated 3D homology model of the active-state CB1 receptor developed by the Doerksen Lab (P Pandey, K K Roy, R J Doerksen, unpublished).

### 2.2.1 Ligand Selection and Design

The ligands selected for this study were from the naphthoylindole and naphthylmethylindole classes of synthetic cannabinoids. Naphthoylindole synthetic cannabinoids consist of a naphthalene group linked to an indole group. In some naphthoylindoles the groups are linked by a carbonyl group. Naphthoylindoles also can contain an N-linked alkyl chain on

the indole group. Naphthylmethylindoles have the same base structure but are linked by a methyl group instead of a carbonyl group.

For this study the known synthetic cannabinoids from the naphthoylindole class used were JWH-175, JWH-073, JWH-018, JWH-122, JWH-210, and JWH-182. Using these known compounds, new structures were designed based on structural similarities and examined using the same methods (Figure 9).

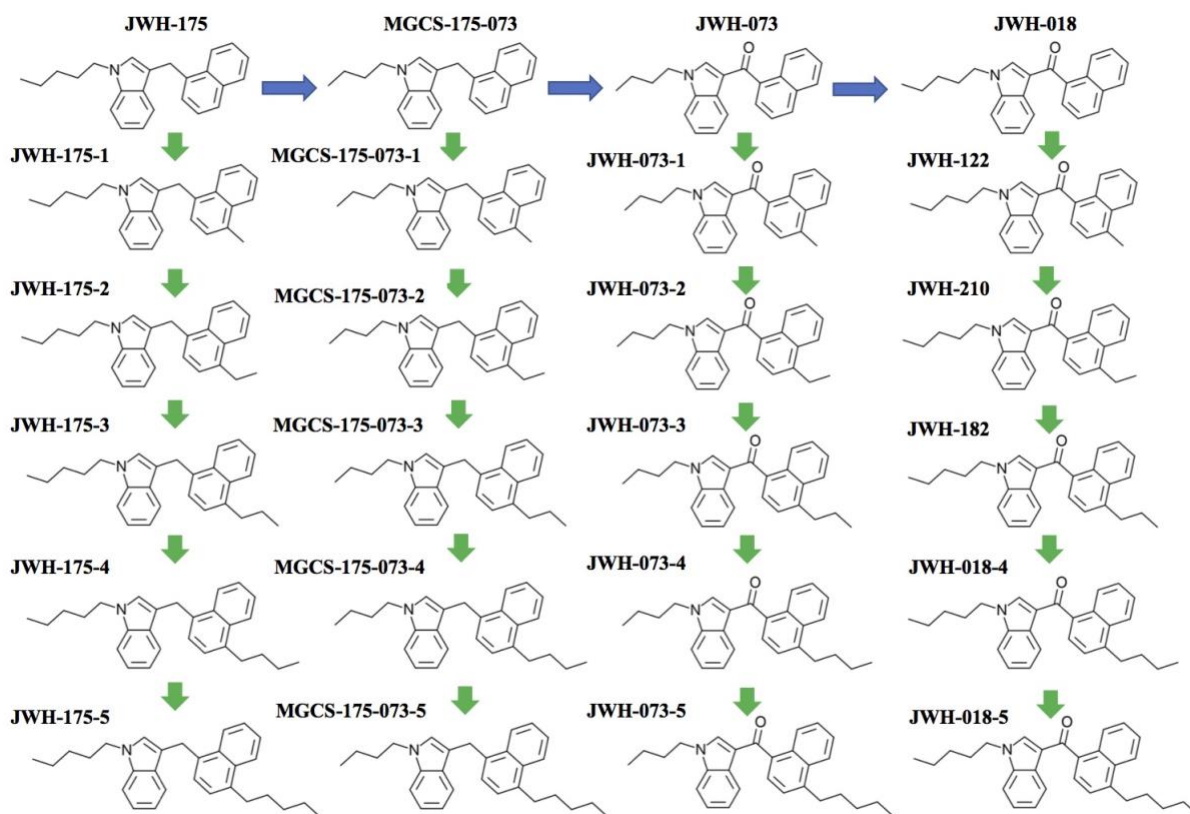


**Figure 9.** Diagram showing the design of the novel synthetic cannabinoids based on structural similarities between the parent compounds JWH-175, JWH-073, JWH-018, JWH-122, JWH-210, and JWH-182.

### 2.2.2 Ligand Preparation

The *LigPrep* protocol was used to successfully convert ligands into three-dimensional structures. The preparation of the ligands involves generating possible states at a target pH of 7.0  $\pm$  2.0 using Epik. Epik is used to predict pKa values and determine all chemically sensible structures.<sup>18,42</sup>

### 2.2.3 Receptor Grid Generation

The *Receptor Grid Generation* application is used to accurately place a grid around the desired binding pocket of the receptor. This was accomplished by selecting the  $\Delta^9$ -THC ligand already in the binding pocket. The grid is generated without constraints, rotatable groups and excluded volumes applied to the receptor. The grid created was used to accurately dock the ligands into the binding pocket of interest in the CB1 receptor model.

### 2.2.4 Ligand Docking

After the grid was generated and the desired ligands were prepared, the next step was *Glide Ligand Docking*. This step allowed for the prepared ligands to be docked into the receptor binding pocket selected during grid generation. Docking was completed using the standard precision (SP) method and force field OPLS3. Flexible ligand sampling was selected and Epik state penalties were added to the docking score. No constraints were selected to use in docking. The Glide program is able to produce potential ligand conformations. The program uses a set of ranked filters to find possible locations on the ligand in the binding pocket of the receptor. The filters include; 1) side-point search, 2a) diameter test, 2b) subset test, 2c) greedy score, 2d) refinement, 3) grid minimization, and 4) final scoring.<sup>43</sup> The *Glide Ligand Docking* process is described by Friesner et al. (2004).<sup>43</sup> For each ligand, up to five possible poses were generated and post-docking minimization was performed. The pose refers to the position and orientation of

the ligand in relation to the receptor.<sup>43</sup> To determine the most accurate pose for each ligand, the docking scores and Glide Emodel scores were analyzed. Docking scores are an estimation of the binding free energy and are used to rank poses of different ligands.<sup>43,44</sup> The Glide Emodel was used to compare poses and determine the best, or most likely, pose for each ligand. Docking scores and Glide Emodel scores are negative. A more negative score means better docking. The docking of each ligand, when using the same procedure, produces the same values. The algorithm used by Glide does not require docking multiple times and will produce the same values each time as long as the same procedure is used. The use of three decimal places is because differences in some of the values between ligands might not have been seen until the second or third decimal place. The software allows for more decimal places to be used, but it was decided to use three decimal places due to some of the small changes observed in the data.

### **2.2.5 Spectral Simulation**

Following the analysis of the known and novel synthetic cannabinoids, spectral data were calculated for each of the novel structures using spectral simulation software. The software ChemDoodle was able to produce <sup>1</sup>H NMR and <sup>13</sup>C NMR spectra as well as a mass parent peak. The known synthetic cannabinoids were also analyzed in this way and compared to data from the NIST library to confirm accuracy.

## **2.3 Results and Discussion**

In this study the length of the alkyl chain both on the naphthalene group, as well as on the indole group, were analyzed. The ligands in this study were examined in two phases, each phase consisting of two groups of ligands. This was done to better understand the influence certain

structural characteristics have on the binding of the ligand to the CB1 receptor and what specific residues interactions are taking place.

### **2.3.1 JWH-073 and MGCS-175-073**

The first groups examined started with JWH-073 and a potential new structure of MGCS-175-073. Both of these parent structures contain an N-linked butyl chain and an alkyl chain is added in increasing length to the naphthalene portion of the structure. In this study the alkyl chain was increased all the way to a five-carbon, pentyl, alkyl chain. The difference between these two parent structures is the presence of the carbonyl group on the JWH-073 group.

As the alkyl chain increased on the naphthalene, a trend was seen in both groups of synthetic cannabinoids in terms of the docking scores (Figure 10). When there was no alkyl chain present on the naphthalene the docking scores of each group were around the same with the MGCS-175-073 group being slightly more positive than the JWH-073 group of ligands. The ligands of the MGCS-175-073 group consistently had more positive docking scores than the JWH-073 group, with the exception of the MGCS-175-073-5 ligand that had a docking score a little more negative than the JWH-073-5 ligand. The trend in docking scores was consistent through the lengthening of the alkyl chain on the naphthalene of each group of ligands. As a methyl was added to the naphthalene the docking scores became more positive and then decreased, became more negative, as that methyl was increased to an ethyl group. The docking scores become more negative again as the ethyl was extended to a propyl. The addition of a propyl group gave the best, or most negative, docking score for each parent ligand. The docking scores saw a significant increase, to a more positive docking score, with the addition of a butyl chain on the naphthalene. The addition of a butyl chain saw the most positive docking scores in

each group of ligands. The docking scores became more negative as the butyl was lengthened to a pentyl chain.

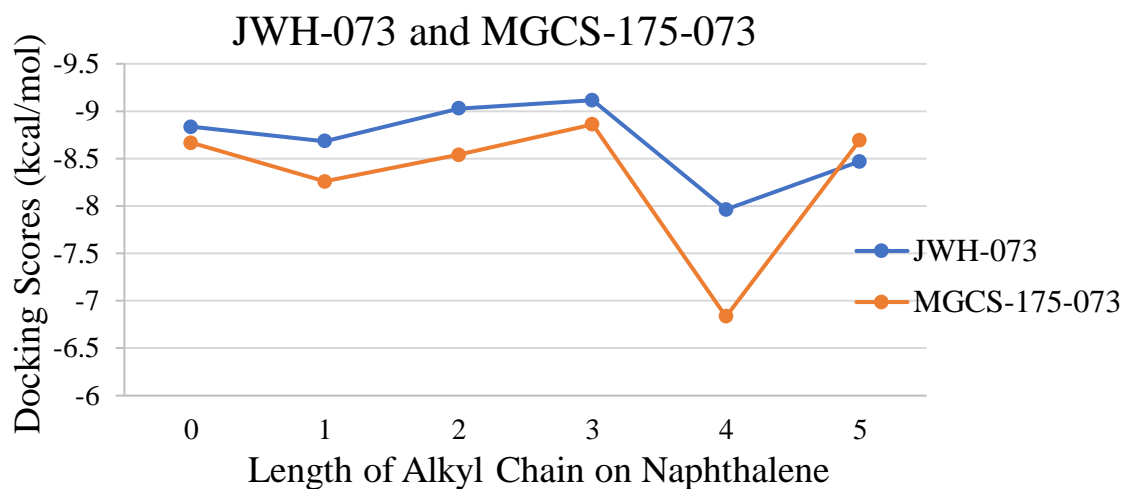


**Figure 10.** Docking scores vs length of alkyl chain graph for the JWH-073 and MGCS-175-073 groups.

To get a better understanding of how the structural characteristics of the ligands influence the binding to the receptor, the specific residue interactions were examined (Figure 11-12).

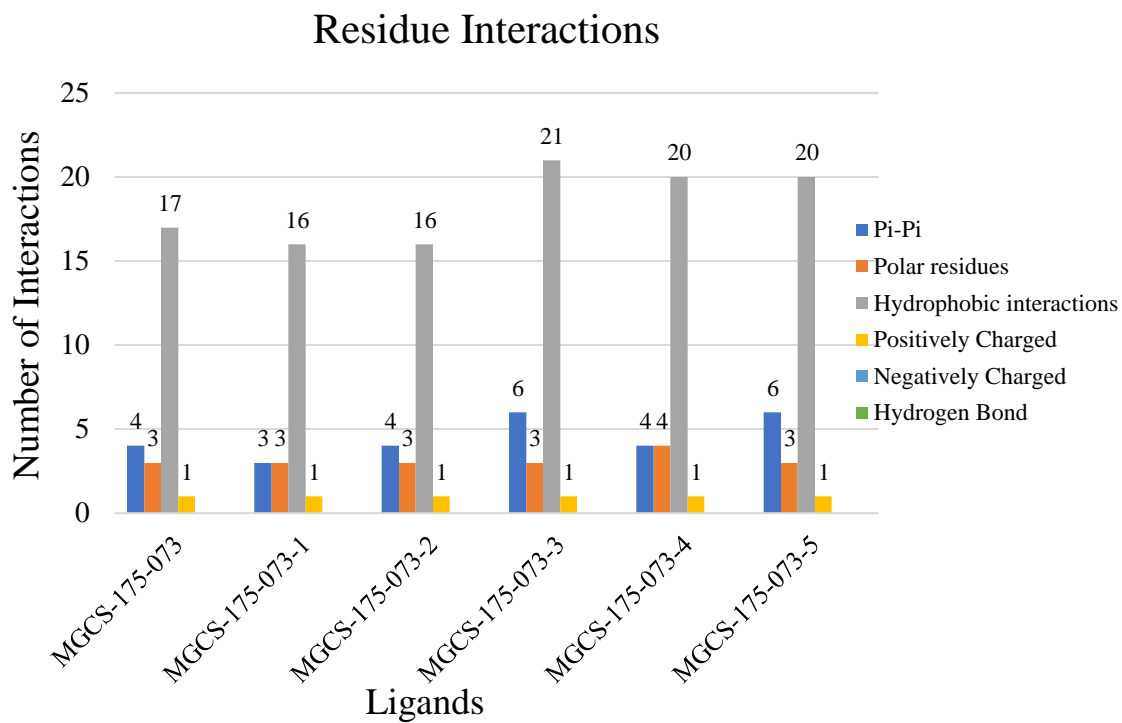


**Figure 11.** Interacting residues observed within 5 Å for the MGCS-175-073 ligand group.



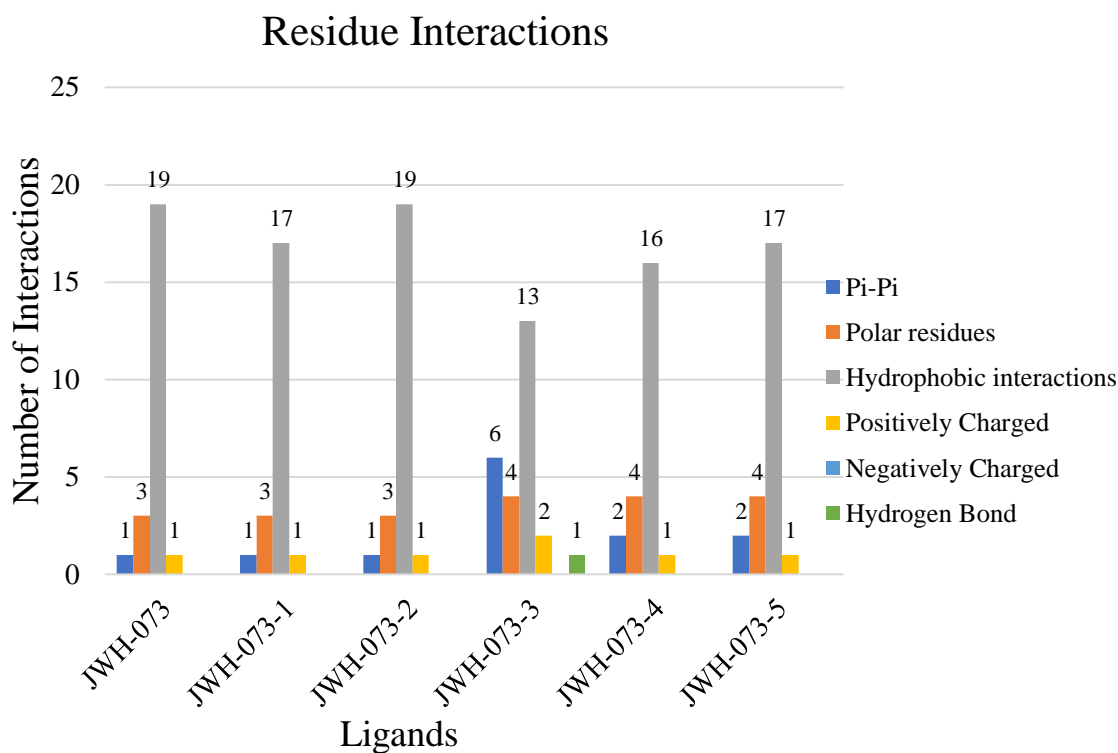


**Figure 12.** Interacting residues observed within 5 Å for the JWH-073 ligand group.

The MGCS-175-073 group of ligands contains a N-linked butyl chain and no carbonyl group was present. For this group of ligands, the number of  $\pi$ - $\pi$  stacking interactions ranged from 3-6. The number  $\pi$ - $\pi$  stacking interactions for the first three ligands, MGCS-175-073, MGCS-175-073-1 and MGCS-175-073-2 were 4, 3 and 4 respectively. The ligand with the lowest number of  $\pi$ - $\pi$  stacking interactions (3) also had the most positive docking score. The number of  $\pi$ - $\pi$  stacking interactions increased to 6 as the alkyl chain was lengthened to a propyl chain. This ligand, MGCS-175-073-3, had the most negative docking score of this group and the highest number of hydrophobic residue interactions (21). The MGCS-175-073-5 ligand had second most negative docking score and it also had 6  $\pi$ - $\pi$  stacking interactions. However, it only had 20 hydrophobic interacting residues compared to the 21 with the MGCS-175-073-3 ligand.

The MGCS-175-073-4 ligand had the most positive docking score. It also displayed the most polar residues (4) of the group. No ligands in this group displayed hydrogen bonding interactions or negatively charged residue interactions within a distance of 5 Å.

The JWH-073 group of ligands also has a N-linked butyl chain but also contains a carbonyl group, methanone. The number of  $\pi$ - $\pi$  stacking interactions in this group ranged from 1-6. The first three ligands, JWH-073, JWH-073-1, and JWH-073-2, all displayed 1  $\pi$ - $\pi$  stacking interaction, 3 polar interactions, and 1 positively charged residue interactions within 5 Å. The only difference in interactions between these first three ligands was the number of hydrophobic residue interactions. JWH-073 and JWH-073-2 each had 19 hydrophobic interactions while JWH-073-1, with the most positive docking score of the three ligands only had 17 hydrophobic interactions. As the alkyl chain was lengthened to a propyl group these number of  $\pi$ - $\pi$  stacking interactions increased to 6 for the JWH-073-3 ligand. The JWH-073-3 ligand had the most negative docking score of this group. It also had the highest number of  $\pi$ - $\pi$  stacking interactions (6) and the lowest number of hydrophobic interactions (13). It was the only ligand with 2 positively charged residues and the only ligand of this group to display hydrogen bonding within 5 Å. The JWH-073-4 ligand had the most positive docking score. It was observed to have 2  $\pi$ - $\pi$  stacking interactions, 4 polar residues, 16 hydrophobic residues and only 1 positively charged residue interaction. The docking score became slightly more negative as the butyl chain was increased to a pentyl chain, JWH-073-5. The only difference observed between JWH-073-4 and JWH-073-5 was the number of hydrophobic interactions, 16 and 17 respectively.

When comparing the interactions between the two groups of ligands it was observed that the MGCS-175-073 group of ligands had more positive docking scores than the JWH-073 group with the exception of MGCS-175-073-5 which was only slightly more negative than JWH-073-5.

The MGCS-175-073 group has had a higher number of  $\pi$ - $\pi$  stacking interactions, ranging from 3-6, while the JWH-073 group's number of  $\pi$ - $\pi$  stacking interactions stayed around 1 or 2 with the only exception being JWH-073-3 that had 6  $\pi$ - $\pi$  stacking interactions. JWH -073-3 was also the ligand with most negative docking score of both groups. It was also the ligand with the lowest number of hydrophobic interactions, the only ligand with 2 positively charged residue interactions and the only ligand with a hydrogen bond interaction. Based on this data it can be determined that the presence of the methanone group (JWH-073) plays an important role in the docking of synthetic cannabinoids to the CB1 receptor. 3D interaction diagrams were then used to better examine the positions of the ligands in the binding pocket of the CB1 receptor. The JWH-073 group of ligands were examined first using the 3D interaction diagram (Figure 13).

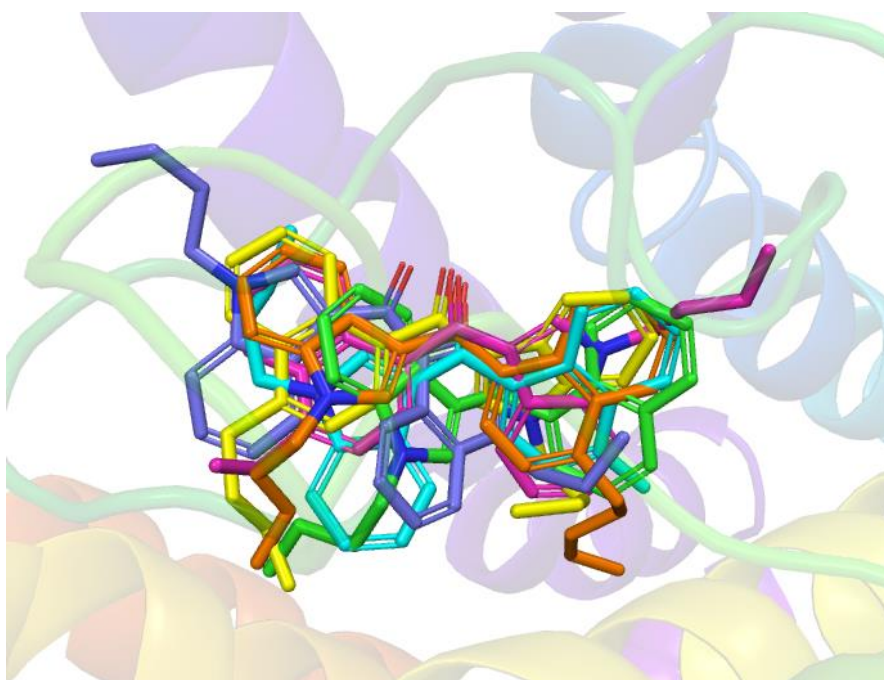


**Figure 13.** 3D interactions diagram of JWH-073 (green), JWH-073-1 (cyan), JWH-073-2 (pink), JWH-073-3 (purple), JWH-073-4 (yellow), and JWH-073-5 (orange).

In the JWH-073 group of ligands significant variation in the position of each ligand was observed as the alkyl chain was lengthened on the naphthalene. However, when the MGCS-175-073 group of ligands were examined, the ligands were found to be in similar positions even as the alkyl chain was lengthened (Figure 14).

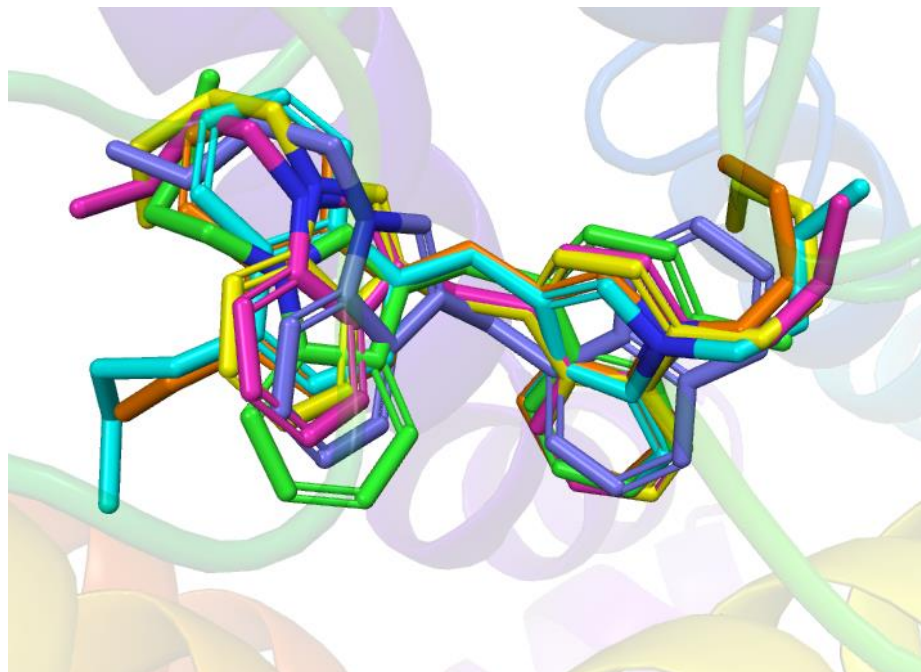


**Figure 14.** 3D interaction diagram of MGCS-175-073 (purple), MGCS-175-073-1 (green), MGCS-175-073-2 (orange), MGCS-175-073-3 (pink), MGCS-175-073-4 (cyan), and MGCS-175-073-5 (yellow).

The MGCS-175-073-2 and MGCS-175-073-4 ligands were found to be in very similar positions. The variations in positions were observed in the alkyl chains of the structures (Figure 15).

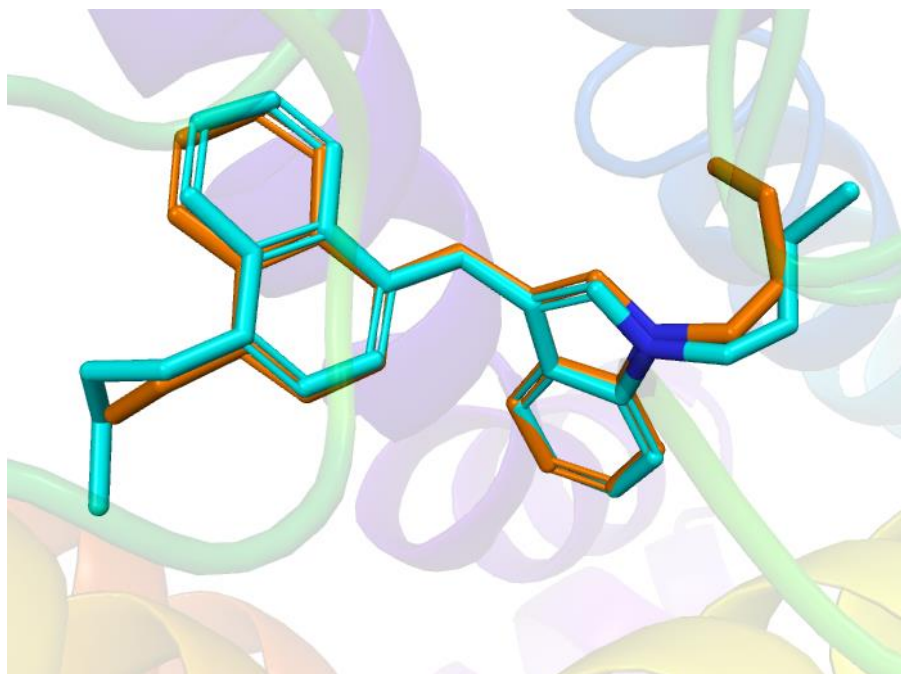


**Figure 15.** 3D interaction diagram of MGCS-175-073-2 (orange) and MGCS-175-073-4 (cyan).

MGCS-175-073-3 and MGCS-175-073-5 were observed to have similar positions to each other, but where opposition of the MGCS-175-073-2 and MGCS-175-073-4 ligands (Figure 16). The notable differences observed between the two ligands were in the position of their alkyl chains in the binding pocket of the CB1 receptor.

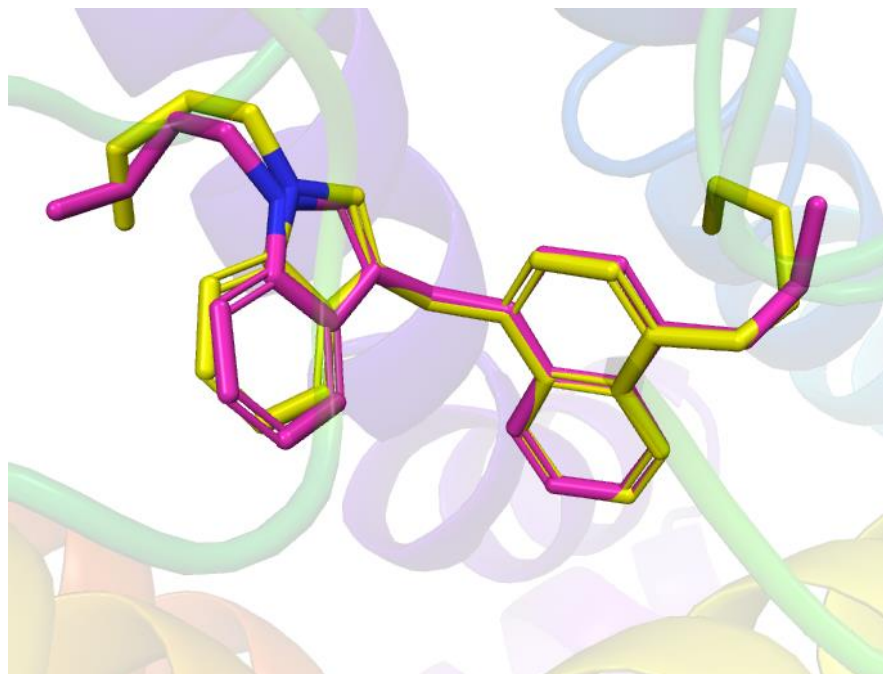


**Figure 16.** 3D interaction diagram of MGCS-175-073-3 (pink) and MGCS-175-073-5 (yellow).

### 2.3.2 JWH-175 and JWH-018

The next groups examined contained the parent structures JWH-175 and JWH-018. Both of the groups contained a N-linked pentyl chain and the alkyl chain on the naphthalene was increased to a five-carbon chain. The group starting with JWH-018 contains a carbonyl linker (methanone) between the naphthalene and indole that is absent in the JWH-175 group.

As the alkyl chain was increased on the naphthalene, a trend was seen between both groups in relation to their docking scores. (Figure 17) A methyl group was then added and both groups saw an increase, becoming more positive, in docking score. The docking scores became slightly more negative as the alkyl chain was increased to a two carbon, ethyl, chain. When a propyl group was present the docking score became more negative for the JWH-175-3 ligand but stayed around the same for the JWH-182 ligand. The docking scores observed from the addition to a butyl chain, and the addition of a pentyl chain displayed more positive docking scores.

However, overall the JWH-175 ligand group, with no carbonyl group, saw consistently better, more negative docking scores with the exception of JWH-018. The most negative docking score was observed for the JWH-018 ligand, while the JWH-018-5 ligand had the most positive docking score.

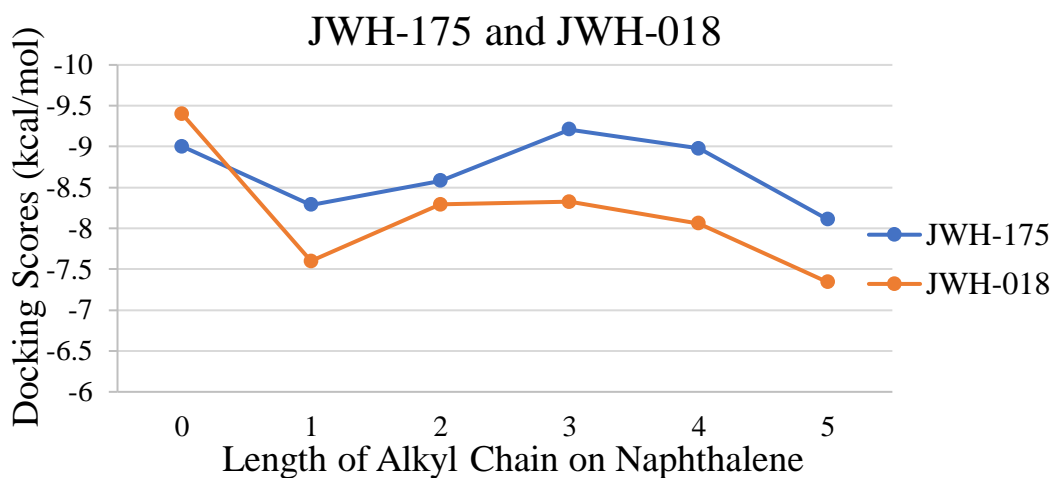


**Figure 17.** Docking scores vs length of alkyl chain for the JWH-175 and JWH-018 groups.

To get a better understanding of how the structural characteristics of the ligands influence the binding to the receptor, the specific residue interactions were examined. (Figure 18-19)

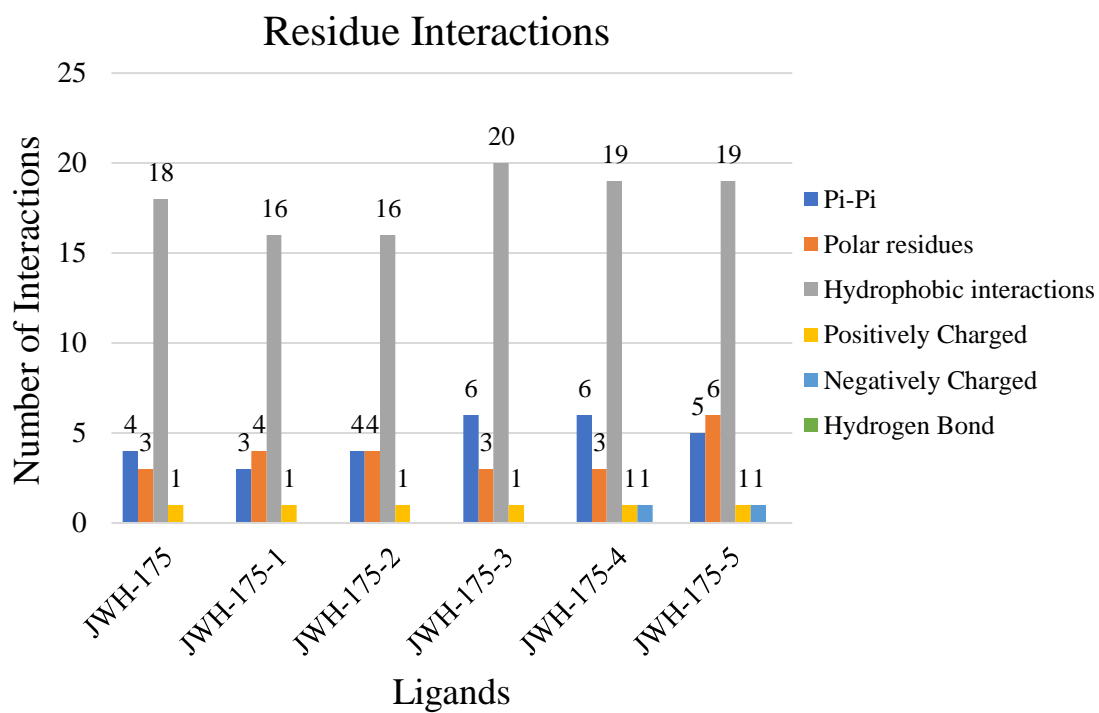


**Figure 18.** Interacting residues observed within 5 Å for the JWH-175 ligand group.



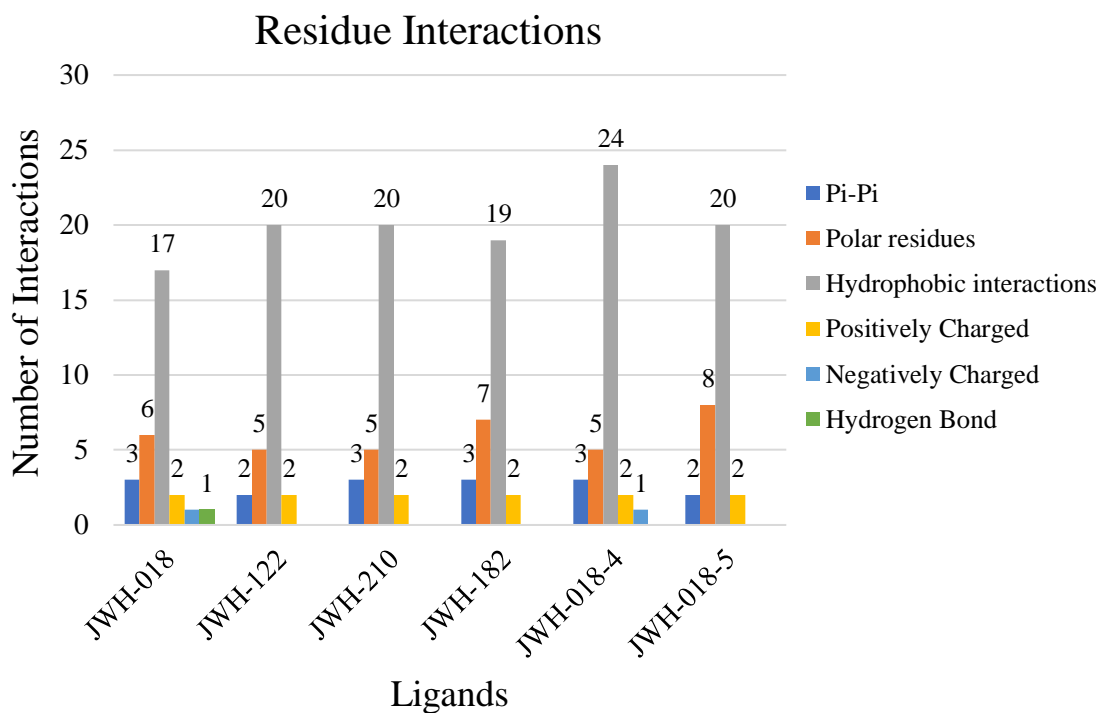


**Figure 19.** Interacting residues observed within 5 Å for the JWH-018 ligand group.

For the JWH-175 ligand group the number of  $\pi$ - $\pi$  stacking interactions was between 3-6. The JWH-175, JWH-175-1 and JWH-175-2 saw the least number of  $\pi$ - $\pi$  stacking interactions, only 3-4. The pattern in  $\pi$ - $\pi$  stacking interactions for these three ligands correlates to their docking scores, with the JWH-175-1 ligand having the least number of  $\pi$ - $\pi$  stacking interactions (3) but the most negative docking score. These three ligands also had the lowest number of hydrophobic residues compared to the ligands with the longer alkyl chains. As the alkyl chain was lengthened to a propyl chain the number of  $\pi$ - $\pi$  stacking interactions increased to 6, the same was also seen for JWH-175-4. The JWH-175-5 ligand only had 5  $\pi$ - $\pi$  stacking interactions. This increase in  $\pi$ - $\pi$  stacking interactions correlates to the docking scores becoming more positive. JWH-175-3 had the most negative docking score. This ligand had 6  $\pi$ - $\pi$  stacking interactions, 3

polar, 20 hydrophobic and 1 positively charged residue interacting within 5 Å. JWH-175-3 had the most hydrophobic residue interactions of the JWH-175 group. The JWH-175-5 ligand had the most positive docking score and it had 5  $\pi$ - $\pi$  stacking interactions, 6 polar, 19 hydrophobic, 1 positively charged and 1 negatively charged residue interacting within 5 Å. This ligand had the most polar residue interactions for this group. Negatively charged residues were only seen for JWH-175-4 and JWH-175-5.

For the group of ligands starting with JWH-018, with the methanone group, the number of  $\pi$ - $\pi$  stacking interactions was between 2-3, significantly lower than the number of interactions observed in the JWH-175 group (3-6). Similar to the JWH-175 group, the trend in docking scores for JWH-018, JWH-122 and JWH-210 correlated to the number of  $\pi$ - $\pi$  stacking interactions observed; 3, 2, and 3 respectively. Of these three ligands the JWH-122 ligand had the most positive docking score and the lowest number of  $\pi$ - $\pi$  stacking interactions. JWH-018 had the most negative docking score of this group of ligands. This ligand also had the lowest number of hydrophobic interactions (17) and displayed a hydrogen bond that was not present on the other ligands. JWH-018-4 and JWH-018-5 were also the only ligands that displayed a negatively charged residue within 5 Å. JWH-018-5 had the most positive docking score of this group. This ligand had 2  $\pi$ - $\pi$  stacking interactions similar to JWH-122 and these ligands saw similar docking scores, JWH-122 had a docking score of -7.598 and JWH-018-5 had a docking score of -7.341. The difference in docking score between these two ligands can be explained by the increased number of polar residues present for JWH-018-5. JWH-018-5 had 8 polar residues while JWH-122 only had 5.

When comparing the interactions between the two groups of ligands it was observed that the JWH-175 group, with no carbonyl, had more  $\pi$ - $\pi$  stacking interactions. The JWH-018 group,

however, had more polar residue interactions than the JWH-175 group. The JWH-175 ligands were also found to have more negative docking scores with the exception of JWH-018. The JWH-175 group of ligands all had 1 positively charged residue where the JWH-018 group all had 2. This could explain the more positive docking scores of the JWH-018 group. 3D interaction diagrams were used to better understand the positions of the ligands in the binding pocket of the CB1 receptor (Figure 20).

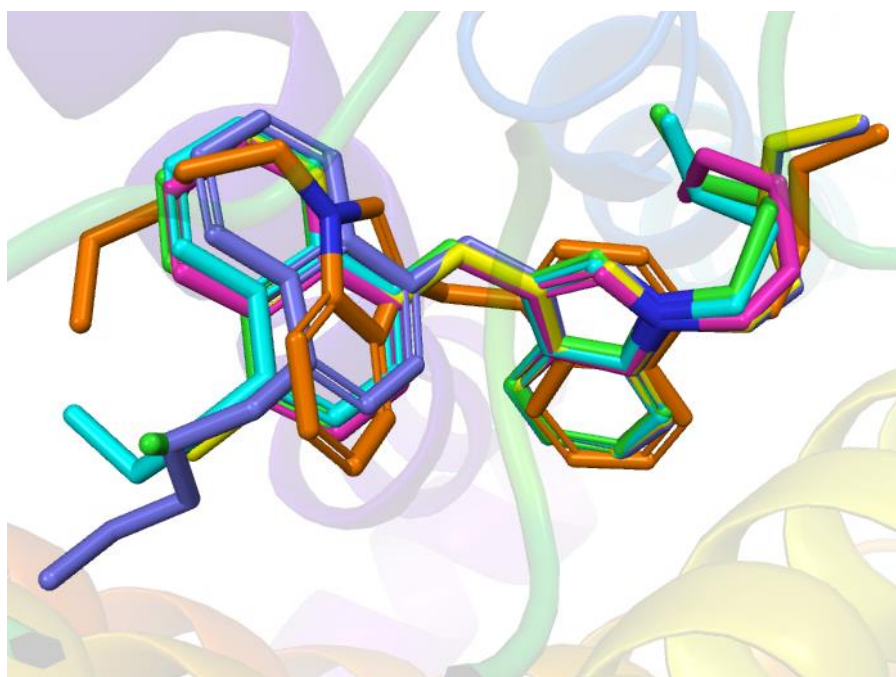


**Figure 20.** 3D interaction diagram of JWH-175 (pink), JWH-175-1 (yellow), JWH-175-2 (green), JWH-175-3 (cyan), JWH-175-4 (orange), and JWH-175-5 (purple).

In the 3D interaction diagram, it was observed that the ligands in the JWH-175 all displayed similar positions in the binding pocket with the exception of JWH-175-4. All the JWH-175 ligands were then examined without the addition of JWH-175-4 (Figure 21).

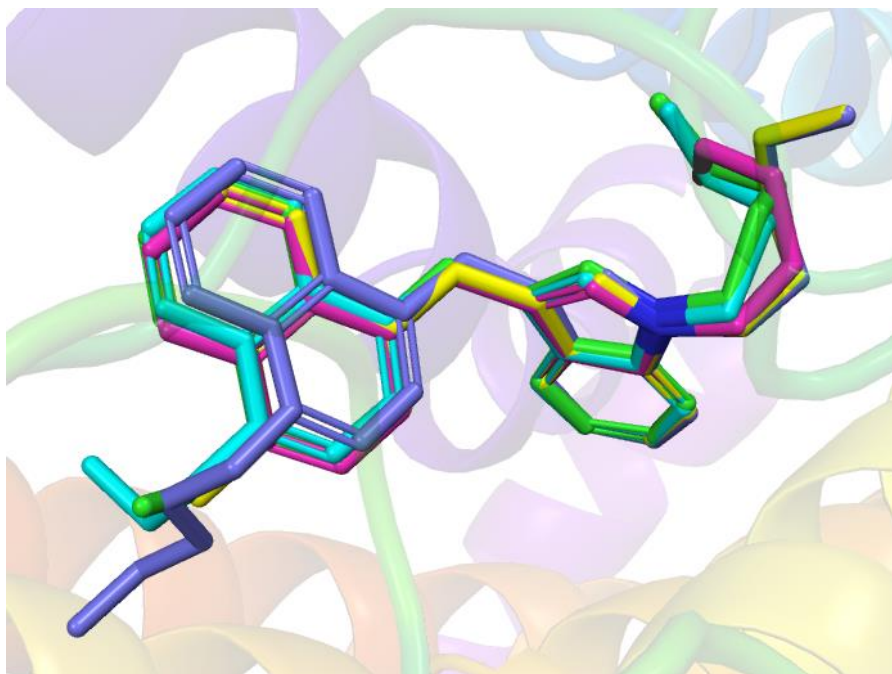


**Figure 21.** 3D interaction diagram of JWH-175 (pink), JWH-175-1 (yellow), JWH-175-2 (green), JWH-175-3 (cyan), and JWH-175-5 (purple).

The 3D interaction diagram showed that the major differences observed in the positions of the JWH-175 ligands was found in alkyl chains of each structure. The JWH-018 group was also examined using the 3D interaction diagram (Figure 22).

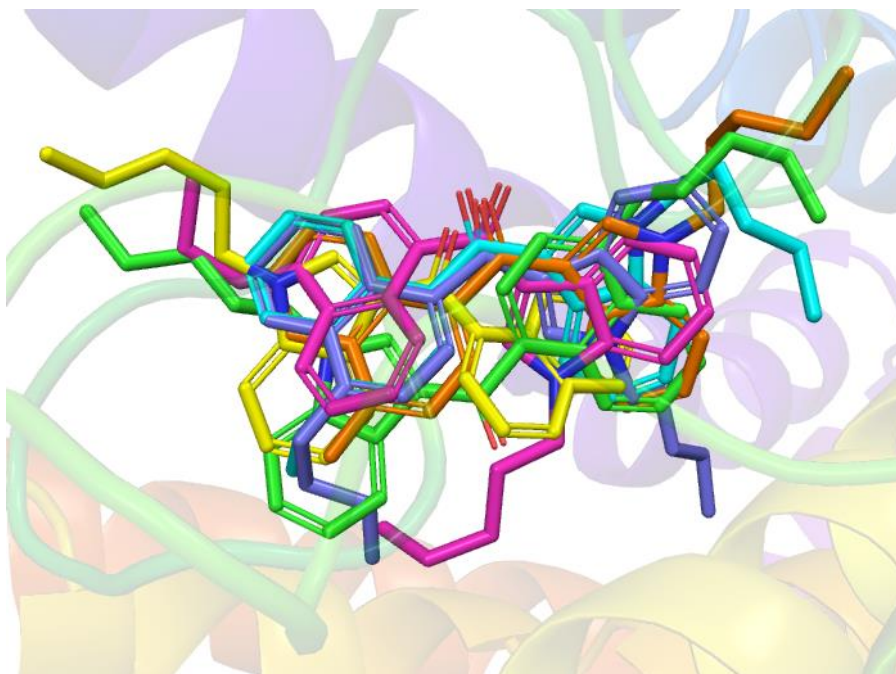


**Figure 22.** 3D interaction diagram of JWH-018 (yellow), JWH-122 (orange), JWH-210 (cyan), JWH-182 (pink), JWH-018-4 (purple), and JWH-018-5 (green).

Unlike the JWH-175 group, the JWH-018 group was observed to have more variation in positions of the structures in the binding pocket of the CB1 receptor. It can be assumed that it is the presence of the carbonyl group in the JWH-018 group that influences the positions of each of the ligands. Only two of the ligands from the JWH-018 group were found to have similar positions, JWH-122 and JWH-210 (Figure 23).

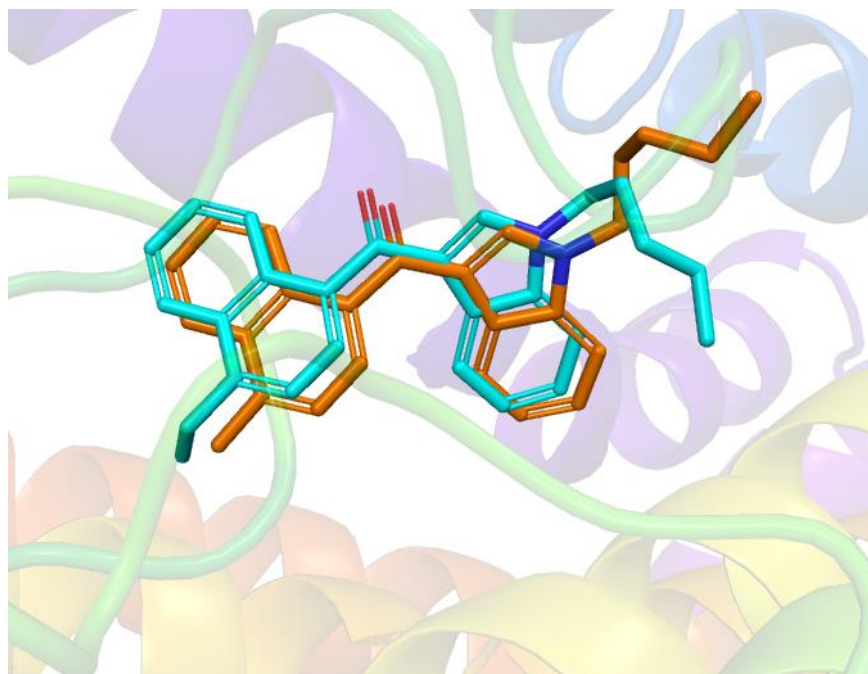


**Figure 23.** 3D interaction diagram of JWH-122 (orange) and JWH-210 (cyan).

Spectral data of the novel synthetic cannabinoid structures were generated using the software ChemDoodle. ChemDoodle is able to produce  $^1\text{H}$  NMR and  $^{13}\text{C}$  NMR spectra of compounds, as well as determine the mass parent peak (Figure 23).

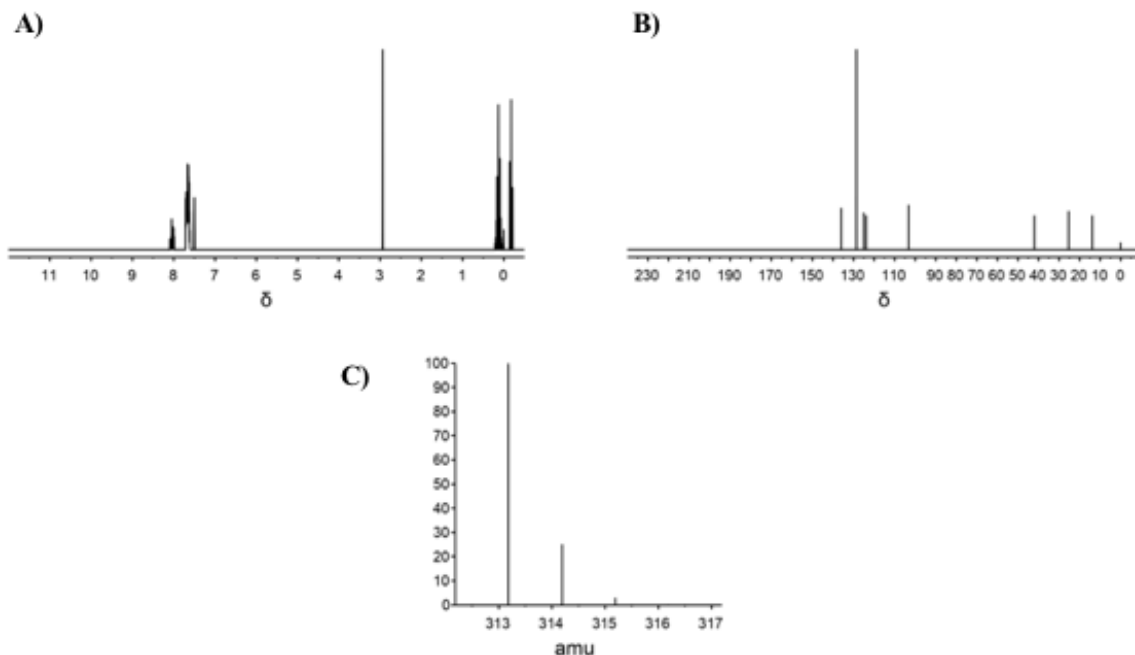


**Figure 24.** Spectral data of the novel synthetic cannabinoid MGCS-175-073; A) <sup>1</sup>H NMR, B) <sup>13</sup>C NMR, C) Mass Parent Peak

## 2.4 Conclusions

The objective of this study was to examine known and novel synthetic cannabinoids from the JWH family and how structural characteristics can influence docking and residue interactions between the synthetic cannabinoids and the CB1 receptor. In this study the length of the alkyl chain both on the naphthalene group was analyzed. The ligands in this study were examined in two phases, each phase consisting of two groups of ligands. This was done to better understand the influence certain structural characteristics have on the binding of the ligand to the CB1 receptor and what specific residues interactions are taking place. Trends were observed in each group of ligands examined in the study when analyzing the docking scores and the number of

interacting residues. It was determined that two structural characteristics were influential on the docking of the ligands to the CB1 receptor, the carbonyl group between the naphthalene and the indole and the length of the N-linked alkyl chain. 3D interaction diagrams were utilized to better understand the influence of the structural characteristics on the position of the ligand in the binding pocket of the CB1 receptor. Through the 3D interaction diagrams, it was determined that the presence of a carbonyl group greatly impacts the positions of the ligands in the binding pocket of the receptor. When there was not a carbonyl present (MGCS-175-073 and JWH-175), the ligands were very similar in their positions. The length of alkyl chain on the naphthalene was determined to influence the position of the alkyl chain; however, it did not appear to influence the overall position of the ligand's core structure in the CB1 receptor. Future studies will include further analysis of what is influencing the varying positions in the core structures of the ligands in the binding pocket of the CB1 receptor.



CHAPTER 3  
THE COMPUTATIONAL STUDY OF KNOWN AND NOVEL HALOGENATED  
DERIVATIVES OF THE SYNTHETIC CANNABINOID JWH-018

### 3.1 Introduction

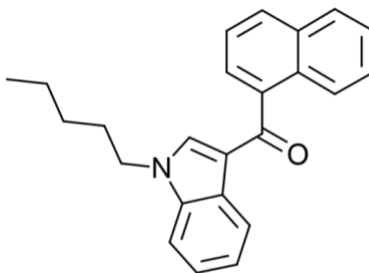
Synthetic cannabinoids are divided into families based on the structure and the designer of the compound. The families include JWH-XXX, CP-XX,XXX, AM-XXX, HU-XXX, WIN-XXX and more. CP-XX,XXX synthetic cannabinoids were designed by Pfizer. The JWH-XXX family of synthetic cannabinoids includes over 400 structures of cannabinoids that were designed by John W. Huffman and his research group at Clemson University. Huffman's compound JWH-018 was one of the first synthetic cannabinoids marketed and sold as "Spice".<sup>38,39</sup>

JWH-018 has been known to have cannabimimetic, similar to cannabis, effects but in lower doses than  $\Delta^9$ -THC.  $\Delta^9$ -THC is only a partial CB1 agonist.<sup>45</sup> JWH-018 is a both a CB1 and CB2 agonist, comparatively. In 2014 the European Monitoring Centre for Drugs and Drug Addiction reported the finding of novel halogenated derivatives, JWH-018 Cl and JWH-018. It has been noted that halogenation of cannabinoid structures can lead to substantial changes in potency and affinity for the cannabinoid receptors.<sup>46</sup>

In 2015, Vigolo et al. studied these novel halogenated derivatives of JWH-018 through examining multiple properties after acute exposure in mice and in vitro competition binding experiments. The authors in this study determined that even though the halogenated derivatives altered sensorimotor response in the mice like the parent compound, JWH-018, they showed

fewer severe adverse effects. Vigolo et al. determined the rank order of potency to be JWH-018  $\geq$  JWH-018 Cl  $\geq$  JWH-018 Br  $\geq$   $\Delta^9$ -THC.<sup>46</sup>

The objectives of this study were to 1) investigate the binding properties of JWH-018 and its known halogenated derivatives JWH-018 Cl and JWH-018 Br to the CB1 receptor and 2) design the novel halogenated derivatives JWH-018 F and JWH-018 I and study their binding to the CB1 receptor through the use of molecular docking.



**JWH-018**

**Figure 25.** Chemical structure of JWH-018, naphthalene-1-yl(1-pentyl-1*H*-indol-3-yl)methanone

### 3.2 Materials and Methods

Schrödinger's molecular modeling software, Maestro, was utilized to examine the binding of JWH-018 and its known halogenated derivatives, JWH-018 Cl and JWH-018 Br, to an active-state CB1 receptor model through molecular docking. Potential new halogenated derivatives, JWH-018 F and JWH-018 I, were also analyzed in this study. Molecular docking is a type of virtual screening that is able to place ligands of interest into the binding pocket of the designated receptor in order to evaluate the binding affinity and ligand-receptor interactions. The prepared 3-D active state model contains  $\Delta^9$ -THC in the binding pocket of the receptor. The

three-dimensional (3D) homology model used in this study was designed and validated by the Doerksen lab at The University of Mississippi, Department of BioMolecular Sciences, Division of Medicinal Chemistry. Since the development of this model, a crystal structure has been published. The crystal structure was published by Hua et al. in 2017.<sup>41</sup> The Doerksen lab has analyzed the crystal structure and compared it to the homology model and found only slight differences in the two structures. The main difference to note is the LYS192 residue. In the crystal structure the side chain of the LYS192 residue is outside the binding pocket, while in the Doerksen model the side chain is pointing towards the binding pocket. It was decided that the study would continue with use of the 3D homology model of the active-state CB1 receptor developed by the Doerksen lab since both structures are comparable. The prepared 3-D active state model contains  $\Delta^9$ -THC in the binding pocket of the receptor. (Figure 26)

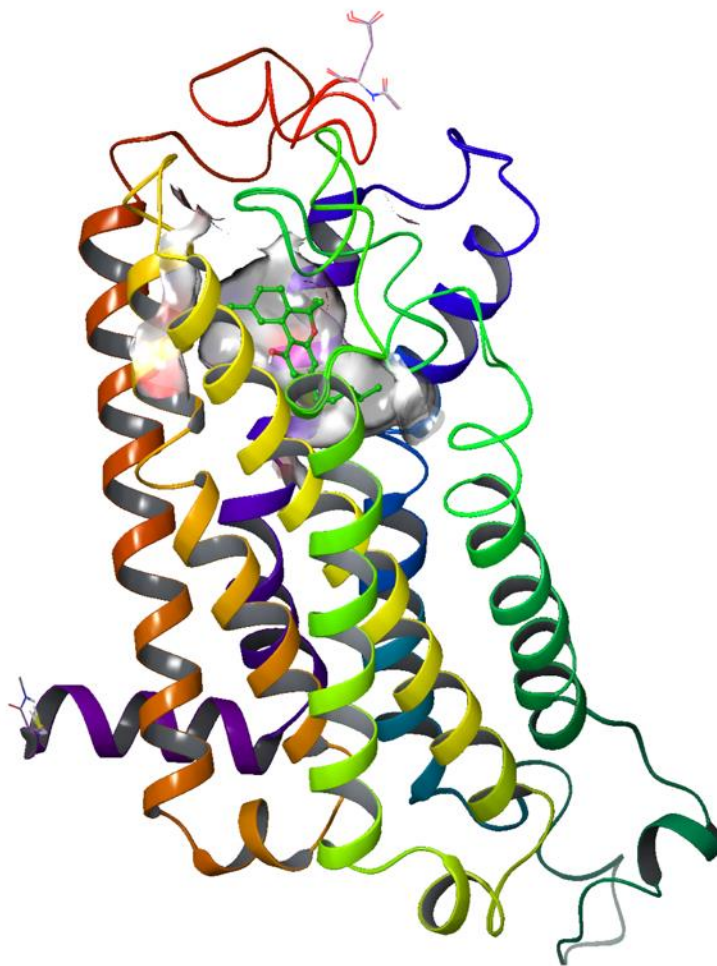


**Figure 26.** Validated 3D homology model of the active-state CB1 receptor, developed by the Doerksen Lab, with a bound  $\Delta^9$ -THC ligand (P Pandey, K K Roy, R J Doerksen, unpublished).

### 3.2.1 Receptor Grid Generation

The *Receptor Grid Generation* application is used to accurately place a grid around the binding pocket of the receptor. This was accomplished by selecting the  $\Delta^9$ -THC ligand already in the binding pocket. The grid generated contained no constraints, rotatable groups and excluded volumes applied to the receptor. The grid created was used to accurately dock the ligands of interest to the receptor.

### 3.2.2 Ligand Selection and Preparation

JWH-018 has two known halogenated derivatives, JWH-018 Cl and JWH-018 Br. For this study all three of these structures were examined as well as the novel halogenated derivatives JWH-018 F and JWH-018 I. The *LigPrep* protocol was used to successfully convert ligands into three-dimensional structures. The preparation of the ligands involves generating possible states at a target pH of 7.0 +/- 2.0 using Epik. Epik is used predict pKa values and determine all chemically sensible structures.<sup>18,42</sup>

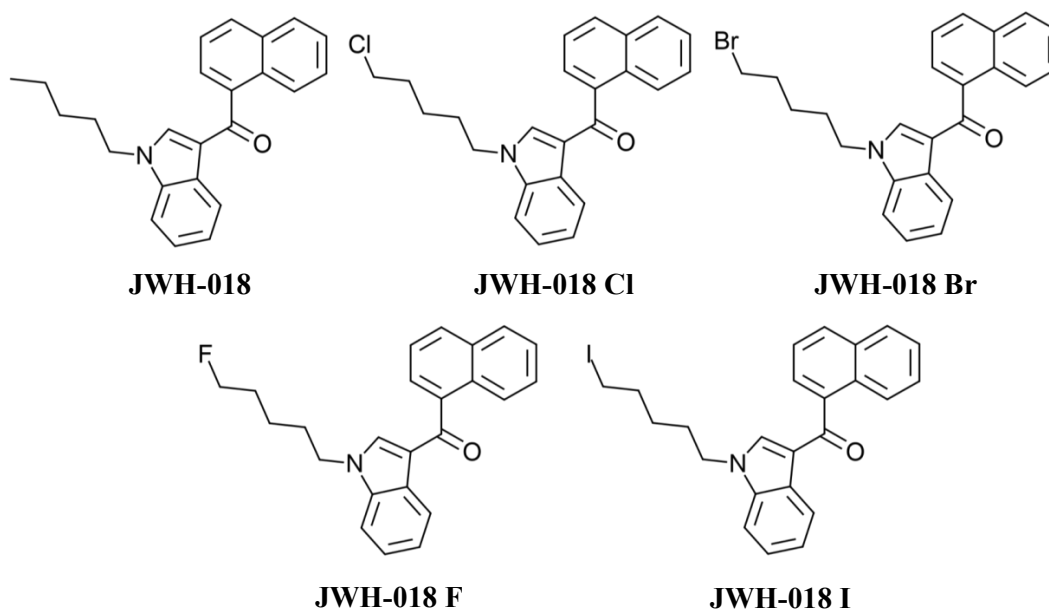


**Figure 27.** Structures of known and novel halogenated derivatives of JWH-018.

### 3.2.3 Ligand Docking

After the grid was generated and the desired ligands were prepared, the next step was *Glide Ligand Docking*. This step allowed for the prepared ligands to be docked into the receptor binding pocket selected during grid generation. Docking was completed using the standard precision (SP) method and force field OPLS3. Flexible ligand sampling was selected and Epik state penalties were added to the docking score. No constraints were selected to use in docking. The Glide program is able to produce potential ligand conformations. The program uses a set of ranked filters to find possible locations on the ligand in the binding pocket of the receptor. The filters include; 1) side-point search, 2a) diameter test, 2b) subset test, 2c) greedy score, 2d) refinement, 3) grid minimization, and 4) final scoring.<sup>43</sup> The *Glide Ligand Docking* process is described by Friesner et al. (2004).<sup>43</sup> For each ligand, up to five possible poses were generated and post-docking minimization was performed. The pose refers to the position and orientation of the ligand in relation to the receptor.<sup>42</sup> To determine the most accurate pose for each ligand, the docking scores and Glide Emodel scores were analyzed. Docking scores are an estimation of the binding free energy and are used to rank poses of different ligands.<sup>43,44</sup> The Glide Emodel was used to compare poses and determine the best, or most likely, pose for each ligand. Docking scores and Glide Emodel scores are negative. A more negative score means better docking. The docking of each ligand, when using the same procedure, produces the same values. The algorithm used by Glide does not require docking multiple times and will produce the same values each time as long as the same procedure is used. The use of three decimal places is because differences in some of the values between ligands might not have been seen until the second or third decimal place. The software allows for more decimal places to be used, but it was decided to use three decimal places due to some of the small changes observed in the data.

### 3.2.4 Binding Energy Estimations: Prime MM-GBSA

The relative binding free energy of each ligand was then estimated using the *Prime MM-GBSA* application and used the following the equation:  $\Delta G_{\text{bind}} = E_{\text{complex}} (\text{minimized}) - (E_{\text{ligand}} (\text{minimized}) - E_{\text{receptor}} (\text{minimized}))$ .<sup>22</sup> The solvation model used was VSGB and calculations were done using OPLS3. Protein flexibility was applied at a distance of 5 Å from the ligand. The Prime MM-GBSA data values are not expected to be the same as the experimental binding affinities. They are generated to give a ranking of the ligands that correlates with the experimental data of binding affinities ( $K_i$  values). A more negative binding free energy values correlates to a stronger binding.<sup>47</sup>

### 3.2.5 Spectral Simulation

Following the analysis of the known and novel synthetic cannabinoids, spectral data were calculated for each of the new structures using spectral simulation software. The program ChemDoodle was able to produce calculated  $^1\text{H}$  NMR,  $^{13}\text{C}$  NMR, and mass parent peak spectra of the novel compounds. The known synthetic cannabinoids were also analyzed by this method and compared to data from the NIST library to confirm accuracy.

## 3.3 Results and Discussion

Binding affinity studies of JWH-018 and its halogenated derivatives, JWH-018 Cl and JWH-018 Br have been done with mouse brain membranes and human CB1 (hCB1) membranes.<sup>46</sup> In this study, the known halogenated derivatives and the novel halogenated derivatives, JWH-018 F and JWH-018 I, were studied through the use of molecular docking. Through molecular docking, the ligands were virtually docked to the 3D validated homology model CB1 receptor developed by the Doerksen lab. Once the ligands were docked their docking

scores were analyzed. The docking scores are estimation of the binding free energy and was used to rank poses of different ligands. The lower, or more negative, the docking score is the stronger the binding is to the CB1 receptor. When docked, each ligand produced up to five possible poses. To determine the best pose of each ligand, the Glide Emodel value was used. The lowest, or most negative, value indicates the best pose for that ligand. Binding energy calculations were then done to determine the relative binding energy of the best pose of each ligand.

**Table 1.** Summary of experimental binding affinities, docking scores, glide Emodel values and binding free energy estimations.

| <b>Ligand</b> | <b>Mouse Brain Membranes<br/>Ki (nM)<sup>46*</sup></b> | <b>hCB1 CHO membranes<br/>Ki (nM)<sup>46*</sup></b> | <b>Docking Scores<br/>(kcal/mol)</b> | <b>Glide Emodel</b> | <b>Binding energy<br/>(kcal/mol)</b> |
|---------------|--|---|--------------------------------------|---------------------|--------------------------------------|
| JWH-018       | 5.82 ± 0.61  | 9.53 ± 0.88   | -9.400                               | -50.914             | -54.416                              |
| JWH-018 F     | -  | -   | -7.337                               | -44.240             | -67.888                              |
| JWH-018 Cl    | 4.21 ± 0.49  | 3.92 ± 0.31   | -7.490                               | -37.855             | -74.287                              |
| JWH-018 Br    | 7.13 ± 0.62  | 6.24 ± 0.53   | -7.470                               | -54.988             | -72.883                              |
| JWH-018 I     | -  | -   | -8.057                               | -71.792             | -75.725                              |

\*0.5 nM [3H]-CP-55,490 was used as the reference ligand for the competitive binding assay.<sup>46</sup>

The Ki values used for comparison in this study were calculated from competitive binding experiments. The experiments performed by Vigolo et al. used 0.5 nM of [3H]-CP-55,490 with both the mouse membranes and the human CB1 receptors. WIN-55,212-2 was added to determine non-specific binding. The authors then determined the free and bound radioactivity. Ki values, inhibitory binding constants, were calculated from the experimental IC<sub>50</sub> values. The IC<sub>50</sub> values express what concentration of the ligand is required to inhibit half of the receptor's biological response. Vigolo et al. determined IC<sub>50</sub> values through the use of cyclic AMP assays where 0.5 nM 4-(3-butoxy-4-methoxybenzyl)-2-imidazolidinone (Ro 20-1724) was added to the



hCB1 CHO membranes as a phosphodiesterase inhibitor. The Cheng and Prusoff equation was used to determine the  $K_i$  values;  $K_i = IC_{50}/(1+[C^*]/K_D^*)$ , C refers to the concentration of the radioligand that was displaced and  $K_D$  is the dissociation constant.<sup>46</sup> The JWH-018 was found to have the best, or most negative, docking score of all the ligands analyzed in this study. Its docking score was determined to be  $-9.400$  kcal/mol, followed by JWH-018 I, JWH-018 Cl, JWH-018 Br and JWH-018F with  $-8.057$ ,  $-7.490$ ,  $-7.470$ , and  $-7.337$  kcal/mol, respectively. Binding free energy (kcal/mol) calculations were also done of the best pose for each ligand. These values are not expected to be the same as the experimental binding affinities but are expected to give a ranking of the ligands that correlates with the experimental data of binding affinities ( $K_i$ ). A more negative binding free energy value correlates to a stronger binding.<sup>35</sup> This data shows JWH-018 has the highest, most positive, binding free energy estimation ( $-54.416$  kcal/mol), and it also has the highest experiment  $K_i$  value with hCB1 CHO ( $9.53 \pm 0.88$  nM). The only other  $K_i$  values available for comparison are for JWH-018 Br and JWH-018 Cl. JWH-018 Cl had the lowest  $K_i$  value ( $3.92 \pm 0.31$  nM) and the lowest, most negative binding free energy ( $-74.287$  kcal/mol). JWH-018 Br fell in the middle with a  $K_i$  value of  $6.24 \pm 0.53$  nM and binding energy estimation of  $-72.883$  kcal/mol. The novel halogenated derivatives JWH-018 F and JWH-018 I do not have experimental  $K_i$  values, but they can be deduced based on the estimated binding energies. It can be hypothesized that JWH-018 F would have a  $K_i$  value lower than JWH-018, but higher than the other halogenated derivatives and JWH 018 I would have the lowest, or better binding affinity, than all the other ligands.

Using the *Ligand Interaction Diagram* application in Maestro, the residues interacting at within distance of  $5 \text{ \AA}$  from the ligand were examined (Table 2). The types of interacting

residues present within the binding pocket were labeled as hydrophobic, polar, negatively charged or positively charged residues.

**Table 2.** Number and identification of interacting residues within 5 Å for JWH-018 and its halogenated derivatives.

| <b>Ligand</b> | <b>Docking Score (kcal/mol)</b> | <b>Binding Energy (kcal/mol)</b> | <b>Hydrophobic</b> | <b>Polar</b> | <b>Negatively Charged</b> | <b>Positively Charged</b> |
|---------------|---------------------------------|----------------------------------|--------------------|--------------|---------------------------|---------------------------|
| JWH-018       | -9.401                          | -54.416                          | 17                 | 6            | 1                         | 2                         |
| JWH-018 F     | -7.337                          | -67.888                          | 21                 | 4            | 1                         | 1                         |
| JWH-018Cl     | -7.490                          | -74.287                          | 22                 | 4            | 1                         | 1                         |
| JWH-018Br     | -7.470                          | -72.883                          | 21                 | 7            | 1                         | 1                         |
| JWH-018 I     | -8.057                          | -75.725                          | 21                 | 6            | 1                         | 1                         |

It was determined that JWH-018, with the most negative docking score, possessed 17 hydrophobic residues, 6 polar residues, 1 negatively charged residue and 2 positively charged residues. When comparing JWH-018 with its halogenated derivatives, it can be seen that some of the major differences included the lower number of hydrophobic residues and the additional positively charged residue for JWH-018. All ligands had the LYS192 residue present within 5 Å and JWH-018 had both LYS192 and LYS376. The positively charged residue LYS376 only appeared when the distance was adjusted for the halogenated derivatives to 6 Å. This could indicate that the distance of specific residues from the ligand could impact the docking score and overall binding of the ligand to the receptor. JWH-018 F and JWH-018 Cl were found to have the least number of polar residues (4), but around the same number of hydrophobic residues as the other halogenated derivatives, JWH-018 Br and JWH-018 I.

After examining the residues present within the binding pocket, the direct interactions taking place between the ligands and the CB1 receptor were analyzed. Interactions can include,  $\pi$ - $\pi$  stacking, hydrogen bonding,  $\pi$ -cation and salt bridges (Table 3).

**Table 3.** Residues interacting with the ligands CB1 receptor within the binding pocket within a distance of 5 Å. Naphthalene 1 is the benzene ring of the naphthalene connected to the carbonyl group and naphthalene 2 is the benzene ring connected to naphthalene 1.

| <b>Ligand</b>     | <b><math>\pi</math>-<math>\pi</math> Stacking<br/>Naphthalene 1</b> | <b><math>\pi</math>-<math>\pi</math> Stacking<br/>Naphthalene<br/>2</b> | <b><math>\pi</math>-<math>\pi</math> Stacking<br/>Benzene<br/>(Indole)</b> | <b><math>\pi</math>-<math>\pi</math> Stacking<br/>Pyrrole<br/>(Indole)</b> | <b>Hydrogen<br/>Bond</b> |
|-------------------|---|---|--|--|--------------------------|
| <b>JWH-018</b>    | TRP279<br>TRP279  | -   | PHE177   | -  | TRP279                   |
| <b>JWH-018 F</b>  | TRP279<br>TRP279  | TRP279<br>TRP279  | TRP356<br>PHE200   | -  | SER383                   |
| <b>JWH-018 Cl</b> | TRP279<br>TRP279  | TRP279<br>TRP279  | TRP356<br>PHE200   | -  | SER383                   |
| <b>JWH-018 Br</b> | PHE200<br>TRP356  | PHE200  | TRP279<br>TRP279   | TRP279<br>TRP279   | SER383                   |
| <b>JWH-018 I</b>  | TRP356  | PHE200  | TRP279<br>TRP279   | TRP279<br>TRP279   | SER383                   |

The only type of interactions seen between the ligands in this study and the CB1 receptor were  $\pi$ - $\pi$  stacking and hydrogen bonding. The one common interaction between all the ligands was a  $\pi$ - $\pi$  stacking interaction with TRP279. However, the location of this interaction on the

ligand varied. The interacting residues between JWH-018 and the CB1 receptor included 2  $\pi$ - $\pi$  stacking interactions with TRP279, 1  $\pi$ - $\pi$  stacking interaction with PHE177 and a hydrogen bond between TRP279 and the oxygen of the carbonyl. JWH-018 F and JWH-018 Cl shared the same interactions. Both ligands had 4  $\pi$ - $\pi$  stacking interactions with TRP279. Two of the  $\pi$ - $\pi$  stacking interactions were with the benzene ring connected to the carbonyl group (naphthalene 1) and the other two were with the benzene ring connected to naphthalene 1 (naphthalene 2). There was hydrogen bonding between SER383 and the double bonded oxygen of the carbonyl group. This interaction with SER383 was seen in all the halogenated derivatives. JWH-018 Br and JWH-018 I had similar interactions. Each ligand had 4  $\pi$ - $\pi$  stacking interactions with TRP279, but, unlike JWH-018 F and JWH-018 Cl the interactions were with the indole portion of the ligands. Of the 4  $\pi$ - $\pi$  stacking interactions with TRP279, 2 were interacting with the pyrrole of the indole and the other 2 were with the benzene of the indole. There was a hydrogen bond between the oxygen of the carbonyl and the SER383 residue. JWH-018 Br had 2  $\pi$ - $\pi$  stacking interactions with PHE 200, one interaction was on naphthalene 1 and the other was on naphthalene 2. JWH-018 Br also had a  $\pi$ - $\pi$  stacking interaction with TRP356 and naphthalene 1. JWH-018 I also had a  $\pi$ - $\pi$  stacking interaction with TRP356 and naphthalene 1. However, JWH-018 I only had 1  $\pi$ - $\pi$  stacking interaction with PHE200 at the naphthalene 2. Over all, the halogenated derivatives had similar interacting residues. The parent structure, JWH-018, had less interactions and interacted with different residues. While JWH-018 had a hydrogen bond between TRP279 and the double bonded oxygen of the carbonyl, all the halogenated derivatives had hydrogen bonding with the residue SER383. The halogenated derivatives overall had an increase in  $\pi$ - $\pi$  stacking interactions compared to JWH-018. These various differences could be responsible for the decreasing docking scores of the halogenated derivatives from the parent structure, JWH-018. Although

there were significant differences in docking scores between JWH-018 and its halogenated derivatives, there was not a significant difference in docking scores between the individual derivatives. These findings indicate that the added number of interactions taking place in the binding pocket influences the docking score and binding of the ligands to the receptor.

Electronegativity could also be a factor in the binding of the halogenated derivatives to the CB1 receptor. Halogens are known to have high electronegativity. Electronegativity is defined as “ the tendency of an atom to attract a bonding pair of electrons”.<sup>36</sup> The periodic table shows the trend of the electronegativity value of an element increases as it moves from left to right and increases as it moves from the bottom to the top of the periodic table. The most electronegative of the halogenated derivatives would be JWH-018 F, which also possess the highest, or least negative docking score,  $-7.337$  kcal/mol. JWH-018 I would be the least electronegative derivative and it has the lowest, or most negative, docking score of  $-8.037$  kcal/mol. JWH-018 Cl and JWH-018 Br have very close docking scores and also similar in electronegativity. To better understand the interactions taking place between each ligand and the CB1 receptor, 3D interaction diagrams were examined.

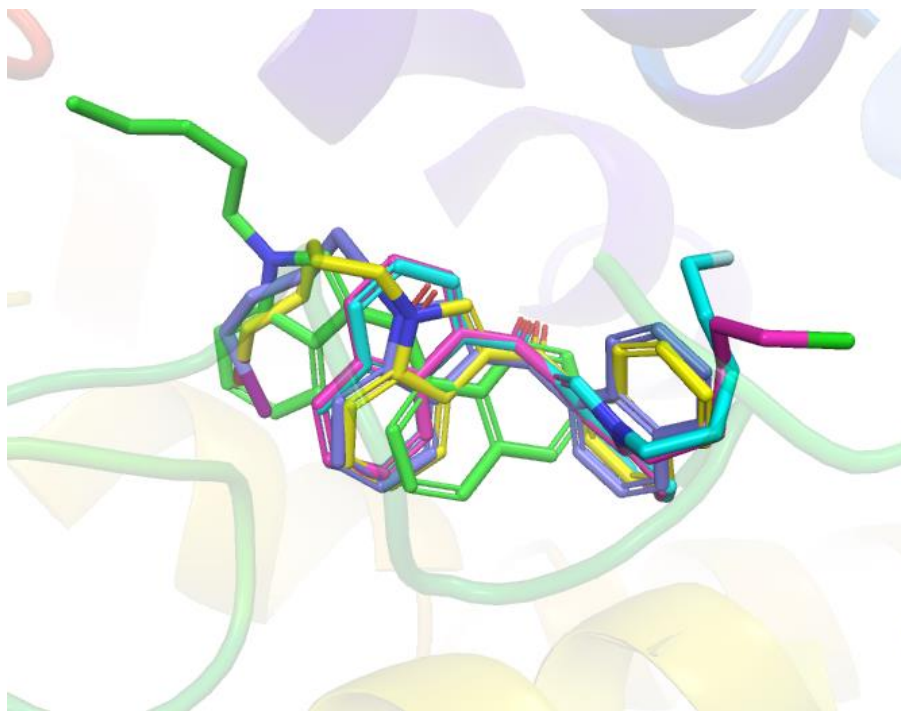


**Figure 28.** 3D interaction diagram of JWH-018 (green) and all the halogenated derivatives; JWH-018 F (cyan), JWH-018 Cl (pink), JWH-018 Br (yellow), and JWH-018 I (purple).

It was observed that JWH-018 differed greatly in its position in the binding pocket compared to the halogenated derivatives. The position of the JWH-018 ligand explains why the interactions varied between the ligand and its halogenated derivatives. JWH-018 contained  $\pi$ - $\pi$  stacking interactions with PHE177, a residue that was not observed in the derivatives, and hydrogen bonding with TRP279 (Figure 29).

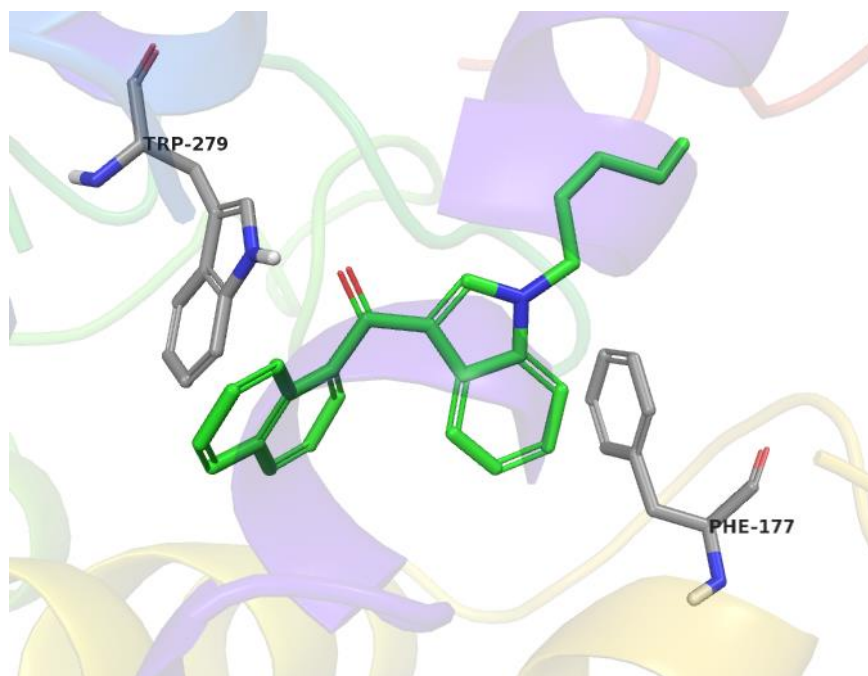


**Figure 29.** 3D interaction diagram of JWH-018 and the PHE177 and TRP279 residues of the CB1 receptor (shown as cartoon). Interacting residues are shown in grey.

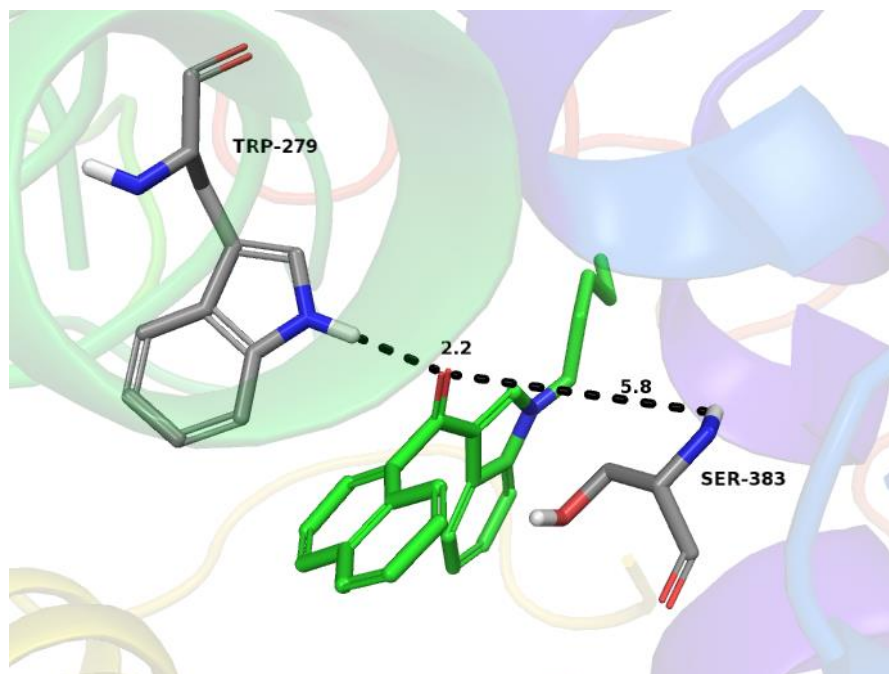


**Figure 30.** 3D interaction diagram of JWH-018 showing the distance from TRP279 (2.2 Å) and SER383 (5.8 Å).

The halogenated derivatives of JWH-018 all displayed hydrogen bonding with SER383 where JWH-018 interacted with TRP279 through a hydrogen bond. Due to the position of JWH-018 in relation to SER383, it was impossible for the ligand to interact with the residue. (Figure 30) The distance between the TRP279 residue and the carbonyl group of the JWH-018 ligand involved in the hydrogen bonding was found to be 2.2 Å, where the SER383 residue was at a distance of 5.8 Å. The positions of the halogenated derivatives were then compared to determine what similarities and differences were found. (Figure 31)



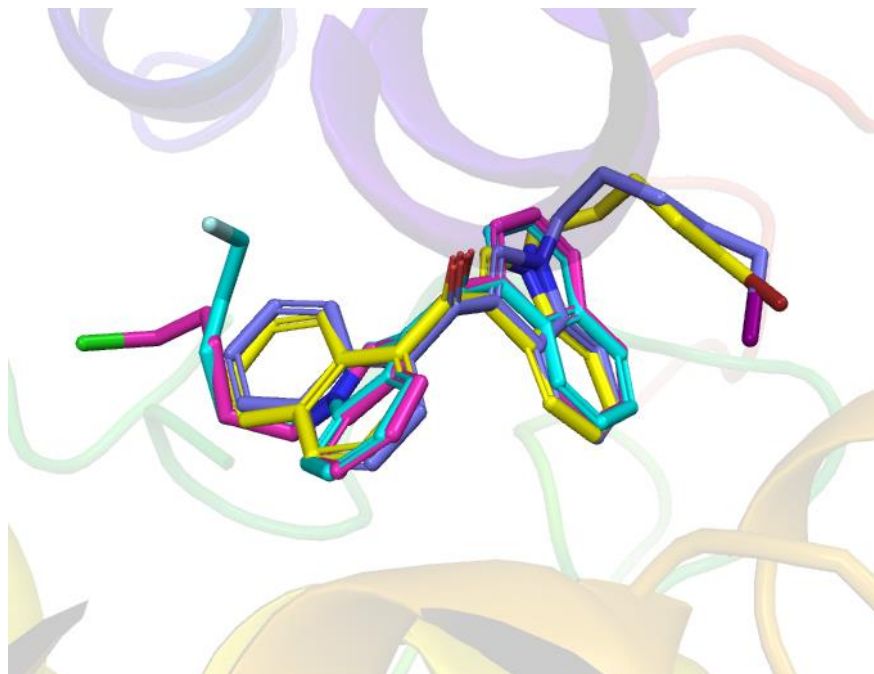


**Figure 31.** 3D interaction diagram of halogenated derivatives; JWH-018 F (cyan), JWH-018 Cl (pink), JWH-018 Br (yellow), and JWH-018 I (purple).

From the 3D interaction diagram, it was observed that JWH-018 F and JWH-018 Cl had similar positions and JWH-018 Br and JWH-018 I had similar positions. All of the halogenated derivatives had  $\pi$ - $\pi$  stacking interactions with TRP279, TRP356, and PHE200. However, the interactions occurred on different locations of the ligand. The position of the JWH-018 F and JWH-018 Cl ligands were opposite of the JWH-018 Br and JWH-018 I ligands.

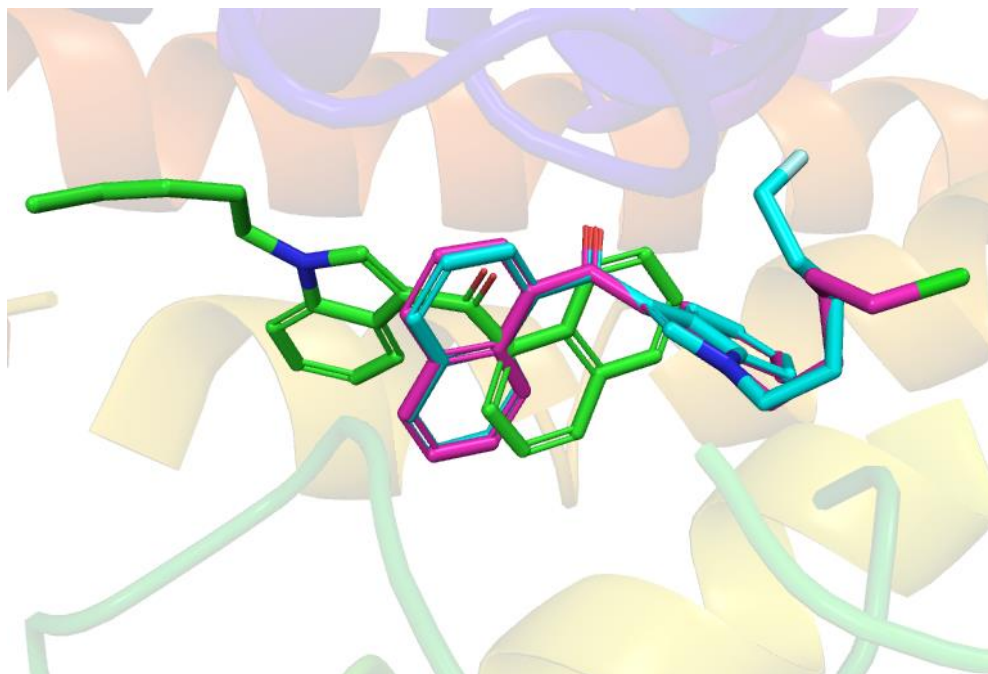


**Figure 32.** 3D interaction diagram with JWH-018 (green), JWH-018 F (cyan), and JWH-018 Cl (pink).

JWH-018 F and JWH-018 Cl were found to be in similar positions in the binding pocket of the CB1 receptor. The main difference was observed at the end of the alkyl chain where then halogens were added. (Figure 32). The common residues observed between these two ligands were examined (Figure 33).

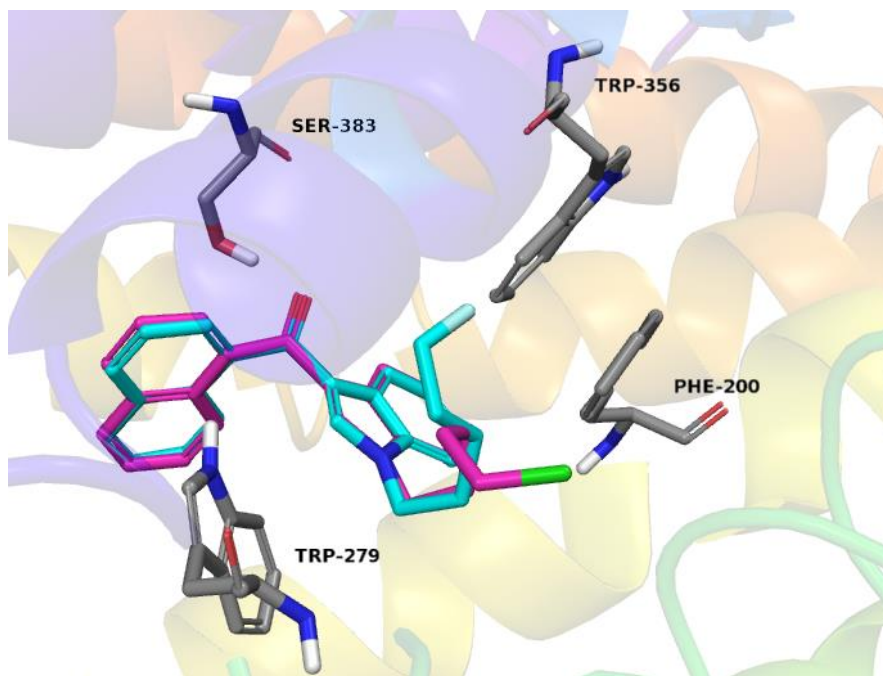


**Figure 33.** 3D interaction diagram of JWH-018 F (cyan) and JWH-018 Cl (pink) and the interacting residues TRP279, TRP356, PHE200, and SER383 (grey).

Both the JWH-018 F and JWH-018 Cl ligand displayed  $\pi$ - $\pi$  stacking interactions with TRP279 and both benzenes of the naphthalene group. TRP356 and PHE200 interacted through  $\pi$ - $\pi$  stacking with the indole portion of each ligand. Hydrogen bonding was observed in both ligands between SER383 and the carboxyl group. The JWH-018 Br and JWH-018 I ligands were then examined (Figure 34-35).

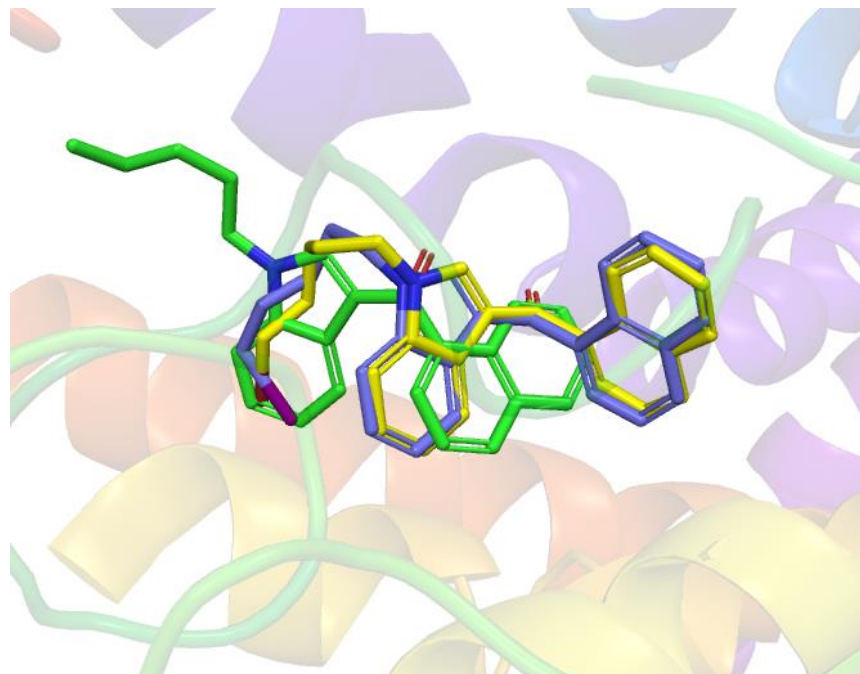


**Figure 34.** 3D interaction diagram with JWH-018 (green), JWH-018 Br (yellow), and JWH-018 I (purple).

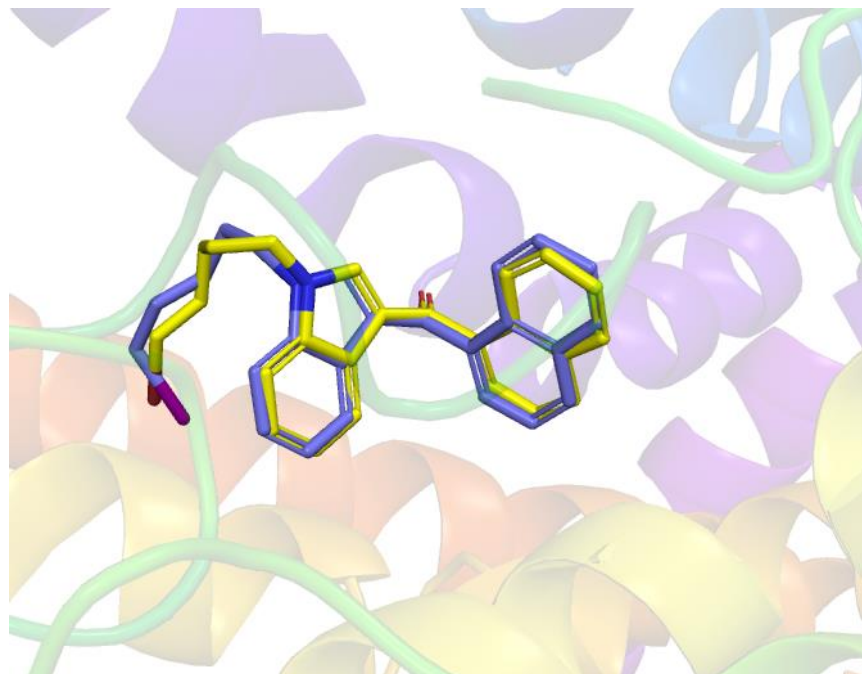


**Figure 35.** 3D interaction diagram of JWH-018 Br (yellow) and JWH-018 I (purple).

The JWH-018 Br and JWH-018 I ligands were found to be in very similar positions in the binding pocket. Only slight differences were observed in the position of the alkyl chain with the halogen added at the end. The interacting residues were examined to better understand how the position of the ligand influenced the residue interactions (Figure 36).

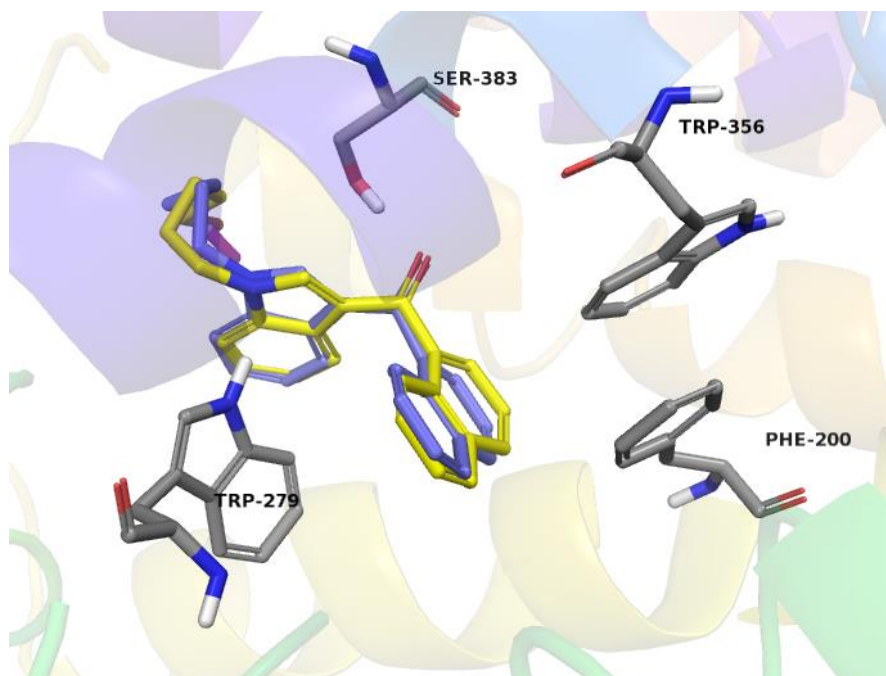


**Figure 36.** 3D interaction diagram of JWH-018 Br (yellow) and JWH-018 I (purple) with the interacting residues TRP279, TRP356, PHE200, and SER383.

JWH-018 Br and JWH-018 I interacted with the same residues as JWH-018 F and JWH-018 Cl. However, the locations of the interactions were different. This is due to the position of the JWH-018 Br and JWH-018 I ligands being opposite of the JWH-018 F and JWH-018 Cl ligands.

The software ChemDoodle was used to calculate spectral data of JWH-018 and its halogenated derivatives. ChemDoodle is able to produce  $^1\text{H}$  NMR and  $^{13}\text{C}$  NMR spectra of compounds, as well as determine the mass parent peak (Figure 37 - 41).

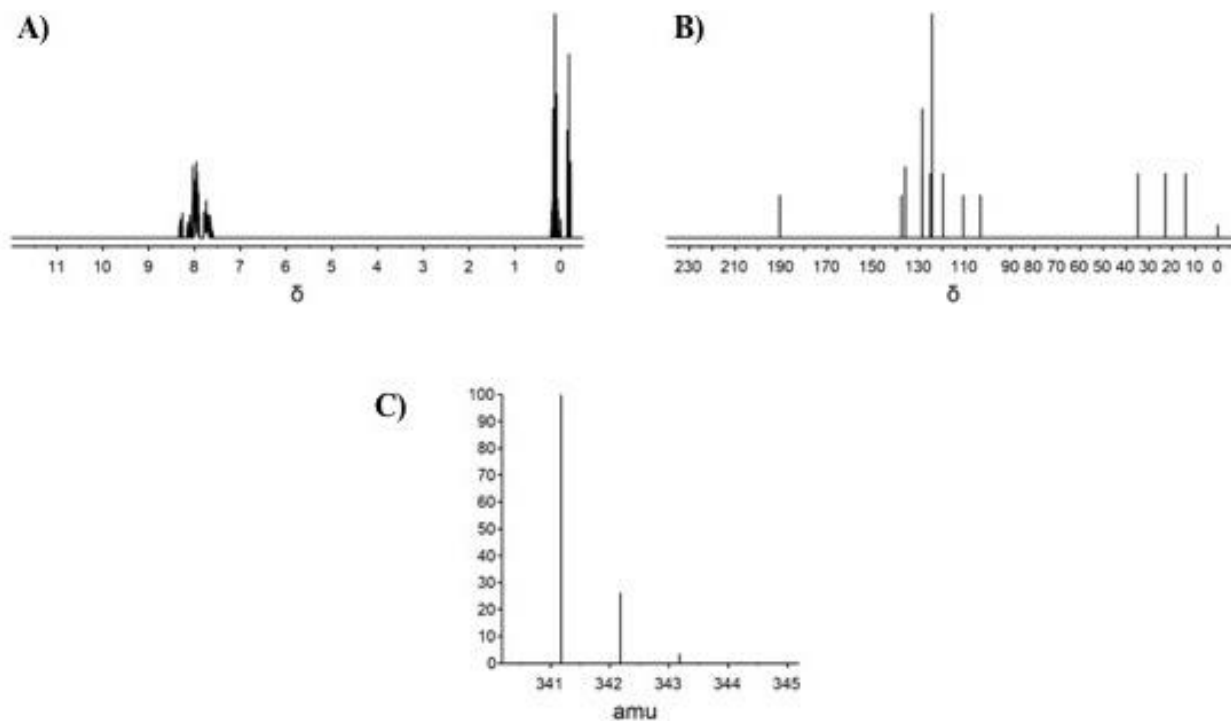


**Figure 37.** Spectral data of JWH-018; A)  $^1\text{H}$  NMR, B)  $^{13}\text{C}$  NMR and C) Mass Parent Peak.

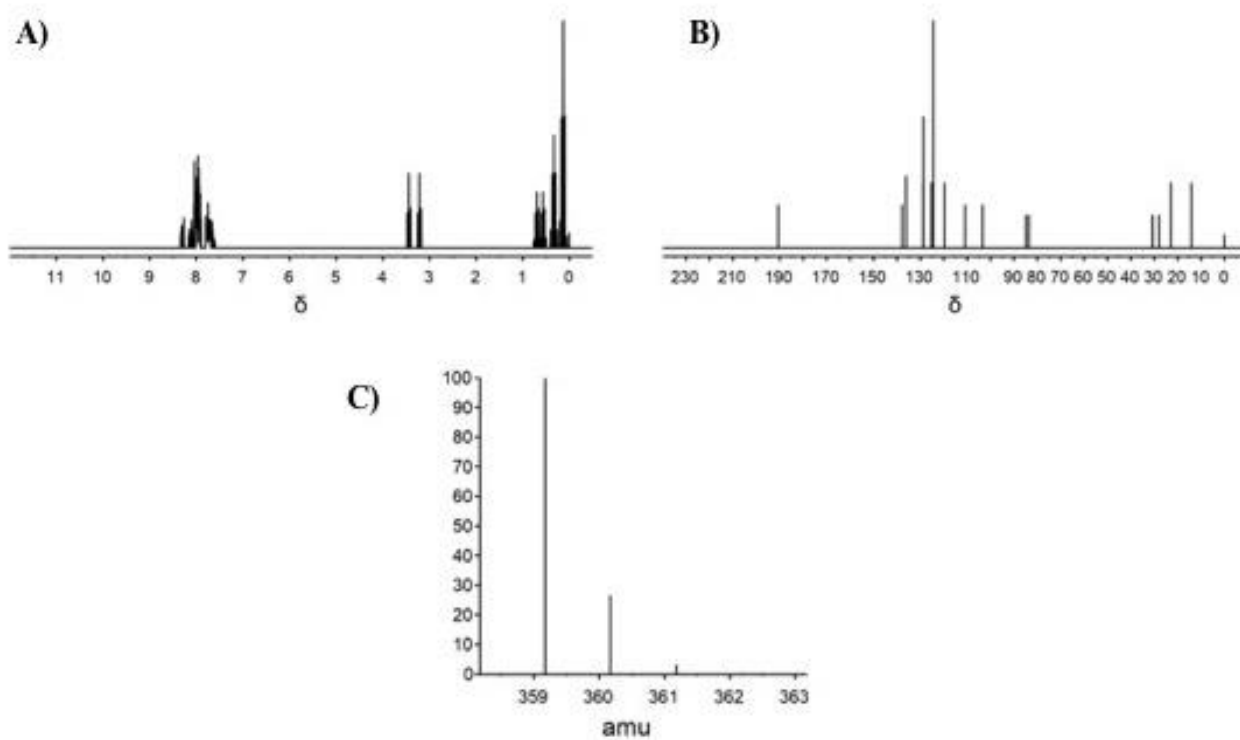


**Figure 38.** Spectral data of JWH-018 F; A)  $^1\text{H}$  NMR, B)  $^{13}\text{C}$  NMR, and C) Mass Parent Peak.



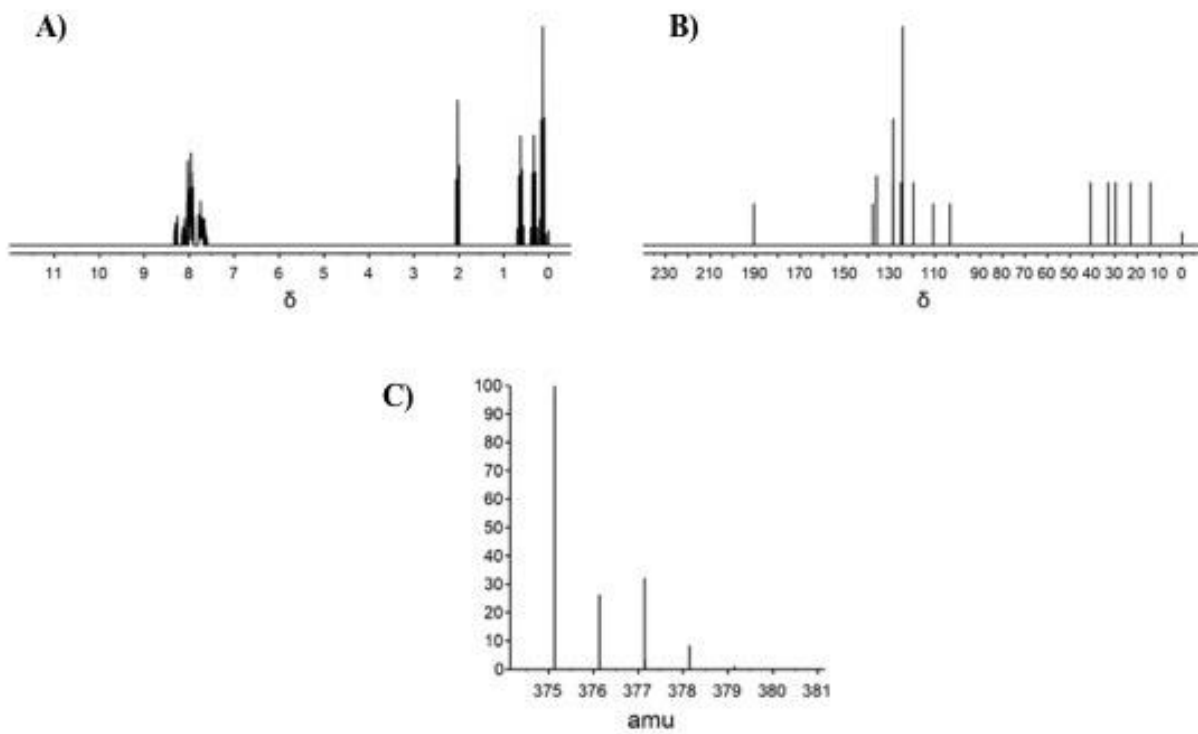


**Figure 39.** Spectral data of JWH-018 Cl; A)  $^1\text{H}$  NMR, B)  $^{13}\text{C}$  NMR, and C) Mass Parent Peak.

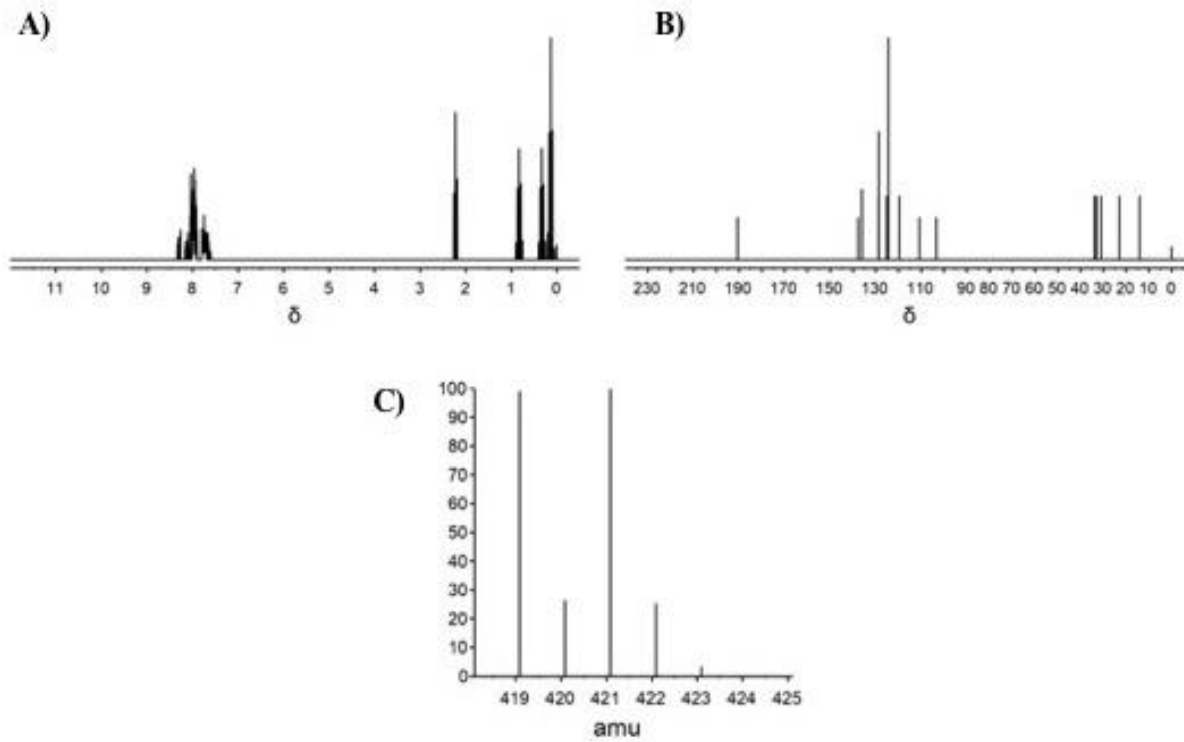


**Figure 40.** Spectral data of JWH-018 Br; A)  $^1\text{H}$  NMR, B)  $^{13}\text{C}$  NMR, and C) Mass Parent Peak.

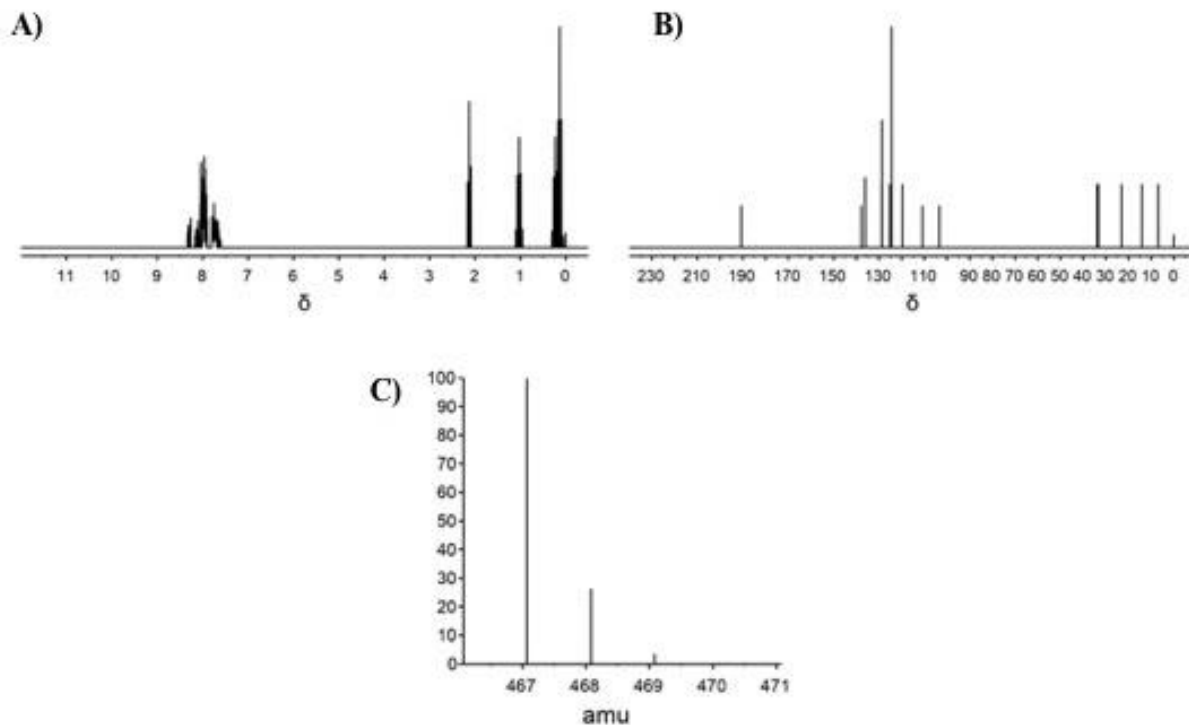


**Figure 41.** Spectral data of JWH-018 I; A) <sup>1</sup>H NMR, B) <sup>13</sup>C NMR, and C) Mass Parent Peak.

### 3.4 Conclusions

This computational study of the known and novel halogenated derivatives of JWH-018 correlated to the rank of potency determined by Vigolo et al., JWH-018 > JWH-018 Cl > JWH-018 Br through the docking scores of these structures. The novel halogenated derivatives of JWH-018, JWH-018 F and JWH-018 I, were also examined in this study. The rank of potency when compare to JWH-018 and its known halogenated derivatives was determined to be JWH-018 > JWH-018 I > JWH-018 Cl > JWH-018 Br > JWH 018 F, based on docking scores. Binding energy estimation calculations were also performed. The binding energy estimation values are not expected to be the same as the experimental binding affinities but are intended to give a ranking of the ligands that correlates with the experimental data of binding affinities.<sup>5647</sup>

Experimental data showed that JWH-018 had the highest  $K_i$  value, which correlated to the binding energy estimation. The experimental  $K_i$  values of JWH-018 Cl and JWH-018 Br also aligned with the calculated binding energies. Based on the binding energy estimations, it can be hypothesized that JWH-018 F would have a smaller  $K_i$  value than JWH-018 but a larger, or weaker binding affinity, compared to the other halogenated derivatives. JWH-018 I can be hypothesized to have the lowest, strongest binding,  $K_i$  value compared to all other ligands in this study. Through 3D interaction diagrams it was observed that the position of JWH-018 inside the binding pocket of the CB1 receptor differed greatly from its halogenated derivations which can explain the differences in interacting residues and the differences in docking scores and binding energy estimations. JWH-018 F and JWH-018 Cl were observed to be in similar positions in the binding pocket, which correlates to the similarities seen in their interacting residues. JWH-018 Br and JWH-018 I were observed in opposite positions, compared to JWH-018 F and JWH-018 C, which is correlates to the differences in residue interactions. Future studies will further examine the cause of varying positions of the core structures in the binding pocket of the CB1 receptor, to better understand the impact halogenation of synthetic cannabinoids has on the binding.

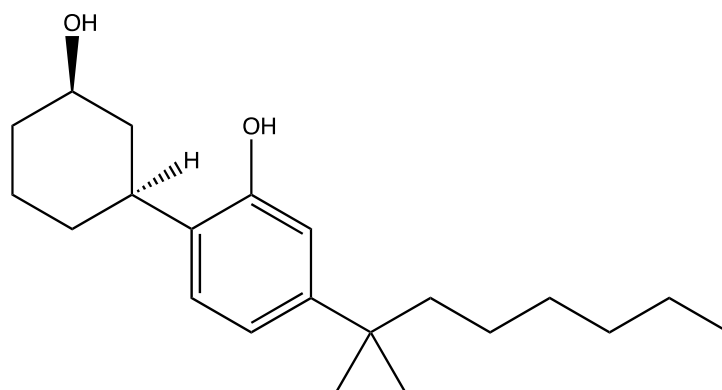
Vigolo et al. hypothesized that the reason for the appearance of the halogenated derivatives on the drug scene was to replace the parent compound, JWH-018.<sup>46</sup> JWH-018 is known to have severe adverse effects. The Vigolo et al. study shows there were not as many severe side effects seen with the halogenated derivatives compared to JWH-018. To further support Vigolo's hypothesis, the novel halogenated derivatives in this study would need to be synthesized and analyzed through in vitro and in vivo studies. The findings from this study

suggests that JWH-018 F would be the halogenated derivative that would produce less severe side effects

CHAPTER 4  
THE COMPUTATIONAL STUDY OF KNOWN AND NOVEL HOMOLOGS OF  
SYNTHETIC CANNABINOIDS IN THE CP FAMILY

#### 4.1 Introduction

The CP-XX,XXX family of synthetic cannabinoids were developed by the company Pfizer. Even though these compounds were developed in the 1970s and 1980s, only recently have these compounds been seen in “spice” drugs on the street, as the synthetic cannabinoid market has grown.<sup>48</sup> Some CP-XX, XXX compounds, like CP-55,940, have been found to be more potent than traditional marijuana and  $\Delta^9$ -THC. This is common with numerous synthetic cannabinoids, even outside the CP-XX,XXX family.<sup>49</sup> There are only a few CP-XX,XXX synthetic cannabinoids, three of the most prominent ones being CP-55,940, CP-47,497 and CP-55,244. These three compounds have structural similarities. Each of these synthetic cannabinoids contains a cyclohexanol group linked to a phenol group and a branched alkyl chain off the phenol group as seen in CP-47,497. (Figure 28) CP-47,497 has known analogs where the length of the phenol linked branched alkyl chain has been altered. The known analogs of CP-47,497 include (C6), (C8), and (C9) CP-47,497. The number following the carbon (C) indicates the length of the phenol linked alkyl chain. These homologs of CP-47,497 first appeared on the market in Germany in 2009. The (C8) homolog, or 1,1-dimethyloctyl analog, was found to be more potent than the parent compound, CP-47,497. Over the next two years following their discovery, CP-47,497 and its analogs were made illegal in several countries including the U.S.<sup>50</sup>



**CP-47,497**

**Figure 42.** Chemical Structure of CP-47,497.

The objectives of this study were to 1) analyze the compounds from the CP family of synthetic cannabinoids and examine how they interact with the CB1 receptor through the use of molecular docking and 2) examine the influence of the length of the phenol linked alkyl chain on the binding to the CB1 receptor.

## 4.2 Materials and Methods

Schrödinger's molecular modeling software, Maestro, was utilized to analyze a set of CP-XX,XXX synthetic cannabinoids through molecular docking. Molecular docking is a type of virtual screening that is able to place ligands of interest into the binding pocket of the designated receptor in order to evaluate the binding affinity and ligand-receptor interactions.<sup>51</sup> The prepared 3-D active state model contains  $\Delta^9$ -THC in the binding pocket of the receptor. The three-dimensional (3D) homology model used in this study was designed and validated by the Doerksen lab at The University of Mississippi, Department of BioMolecular Sciences, Division of Medicinal Chemistry. Since the development of this model, a crystal structure has been published. The crystal structure was published by Hua et al. in 2017.<sup>41</sup> The Doerksen lab has

analyzed the crystal structure and compared it to the homology model and found only slight differences in the two structures. The main difference to note is the LYS192 residue. In the crystal structure the side chain of the LYS192 residue is outside the binding pocket, while in the Doerksen model the side chain is pointing towards the binding pocket. It was decided that the study would continue with use of the 3D homology model of the active-state CB1 receptor developed by the Doerksen lab since both structures are comparable. The prepared 3-D active state model contains  $\Delta^9$ -THC in the binding pocket of the receptor. (Figure 43)

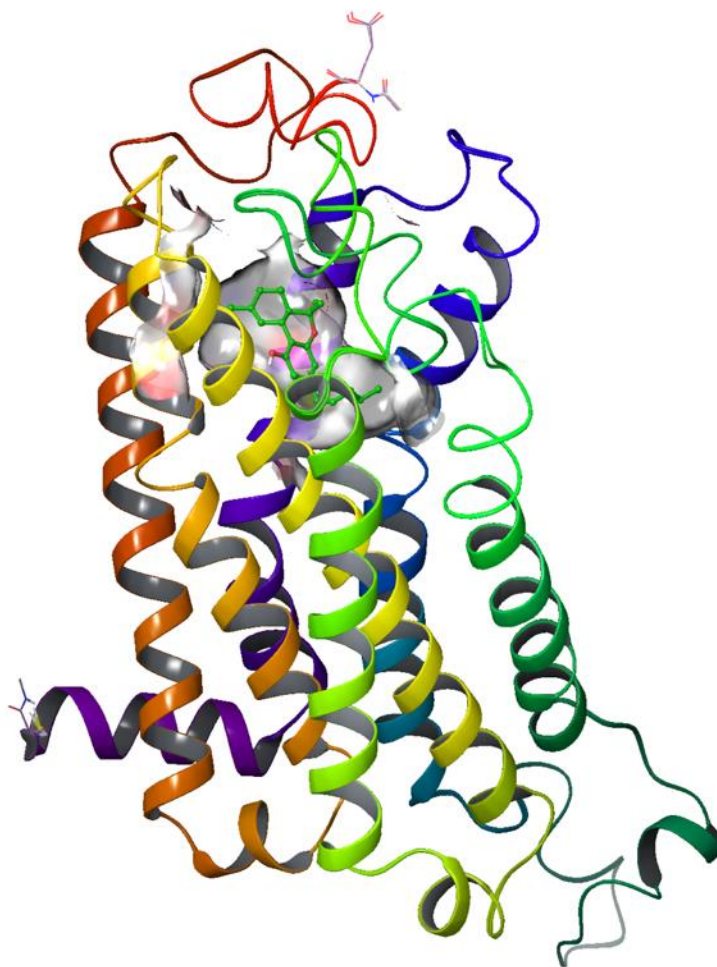


**Figure 43.** Validated 3D homology model of the active-state CB1 receptor, developed by the Doerksen Lab, with a bound  $\Delta^9$ -THC ligand. (P Pandey, K K Roy, R J Doerksen, unpublished).



### 4.2.1 Ligand Selection and Design

The focus of this study was the CP-XX,XXX family of synthetic cannabinoids. Three cannabinoids were examined; CP-44,497, CP-55,244 and CP-55,940. These cannabinoids share a common structural characteristic of a phenol linked, branched heptane chain, the phenol is connected to a cyclohexanol group, but the structures vary on the substituent that is connected to the cyclohexanol (Figure 44).

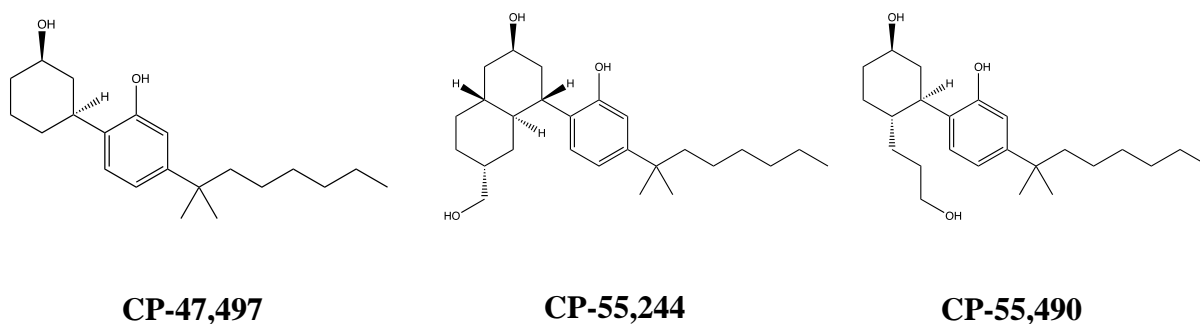
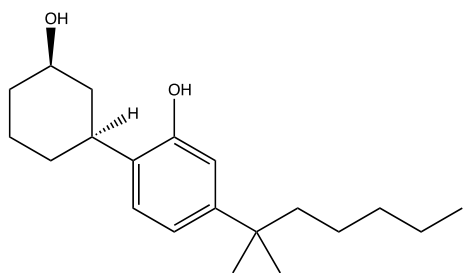
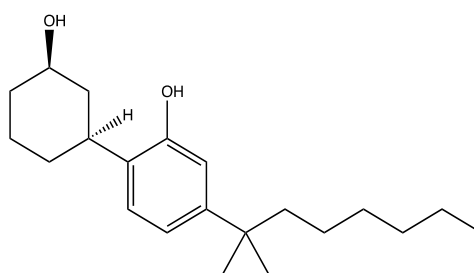


**Figure 44.** Chemical structures of CP-47,497, CP-55,244 and CP-55,940.

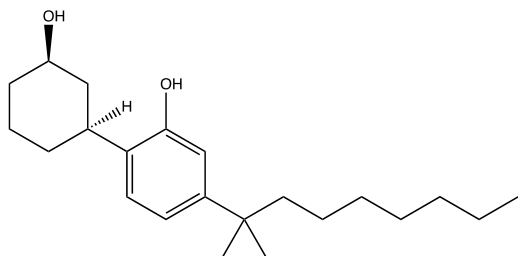
The synthetic cannabinoid CP-44,497 has three known homologs including (C6), (C8), and (C9)- CP-47,497. The number following the carbon (C) indicates the length of the phenol linked alkyl chain. For this study the same homologs were analyzed for CP-55,940 and CP-55,244. (Figure 45-47).



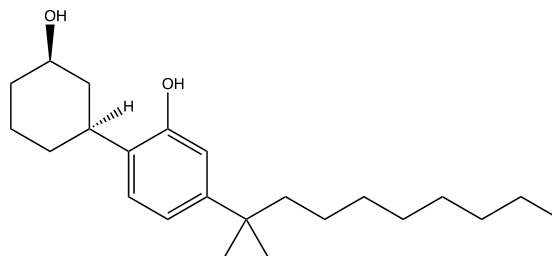
**(C6)-CP-47,497**



**(C7)-CP-47,497\***

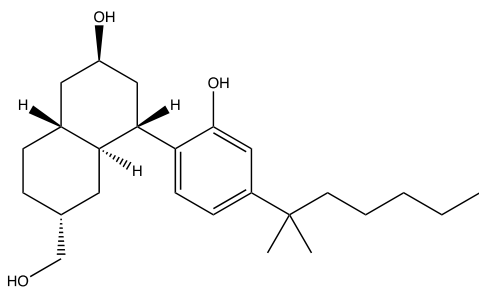


**(C8)-CP-47,497**

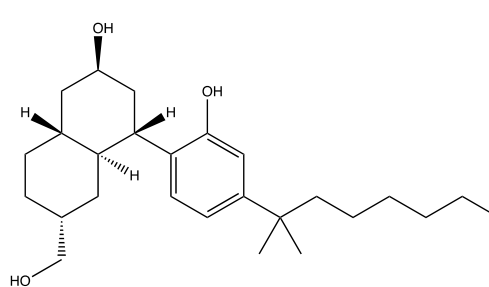


**(C9)-CP-47,497**

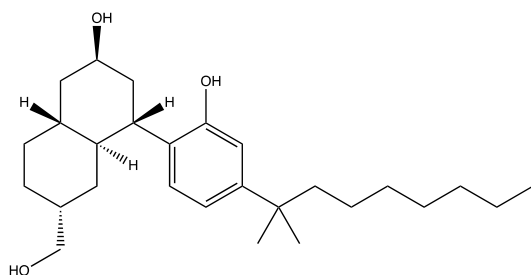
**Figure 45.** Structures of the CP-47,497 homologs. (C7)-CP-47,497\* is the parent structure.



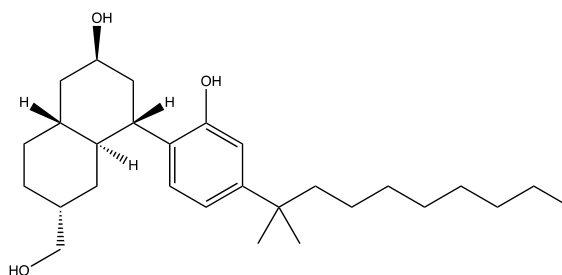
**(C6)-CP-55,244**



**(C7)-CP-55,244\***



**(C8)-CP-55,244**



**(C9)-CP-55,244**

**Figure 46.** Structures of the CP-55,244 homologs. (C7)-CP-55,244\* is the parent structure.

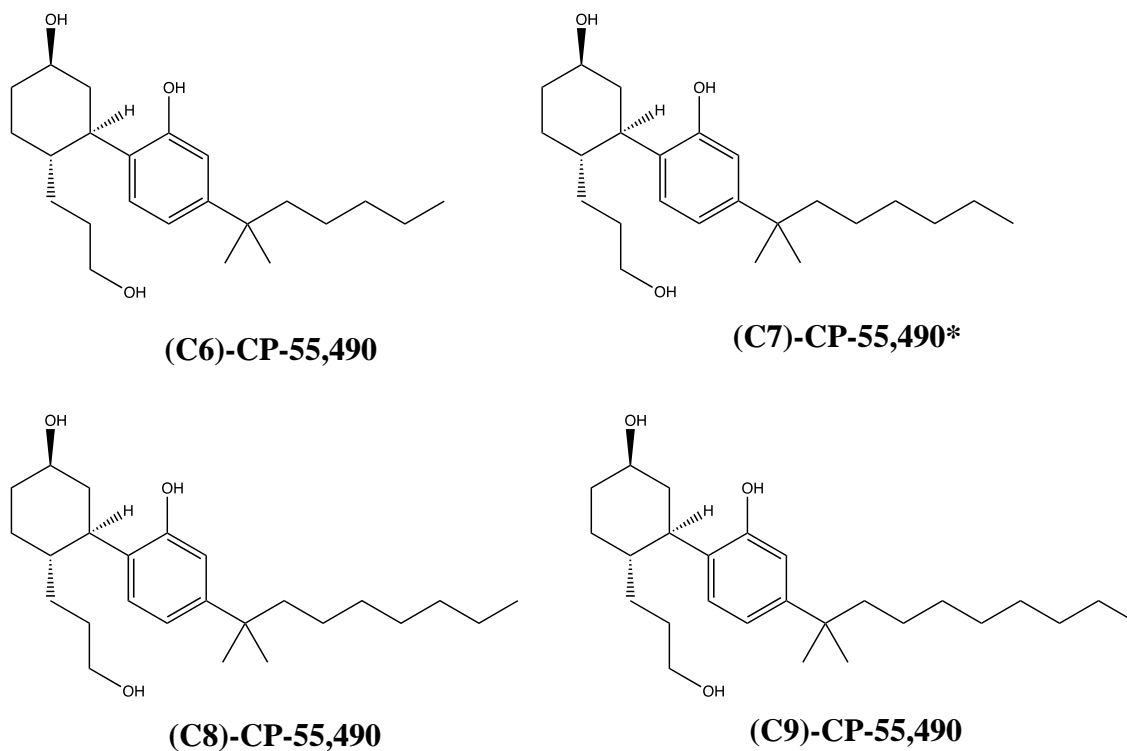


**Figure 47.** Structures of the CP-55,490 homologs. (C7)-CP-55,490\* is the parent structure.

#### 4.2.2 Ligand Preparation

The *LigPrep* protocol is used to successfully convert ligands into three-dimensional structures. The preparation of the ligands involves generating possible states at a target pH of 7.0  $\pm$  2.0 using Epik. Epik is used to predict pKa values and determine all chemically sensible structures.<sup>18,42</sup>

#### 4.2.3 Receptor Grid Generation

The *Receptor Grid Generation* application is used to accurately place a grid around the desired binding pocket of the receptor. This was achieved by selecting the  $\Delta^9$ -THC ligand already in the binding pocket. The grid was generated without constraints, rotatable groups and excluded volumes applied to the receptor. The grid created was used to accurately dock the ligands into the binding pocket of interest in the CB1 receptor model.

#### 4.2.4 Ligand Docking

After the grid was generated and the desired ligands were prepared, the next step was *Glide Ligand Docking*. This step allowed for the prepared ligands to be docked into the receptor binding pocket selected during grid generation. Docking was completed using the standard precision (SP) method and force field OPLS3. Flexible ligand sampling was selected and Epik state penalties were added to the docking score. No constraints were selected to use in docking. The Glide program is able to produce potential ligand conformations. The program uses a set of ranked filters to find possible locations on the ligand in the binding pocket of the receptor. The filters include; 1) side-point search, 2a) diameter test, 2b) subset test, 2c) greedy score, 2d) refinement, 3) grid minimization, and 4) final scoring.<sup>43</sup> The *Glide Ligand Docking* process is described by Friesner et al. (2004).<sup>43</sup> For each ligand, up to five possible poses were generated and post-docking minimization was performed. The pose refers to the position and orientation of the ligand in relation to the receptor.<sup>43</sup> To determine the most accurate pose for each ligand, the docking scores and Glide Emodel scores were analyzed. Docking scores are an estimation of the binding free energy and are used to rank poses of different ligands.<sup>43,44</sup> The Glide Emodel was used to compare poses and determine the best, or most likely, pose for each ligand. Docking scores and Glide Emodel scores are negative. A more negative score means better docking. The docking of each ligand, when using the same procedure, produces the same values. The algorithm used by Glide does not require docking multiple times and will produce the same values each time as long as the same procedure is used. The use of three decimal places is because differences in some of the values between ligands might not have been seen until the second or third decimal place. The software allows for more decimal places to be used, but it was decided to use three decimal places due to some of the small changes observed in the data.

#### 4.2.5 Binding Energy Estimations: Prime MM-GBSA

The relative binding free energy of each ligand was then estimated using the *Prime MM-GBSA* application. These calculations are done following the equation:  $\Delta G_{\text{bind}} = E_{\text{complex}} (\text{minimized}) - (E_{\text{ligand}} (\text{minimized}) + E_{\text{receptor}} (\text{minimized}))$ .<sup>22</sup> The solvation model used was VSGB and calculations were done using OPLS3. Protein flexibility was applied at a distance of 5 Å from the ligand. The Prime MM-GBSA data values are not the expected to be the same as the experimental binding affinities. They are generated to give a ranking of the ligands that correlates with the experimental data of binding affinities ( $K_i$  values). A more negative binding free energy value correlates to a stronger binding of the ligand to the receptor.<sup>47</sup>

#### 4.2.6 Spectral Simulation

Following the analysis of the known and novel synthetic cannabinoids, spectral data were calculated for each of the new structures using spectral simulation software. The program ChemDoodle was able to produce <sup>1</sup>H NMR, <sup>13</sup>C NMR, and mass parent peak spectra of the novel compounds. The known synthetic cannabinoids were also by this method and compared to data from the NIST library to confirm accuracy.

### 4.3 Results and Discussion

The homologs of CP-47, 497 we first noted in the drug market in 2009 in Germany. In this study we analyzed the known homologs of CP-47,497 and the novel homologs of similar CP synthetic cannabinoids, CP-55,244 and CP-55,490. Through molecular docking the ligands were virtually docked to the 3D validated homology model CB1 receptor developed by the Doerksen lab. Once the ligands were docked their docking scores were analyzed. The docking scores are estimation of the binding free energy and was used to rank poses of different ligands. The lower,

or more negative, the docking scores correlate to stronger binding of the ligand to the CB1 receptor. Once docked, each ligand produced up to five possible poses. To determine the best pose of each ligand, the Glide Emodel value was used. The lowest, or most negative, value indicates the best pose for that ligand. Binding energy calculations were then done to determine the relative binding energy of the best pose of each ligand.

**Table 4.** Summary of results showing experimental binding affinities, docking scores, glide Emodel values and binding energy estimations.

| <b>Ligand</b>          | <b>Ki<br/>(nM)<sup>(50,52)**</sup></b> | <b>Docking Score<br/>(kcal/mol)</b> | <b>Glide Emodel</b> | <b>Binding energy<br/>(kcal/mol)</b> |
|------------------------|--|-------------------------------------|---------------------|--------------------------------------|
| <b>(C6)-CP-47,497</b>  | -                                      | -7.990                              | -53.358             | -71.220                              |
| <b>(C7)-CP-47,497*</b> | 2.20 ± 0.5                             | -8.053                              | -54.956             | -60.730                              |
| <b>(C8)-CP-47,497</b>  | -                                      | -8.151                              | -38.859             | -59.640                              |
| <b>(C9)-CP-47,497</b>  | -                                      | -6.657                              | -36.772             | -56.534                              |
| <b>(C6)-CP-55,244</b>  | -                                      | -7.521                              | -43.390             | -82.542                              |
| <b>(C7)-CP-55,244*</b> | 0.21 ± 0.04                            | -7.265                              | -50.029             | -77.262                              |
| <b>(C8)-CP-55,244</b>  | -                                      | -8.058                              | -27.336             | -80.369                              |
| <b>(C9)-CP-55,244</b>  | -                                      | -7.688                              | -4.907              | -69.6855                             |
| <b>(C6)-CP-55,490</b>  | -                                      | -8.256                              | -53.254             | -72.067                              |
| <b>(C7)-CP-55,490*</b> | 1.14 ± 0.04                            | -9.011                              | -66.084             | -72.133                              |
| <b>(C8)-CP-55,490</b>  | -                                      | -9.305                              | -56.443             | -71.981                              |
| <b>(C9)-CP-55,490</b>  | -                                      | -8.361                              | -53.223             | -72.957                              |

\*parent structure

\*\*Ki determined from inhibition of adenylyl cyclase activity<sup>50</sup>

Ki determined from inhibition of radio ligand binding<sup>52</sup>

The  $K_i$ , inhibitory binding constant, values for CP-47,497 and CP-55,490 used for comparison in this were determined through competitive binding assays. 100 fmol/mL [3H]-CP-55,490 was used by Melvin et al. as the radioligand to measure displacement. 100 nM of desacetyllevonantradol was also added to the assay to determine non-specific binding. After incubation and centrifugation, the free radioligand concentration was determined in the supernatant of the sample and the bound ligand was calculated from the pellet. The authors used linear regressions to determine the  $IC_{50}$  value, or the concentration of the ligand is required to inhibit half of the receptor's biological response. The  $K_i$  values was calculated using the Cheng and Prusoff equation;  $K_i = IC_{50}/(1+[C^*]/K_D^*)$ .<sup>50</sup> The  $K_i$  value used for CP-55,244 was determined by Griffin et al.<sup>52</sup> The authors used the radioligand [3H]-SR141716A for the competitive binding assays. The  $IC_{50}$  values were calculated by Griffin et al. through non-linear regressions of the log concentration-percentage.  $K_i$  values were then determined using the Cheng and Prusoff equation.<sup>52</sup> (C8)-CP-55.490 was found to have the best, or most negative, docking score of all the ligands in this study. It was also discovered that in each group of homologs for each ligand that the (C8) homolog always had the best, or most negative docking score. Previous studies determined that the (C8) homolog of CP-47,497 was several times more potent than the parent ligand.<sup>38</sup> Based on the docking score it can be hypothesized that the same is true for the other (C8) homologs. For the CP-47,497 group, the rank of docking scores was found to be (C8) > (C7)\* > (C6) > (C9). The rank of docking scores for CP-55,244 was determined to be (C8) > (C9) > (C6) > (C7)\* and for CP-55,490 the rank was (C8) > (C7)\* > (C9) > (C6).

Binding free energy (kcal/mol) calculations were also done of the best pose for each ligand. These values are not expected to be the same as the experimental binding affinities but are expected to give a ranking of the ligands that aligns with the experimental data of binding

affinities ( $K_i$ ). A more negative binding free energy values correlates to a stronger binding. The binding energy estimations calculated in this study correlated to the experiment  $K_i$  values of the parent synthetic cannabinoids; the smaller  $K_i$  values correlated to more negative binding energies. CP-47,497 ( $K_i = 2.1$  nM) had a binding energy of -60.730 kcal/mol, CP-55,244 ( $K_i = 0.21$  nM) had a binding energy of -77.262 kcal/mol and CP-55,490 ( $K_i = 0.58$  nM) had a binding energy of -72.133 kcal/mol. The rank of binding energy estimations for the parent synthetic cannabinoids was determined to be CP-47,497 > CP-55,244 > CP-55,490, which is consistent with the ranking order of  $K_i$  values. Based on this data it can be assumed that the  $K_i$  values of each of the homologs will be ranked in this way; for CP-47,497: (C9) > (C8) > (C7) > (C6), for CP-55,244: (C9) > (C7)\* > (C8) > (C6) and for CP-55,490: (C8) > (C6) > (C7) > (C9). Further studies will need to be done to confirm this hypothesis.

Using the *Ligand Interaction Diagram* application in Maestro, the residues interacting within a distance of 5 Å from the ligand were examined (Table 5). The types of interacting residues present within the binding pocket were labeled as hydrophobic, polar, negatively charged or positively charged residues.



**Table 5.** Number and identification of residues interacting with each homolog

| <b>Ligand</b>          | <b>Docking score (kcal/mol)</b> | <b>Binding energy (kcal/mol)</b> | <b>Hydrophobic</b> | <b>Polar</b> | <b>Negatively Charged</b> | <b>Positively Charged</b> |
|------------------------|---------------------------------|----------------------------------|--------------------|--------------|---------------------------|---------------------------|
| <b>(C6)-CP-47,497</b>  | -7.990                          | -71.220                          | 21                 | 5            | 1                         | -                         |
| <b>(C7)-CP-47,497*</b> | -8.053                          | -60.730                          | 21                 | 4            | 1                         | -                         |
| <b>(C8)-CP-47,497</b>  | -8.151                          | -59.640                          | 22                 | 6            | 1                         | 2                         |
| <b>(C9)-CP-47,497</b>  | -6.657                          | -56.534                          | 23                 | 6            | 1                         | 2                         |
| <b>(C6)-CP-55,244</b>  | -7.521                          | -82.542                          | 22                 | 7            | 1                         | 1                         |
| <b>(C7)-CP-55,244*</b> | -7.265                          | -77.262                          | 24                 | 7            | 1                         | 1                         |
| <b>(C8)-CP-55,244</b>  | -8.058                          | -80.369                          | 23                 | 7            | 1                         | 1                         |
| <b>(C9)-CP-55,244</b>  | -7.688                          | -69.6855                         | 21                 | 8            | 3                         | 3                         |
| <b>(C6)-CP-55,490</b>  | -8.256                          | -72.067                          | 21                 | 5            | 1                         | 1                         |
| <b>(C7)-CP-55,490*</b> | -9.011                          | -72.133                          | 21                 | 5            | 1                         | 1                         |
| <b>(C8)-CP-55,490</b>  | -9.305                          | -71.981                          | 21                 | 6            | 1                         | 1                         |
| <b>(C9)-CP-55,490</b>  | -8.361                          | -72.957                          | 21                 | 6            | 1                         | 1                         |

All ligands had between 21 and 24 hydrophobic residues. A trend was seen in the polar residues. The number of polar residues interacting in the binding pocket were at its highest when the alkyl chains were increased to 8 and 9 carbons. There also was a correlation seen between  $K_i$  values and polar residues. There were fewer polar residues (4) observed for CP-47,497 which had the highest, weakest binding,  $K_i$  value (2.1 nM) compared to the 5 polar residues and a  $K_i$  value of 0.58 nM for CP-55,490. CP-55,244 had the highest number of polar residues (7) and the lowest, strongest binding,  $K_i$  value (0.21 nM). All ligands had the positively charged residue LYS192 present, within a distance of 5 Å, in the binding pocket. However, (C8) and (C9)-CP-

47,497 interacted with an additional residue, LYS376. (C9)-CP-55,244 had three positively charged residues present within 5 Å; LYS192, LYS276 and ARG182. All the ligands that contained a negatively charged residue shared the same negatively charged residue, ASP272. Again, (C9)-CP-55,244 had three negatively charged residues; ASP272, GLU100 and GLU94. For (C9)-CP-47,487 and (C9)-CP-55,244 there were additional residues present not listed in the previous table. Both of these ligands had the GLY 99 residue present, which was not observed with any other ligands within 5 Å, and (C9)-CP-47,487 possessed solvent exposure at the end of the lengthened alkyl chain.

After examining the residues present within the binding pocket, the direct interactions taking place between the ligands and the CB1 receptor were analyzed. Interactions can include,  $\pi$ - $\pi$  stacking, hydrogen bonding,  $\pi$ -cation and salt bridges. (Table 6)

**Table 6.** Residues interacting with the ligands and the CB1 receptor within the binding pocket within a distance of 5 Å

| <b>Ligand</b>          | <b><math>\pi</math>-<math>\pi</math> Stacking</b> | <b>Hydrogen Bond</b>       |
|------------------------|---|----------------------------|
| <b>(C6)-CP-47,497</b>  | TRP279<br>TRP279                                  | LYS192                     |
| <b>(C7)-CP-47,497*</b> | TRP279<br>TRP279                                  | -                          |
| <b>(C8)-CP-47,497</b>  | TRP279<br>TRP279                                  | PHE278                     |
| <b>(C9)-CP-47,497</b>  | TRP279<br>TRP279                                  | -                          |
| <b>(C6)-CP-55,244</b>  | TRP279<br>TRP279                                  | PHE278<br>VAL196           |
| <b>(C7)-CP-55,244*</b> | TRP279<br>TRP279                                  | PHE278                     |
| <b>(C8)-CP-55,244</b>  | TRP279<br>TRP279                                  | PHE278<br>VAL196           |
| <b>(C9)-CP-55,244</b>  | -   | PHE177<br>LYS376<br>THR377 |
| <b>(C6)-CP-55,490</b>  | TRP279  | TRP279                     |
| <b>(C7)-CP-55,490*</b> | TRP279  | TRP279                     |
| <b>(C8)-CP-55,490</b>  | TRP279  | TRP279<br>LYS192           |
| <b>(C9)-CP-55,490</b>  | TRP279  | TRP279                     |

The only types of interactions observed in this study was  $\pi$ - $\pi$  stacking and hydrogen bonding. All ligands, with the exception of (C9)-CP-55,244 displayed  $\pi$ - $\pi$  stacking with the TRP279 residue and the phenol group of the ligand. Even though (C9)-CP-55,244 did not have any  $\pi$ - $\pi$  stacking, it had the most hydrogen bonding. (C9)-CP-55,244 had the following three hydrogen bonds: 1) PHE177 and the methanol group, 2) LYS376 and the hydroxyl of the phenol group, and 3) THR377 with the hydroxyl of the cyclohexanol group. The CP-55,490 group only contained one  $\pi$ - $\pi$  stacking interaction with TRP279, while all the other ligands displayed two  $\pi$ - $\pi$  stacking interactions with TRP279. (C7)-CP-47,497\* and (C9)-CP-47,497 were the only ligands that did not have any hydrogen bonding present. The (C6) and (C8) homolog ligands each had 1 hydrogen bond present between the ligand and the receptor. (C6) had a hydrogen bond present between LYS192 and the hydroxyl of the cyclohexanol and (C8) had a hydrogen bond between PHE279 and the hydroxyl of the cyclohexanol. Every ligand in the CP-55,244 group displayed hydrogen bonding. (C6) had two instances of hydrogen bonding; PHE 278 with the hydroxyl of the methanol group and VAL196 with the hydroxyl of the cyclohexane. (C7)-CP-47,497\* had only one hydrogen bond present between the hydroxyl of the methanol and PHE278. Hydrogen bonding for the (C8) homolog was the same as the (C6); PHE278 with the hydroxyl of the methanol group and VAL196 with the hydroxyl of the cyclohexane. (C9)-CP-55,244, as mentioned previously, had three hydrogen bonds. The first hydrogen bond was with PHE177 and the hydroxyl of methanol group, then LYS376 and the hydroxyl of the phenol, and THR377 with the hydroxyl of the cyclohexanol. All of the CP-55,940 ligands in this study had the same hydrogen bond with TRP279 and the hydroxyl of the propanol group. The (C8) homolog had an addition hydrogen bonding instance with LYS192 and the hydroxyl of the phenol group. This additional hydrogen bond for the (C8) homolog could be the catalyst for the

better, more negative, docking score of this ligand compared to the other ligands in the CP-55,490 group.

Following the analysis of the interacting residues, 3D interaction diagrams of the ligands were examined to better understand how the position of the ligand in the binding pocket influenced the docking and binding energy estimations.

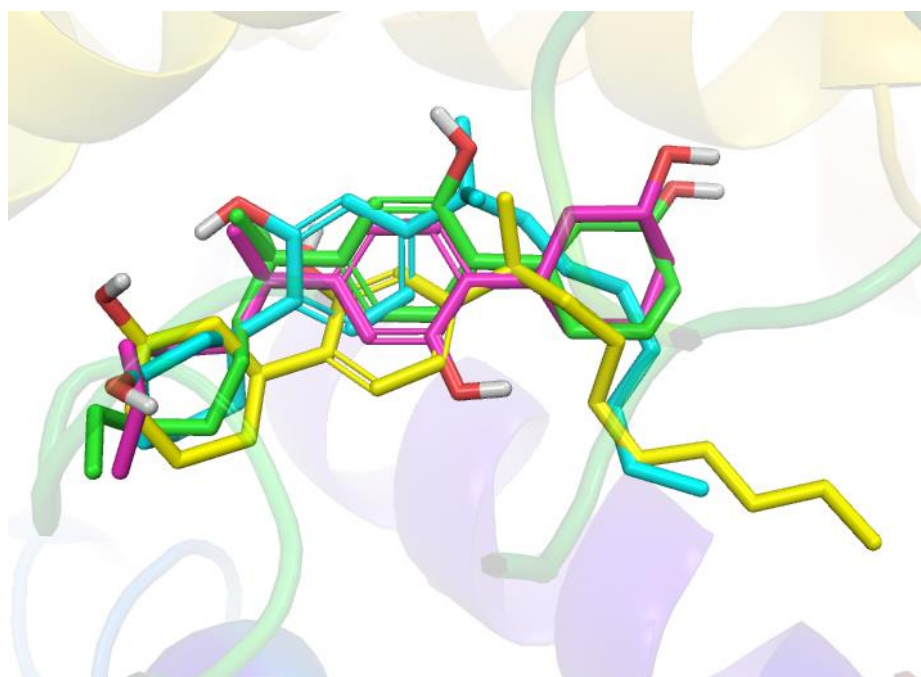


**Figure 48.** 3D interaction diagram of CP-47,497 (green) and its homologs (C6)-CP-47,497 (pink), (C8)-CP-47,497 (cyan), and (C9)-CP-47,497 (yellow).

The CP-47,497 set of ligands were all observed to varying positions in the binding pocket of the CB1 receptor. The previous study by Melvin et al. was determined that the (C8) homolog of CP-47,497 was more potent than its parent compound.<sup>50</sup> The results of this study were found to support the findings by Melvin et al. The 3D interaction diagrams of these two ligands were further examined (Figure 49).

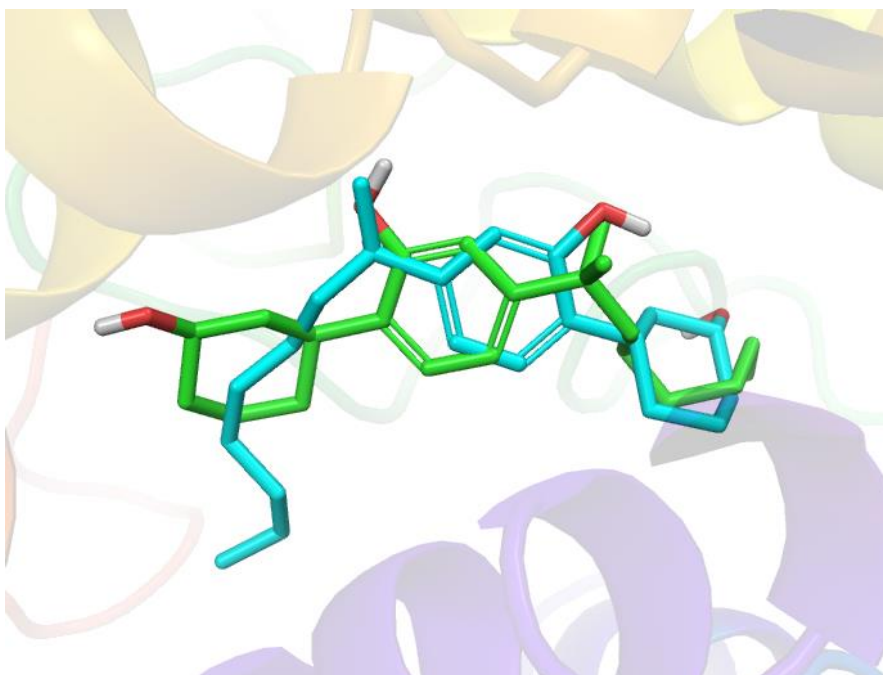


**Figure 49.** 3D interaction diagram of CP-47,497 (green) and (C8)-CP-47,497 (cyan).

The CP-47,497 ligand and its (C8) homolog were observed to be in very different positions in the binding pocket of the CB1 receptor. The alkyl chains of each ligand were in opposite directions of the binding pocket.

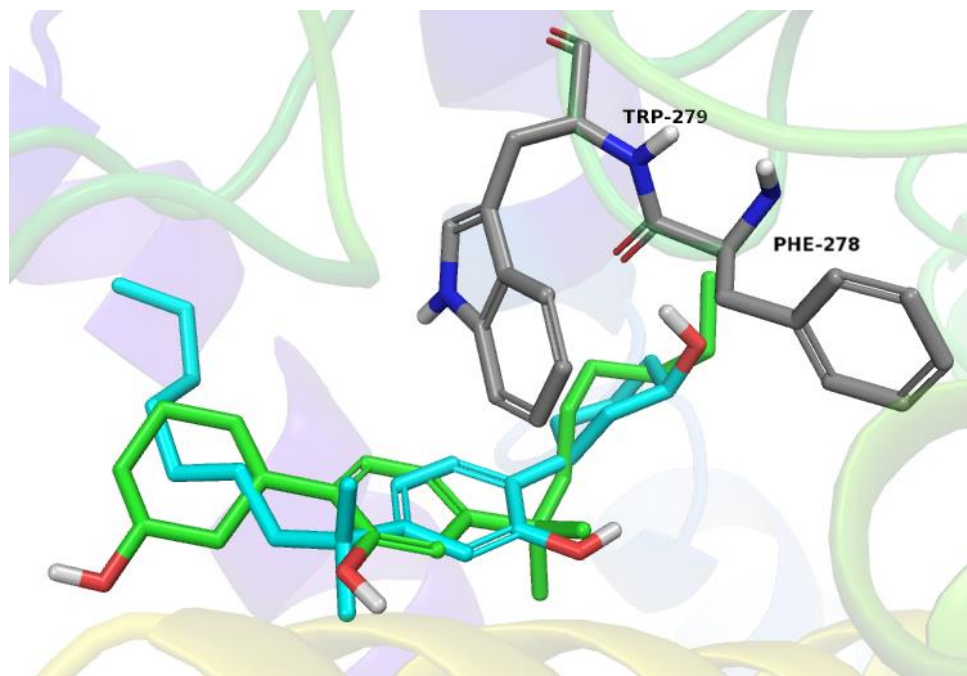


**Figure 50.** 3D interaction diagram of CP-47,497 (green) and (C8)-CP-47,497 (cyan) and the residues TRP279 and PHE278. PHE278 only interacted with (C8)-CP-47,497 (cyan) through a hydrogen bond.

CP-47,497 and the (C8) homolog both interacted through  $\pi$ - $\pi$  stacking with the residue TRP279. However, the (C8) homology was found to have an additional interaction with PHE278 through hydrogen bonding. This hydrogen bonding was able to take place due to the position of the (C8) homolog, which allows for the first hydroxyl group to be in close proximity to the PHE278 residue in order to form that bond (Figure 51).

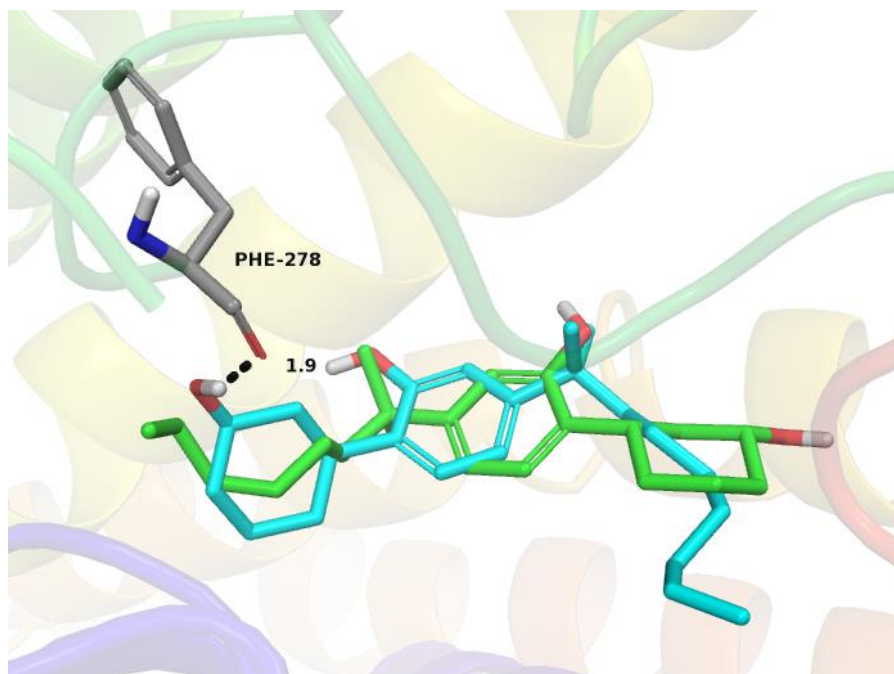


**Figure 51.** 3D interaction diagram of CP-47,497 (green) and (C8)-CP-47,497 (cyan) and the residue PHE278. PHE278 only interacted with (C8)-CP-47,497 (cyan) through a hydrogen bond within a distance of 1.9 Å.

The variations in hydrophobic residues interacting with each homolog were then examined to better understand the influence of increasing the alkyl chain and position of the ligand in the binding pocket (Figure 52).



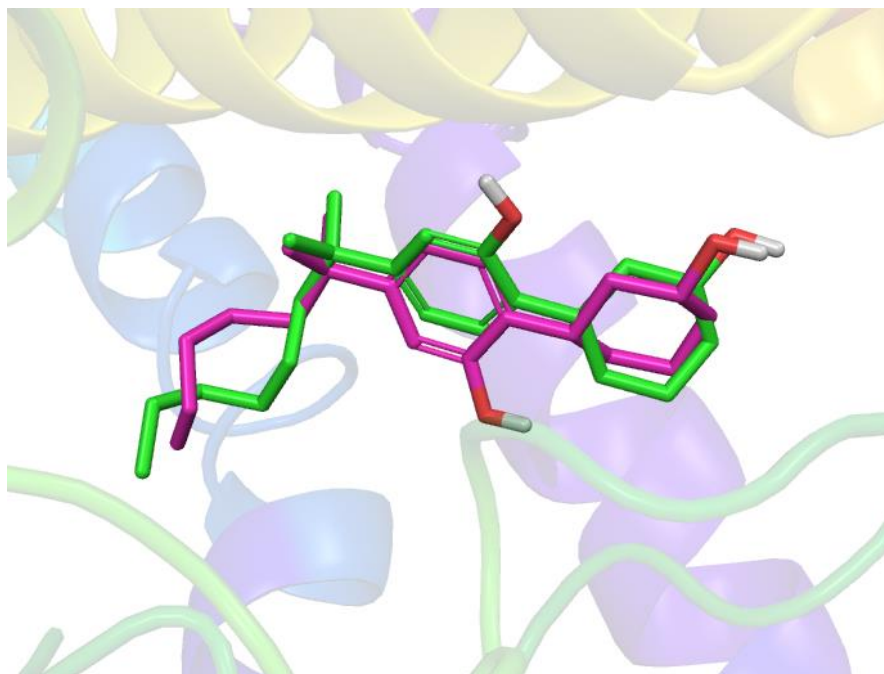


**Figure 52.** 3D interaction diagram of CP-47,497 (green) and (C6)-CP-47,497 (pink).

CP-47,497 and the (C6) homolog were observed to be in similar positions in the binding pocket. Differences were found in the position of the alkyl chain and the phenol group. CP-47,497 and the (C6) homolog were found to interact with the same 21 hydrophobic residues; LEU287, MET277, LEU286, MET363, PHE278, LEU360, PHE200, TRP356, LEU359, TRP279, PHE379, ILE271, ALA383, PHE174, PHE177, LEU193, PHE189, VAL196, CYS386, PHE170, AND VAL291. Both ligands displayed  $\pi$ - $\pi$  stacking with TRP279, but the (C6) homolog also displayed a hydrogen bond when LYS192. The position of the phenol group in the (C6) homolog can explain this additional interaction of hydrogen bonding. The hydrogen bond can also explain the better binding energy estimation calculated for the (C6) homolog compared to the CP-47,497 parent structure.

After the CP-47,497 ligand, with a 7-carbon alkyl chain (C7), was increased to the (C8) homolog, an increase in hydrophobic residue interactions was also observed.

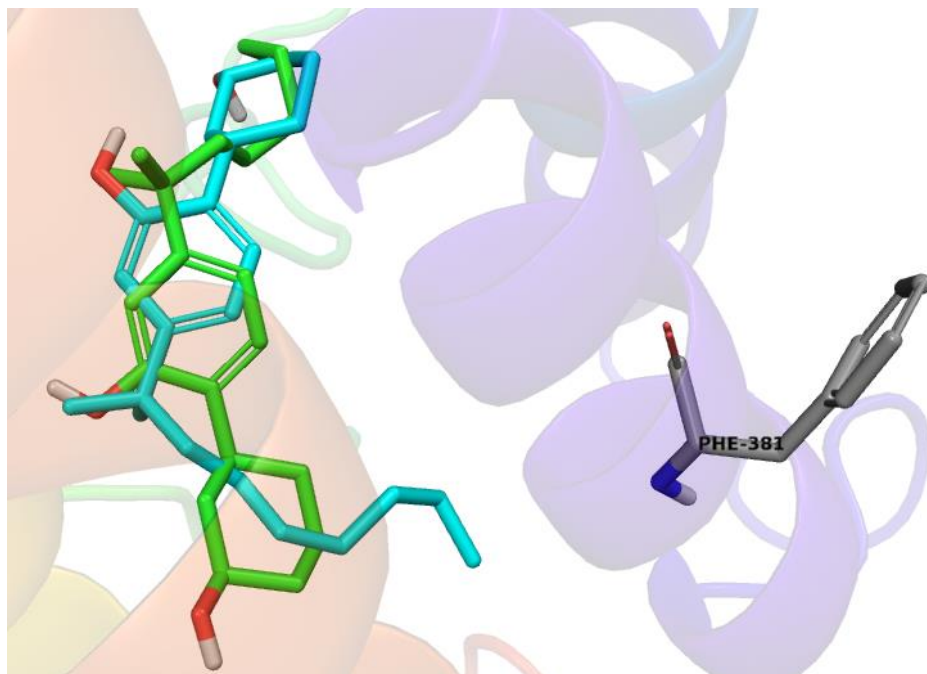


**Figure 53.** 3D interaction diagram of CP-47,497 (green) and (C8)-CP-47,497 (cyan) and the hydrophobic residue PHE381. PHE381 was only observed with the (C8)-CP-47,497 (cyan).

The (C8) homolog of CP-47,497 was found to have 22 hydrophobic interactions, compared to the 21 observed in the (C6) homolog and CP-47,497. The (C8) homolog had the same 21 hydrophobic interactions but contained an additional hydrophobic residue, PHE381. The PHE381 residue was observed near the end of the alkyl chain of the (C8) homolog. The number of hydrophobic residues also increased as the alkyl chain was lengthened to the (C9) homolog, so the variation in hydrophobic residues was further examined (Figure 54).

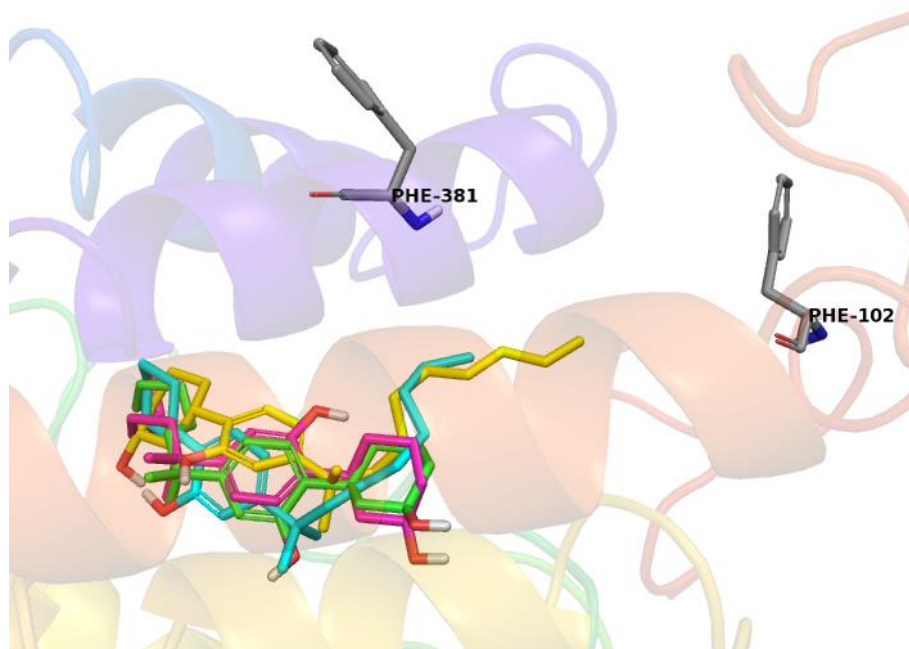


**Figure 54.** 3D interaction diagram of CP-47,497 (green) its homologs (C6)-CP-47,497 (pink), (C8)-CP-47,497 (cyan), and (C9)-CP-47,497 (yellow) shown with the hydrophobic residues PHE381 and PHE102. PHE381 was observed in both the (C8) and (C9) homolog, and PHE102 was only observed for the (C9) homolog.

The (C9) homolog of CP-47,497 was found to have 23 hydrophobic interacting residues. It was determined to have 21 hydrophobic residues in common with CP-47,497 and the (C6) homolog and it had the same addition PHE 381 residue observed in (C8). The 23<sup>rd</sup> residue was determined to be PHE102. The location of this residue was found near the end of lengthened alkyl chain of the (C9) homolog in the binding pocket of the CB1 receptor.

The CP-55,244 ligand and its homologs were then analyzed through 3D interaction diagrams to better understand how the position of the ligand in the binding pocket influenced the docking and binding energy estimations.

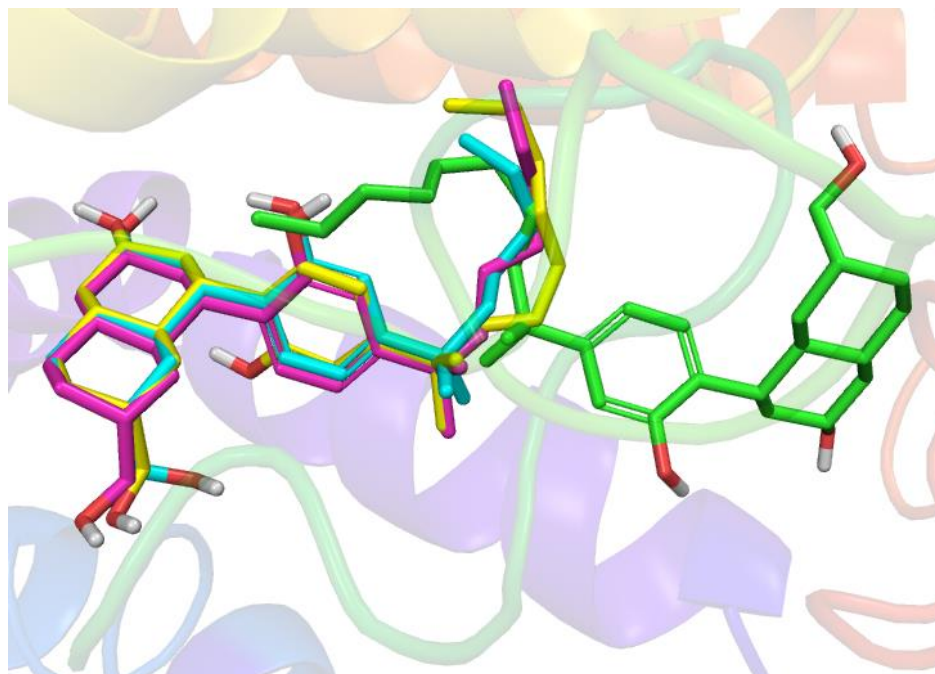


**Figure 55.** 3D interaction diagram of CP-55,244 (pink) and its homologs (C6)-CP-55,244 (cyan), (C8)-CP-55,244 (yellow), and (C9)-CP-55,244 (green).

The position of CP-55,244 and its homologs in the binding pocket of the CB1 receptor were analyzed through 3D interaction diagrams. CP-55,244 and its (C6) and (C8) homologs were all in similar positions with only a few differences observed. The (C9) homolog, however, was observed to be in a different location in the binding pocket. The location of the (C9) homolog compared to the other CP-55,244 ligands explains the differences observed in the interacting residues and its binding energy estimation.

The (C8) homolog of CP-55,244 was determined to have a better docking score and binding energy estimation than CP-55,244. The 3D interaction diagram was used to compare CP-55,244 and its (C8) homolog (Figure 56).

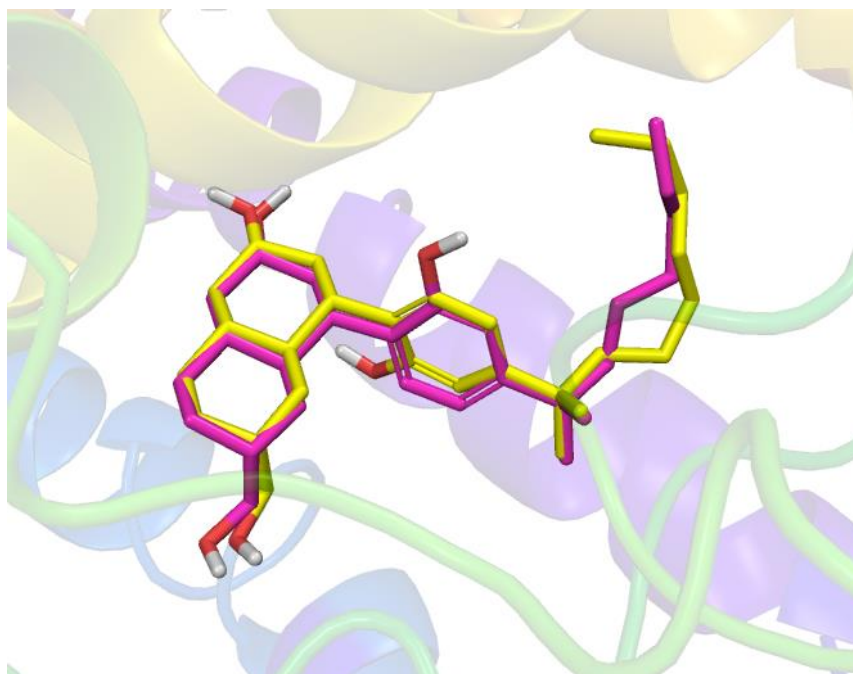


**Figure 56.** 3D interaction diagram of CP-55,244 (pink) and (C8)-CP-55,244 (yellow).

CP-55,244 and the (C8) homolog displayed similar positions in the binding pocket of the CB1 receptor. Some of the differences observed included the position of the hydroxyl groups. The phenol group of the (C8) homolog was opposite of CP-55,244. There were also slight differences in the position of the alkyl chain.

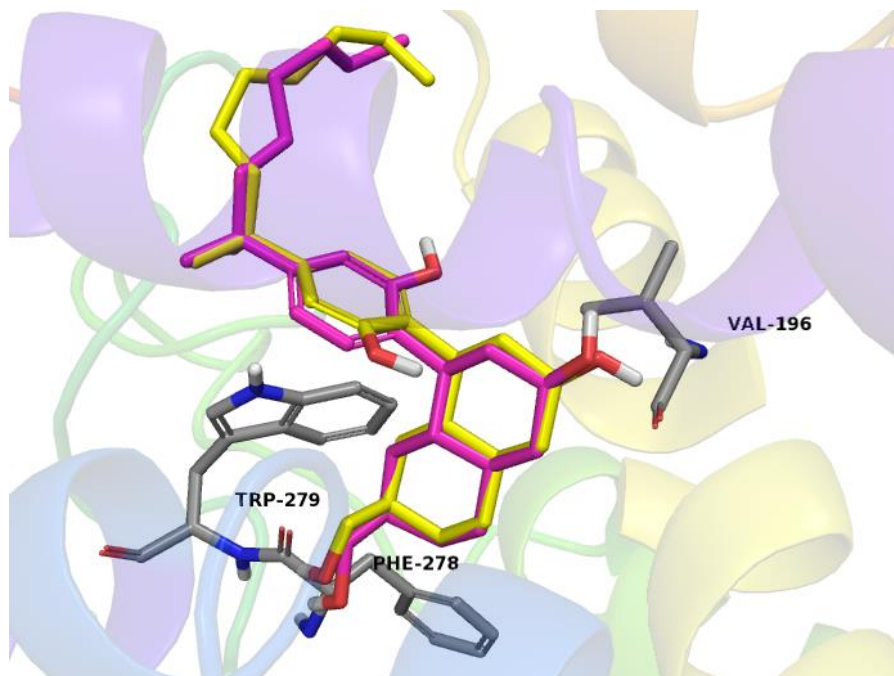


**Figure 57.** 3D interaction diagram of CP-55,244 (pink) and (C8)-CP-55,244 (yellow) and the residues TRP279, PHE278 and VAL196. VAL196 only interacted with (C8)-CP-55,244 (yellow) through a hydrogen bond.

CP-55,244 and the (C8) homolog displayed  $\pi$ - $\pi$  stacking interactions with TRP279 and hydrogen bonding with PHE278. However, the (C8) homolog was the only one to have additional hydrogen bonding occur with VAL196. It is possible that the CP-55,244 ligand did not interact with VAL196 through hydrogen bonding due to the increased distance between the residue and the nearest hydroxyl group of the ligand (Figure 58). The additional hydrogen bonding can explain the better docking score and binding free energy estimation of the (C8) homolog.

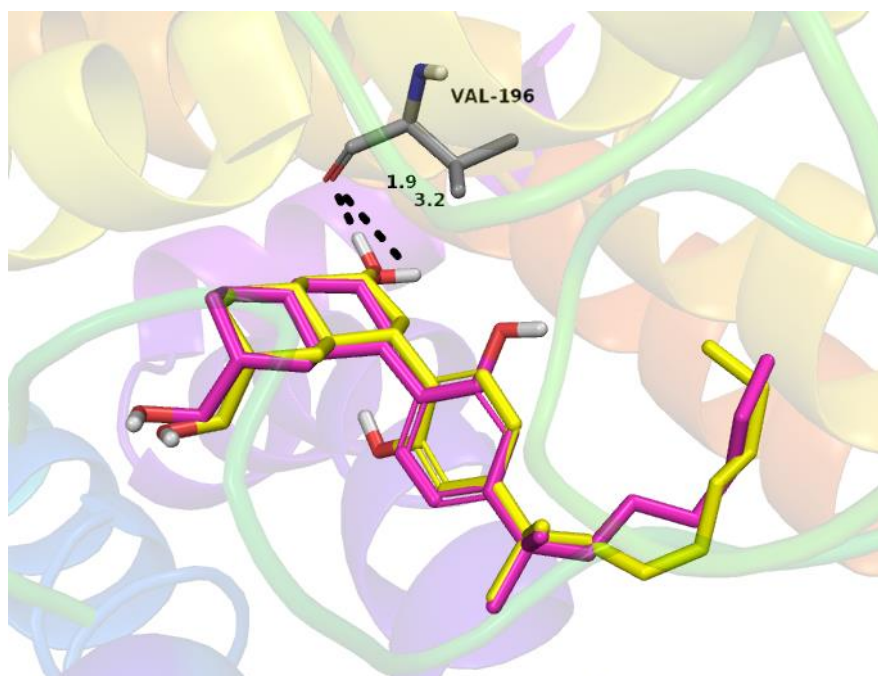


**Figure 58.** 3D interaction diagram of CP-55,244 (pink) and (C8)-CP-55,244 (yellow) and the residue VAL196. VAL196 only interacted with (C8)-CP-55,244 (yellow) through a hydrogen bond within a distance of 1.9 Å.

CP-55,244 and the (C6) homolog shared 22 hydrophobic interacting residues; LEU359, LEU360, MET363, LEU286, TRP356, PHE200, ALA198, CYS386, PHE170, VAL196, TRP279, LEU193, PHE177, PHE174, PHE189, PHE379, ALA380, ILE271, VAL291, MET277, LEU287, AND PHE278. CP-55,244 also had two additional hydrophobic interacting residues, ILE175 and LEU387. The length and the position of the CP-55,244 ligand in the binding pocket can explain the additional hydrophobic residues observed (Figure 59).

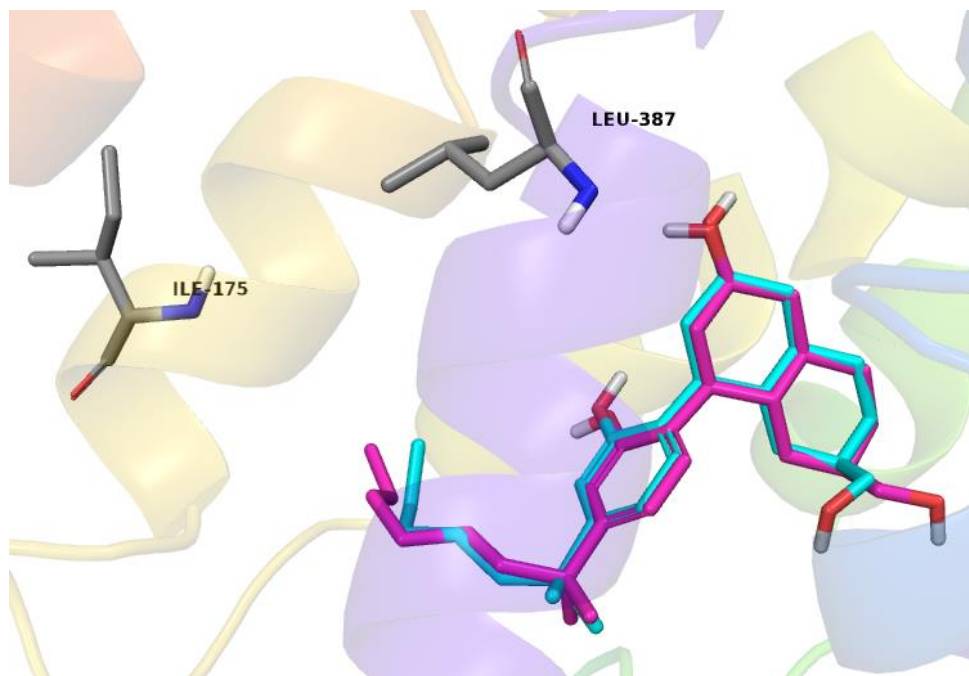


**Figure 59.** 3D interaction diagram of CP-55,244 (pink) and (C6)-CP-55,244 (cyan) and the hydrophobic residues ILE175 and LEU387. ILE175 and LEU387 were only observed with CP-55,244 (pink).

As the alkyl chain was lengthened to 8 carbons, the (C8) homolog, the number of hydrophobic interactions observed was 23. The (C8) homolog had the same 21 hydrophobic residues as CP-55,244 and the (C6) homolog. It also had the ILE175 hydrophobic residue present like CP-55,244, but the LEU387 observed in CP-55,244 was not found to interact with the (C8) homolog. The variations in hydrophobic interacting residues can be contributed to the lengths and positions of the alkyl chains. (Figure 60) The (C9) homolog's position in the binding pocket was very different than the other ligands in the group. The (C9) homolog had 21 hydrophobic interactions and of those 21, only 11 of the residues were the same as the other CP-55,244 ligands.



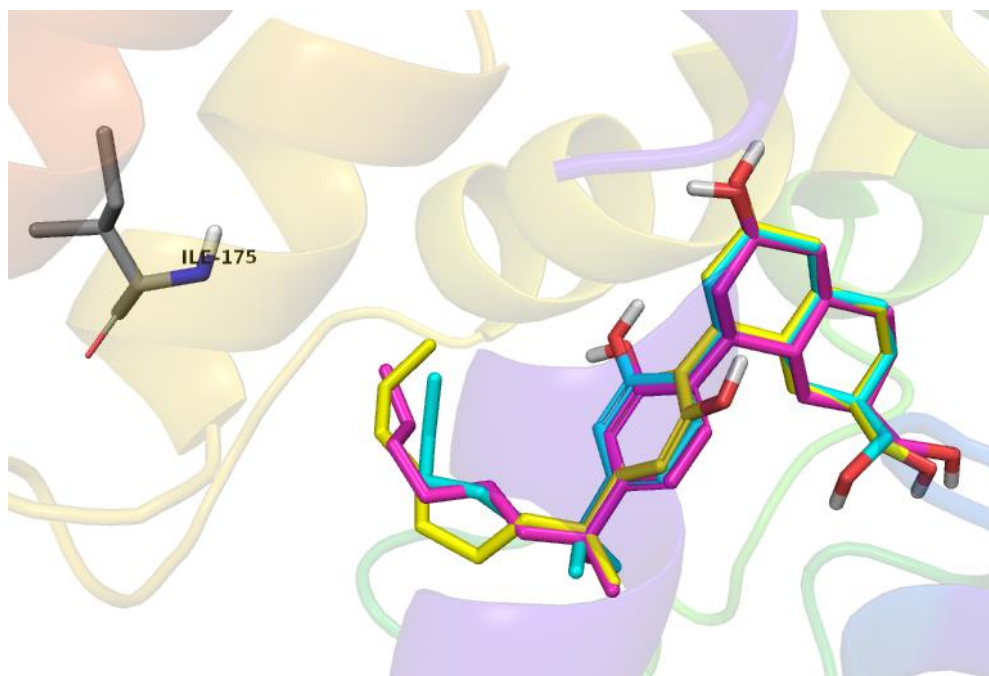


**Figure 60.** 3D interaction diagram of CP-55,244 (pink), (C6)-CP-55,244 (cyan) and (C8)-CP-55,244 (yellow) the hydrophobic residue ILE175. ILE175 was only observed with CP-55,244 (pink) and (C8)-CP-55,244 (yellow).

The CP-55,490 ligand and its homologs were then analyzed through 3D interaction diagrams to better understand how the position of the ligand in the binding pocket influenced the docking and binding energy estimations.

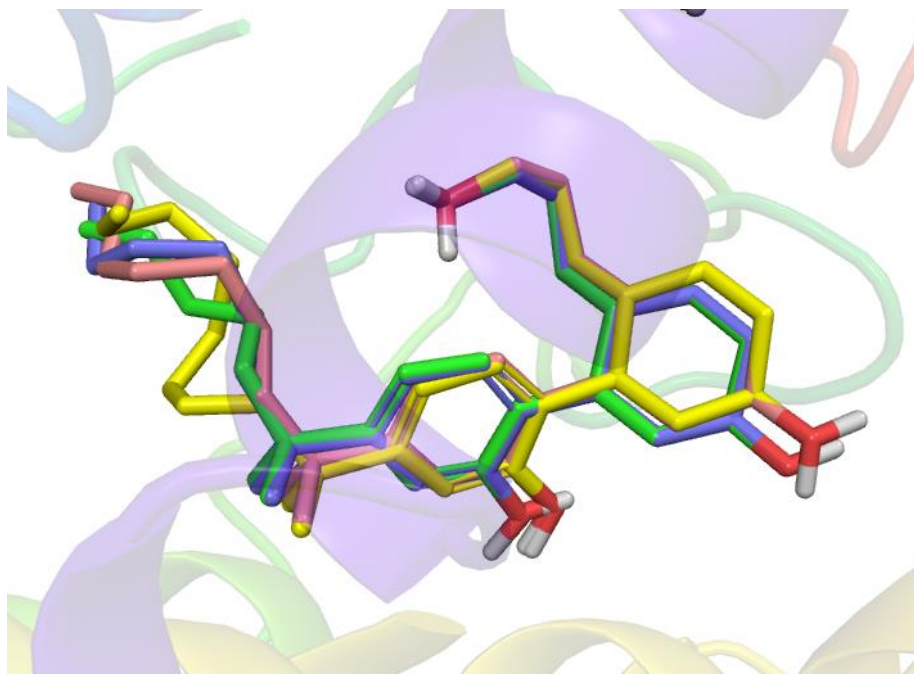


**Figure 61.** 3D interaction diagram with CP-55,490 (purple), (C6)-CP-55,490 (green), (C8)-CP-55,490 (orange), and (C9)-CP-55,490 (yellow).

CP-55,490 and its homologs were all observed to be in similar positions in the binding pocket of the CB1 receptor through the 3D interaction diagram. Some differences observed were in the position of the alkyl chain as it was lengthened and positions of the hydroxyl groups. As seen in the other two groups of ligands, the (C8) homolog was determined to have a better docking score than the CP-55,490 ligand. However, the binding free energy of the (C8) homolog was slightly higher than the CP-55,490 ligand. CP-55,490 and the (C8) homolog were further examined through 3D interaction diagrams (Figure 62).

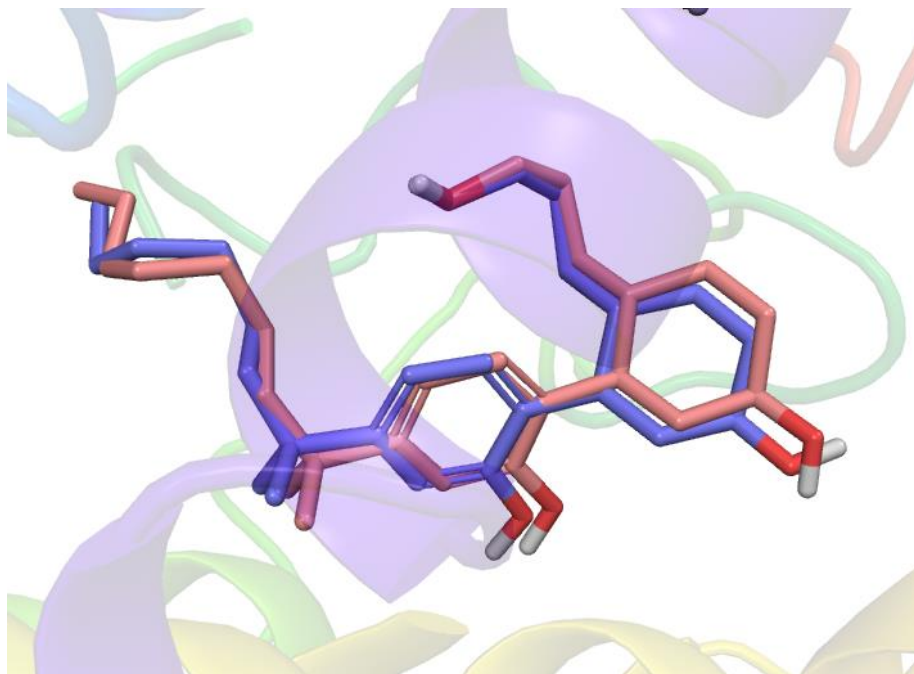


**Figure 62.** 3D interaction diagram with CP-55,490 (purple) and (C8)-CP-55,490 (orange).

The CP-55,490 ligand and its (C8) homolog were observed in similar positions in the binding pocket of the CB1 receptor. Some of the differences observed were in the position of the alkyl chain and the position of the hydroxyl group on the cyclohexanol.

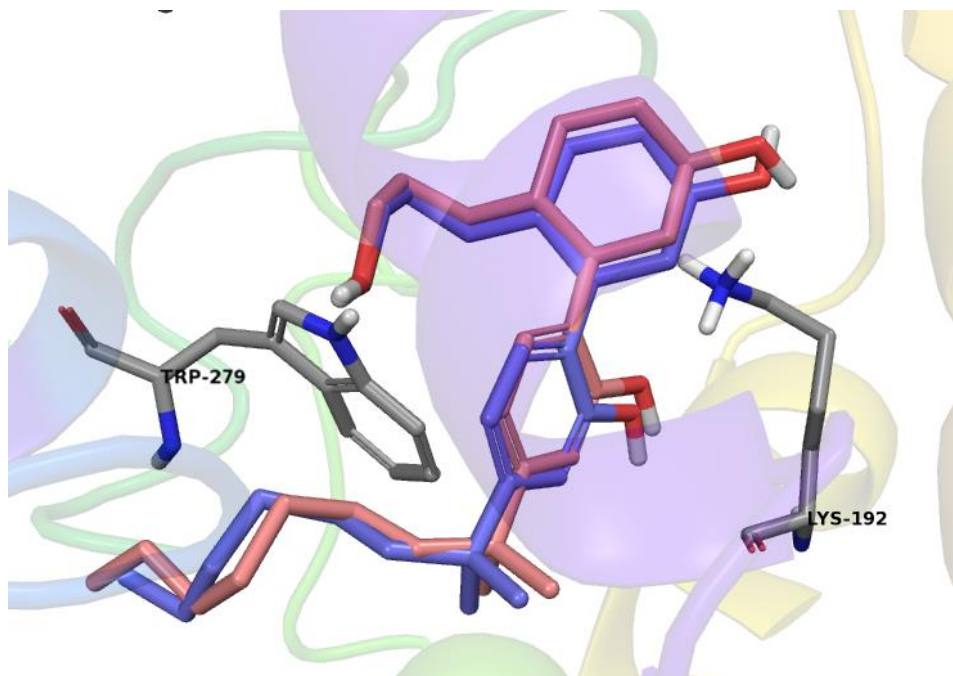


**Figure 63.** 3D interaction diagram with CP-55,490 (purple) and (C8)-CP-55,490 (orange) with the residues TRP279 and LYS192. LYS192 was only observed interacting with (C8)-CP-55,490 (orange) through a hydrogen bond.

CP-55,490 and the (C8) homolog were found to interact through  $\pi$ - $\pi$  stacking with TRP279, and through a hydrogen bond with TRP279. The (C8) homolog was also observed to have an additional hydrogen bond interaction with the residue LYS192. The difference in position of the (C8) homolog compared to CP-55,490 allowed for the addition hydrogen bond to occur with LYS192. The additional hydrogen bond can explain the better docking score of the (C8) homolog, as was also seen in CP-47,497 group and the CP-55,244 group of ligands.

The software ChemDoodle was used to calculate spectral data of the novel analogs designed in this study. ChemDoodle is able to produce calculated  $^1\text{H}$  NMR and  $^{13}\text{C}$  NMR spectra of the analogs, as well as determine the mass parent peak. (Figure 64-66)

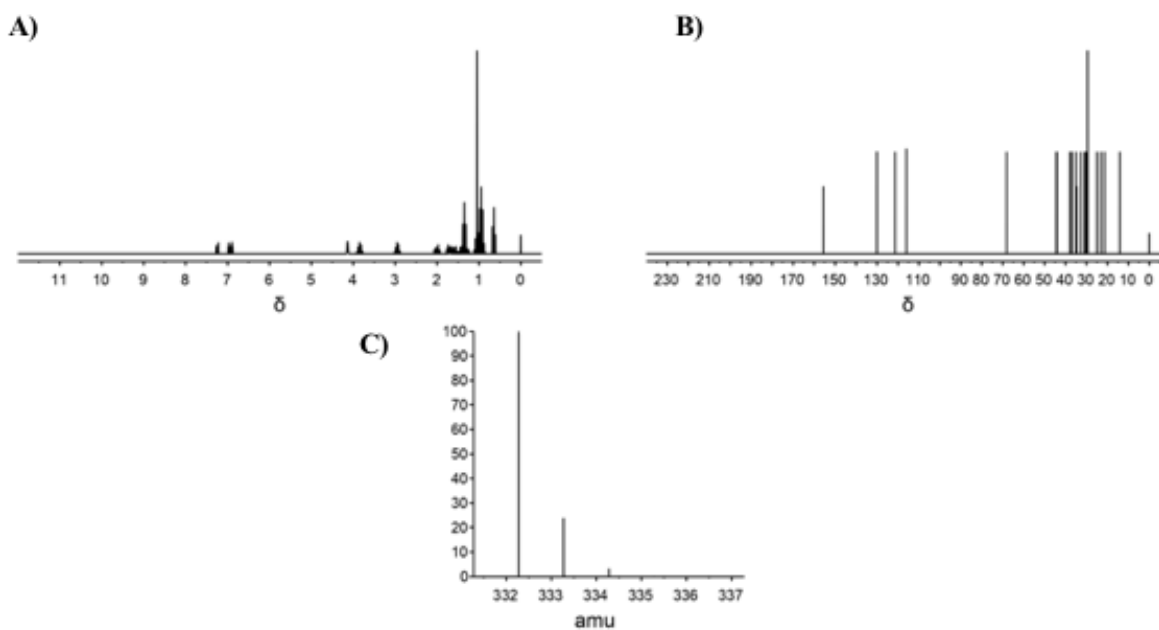


**Figure 64.** Spectral data for CP-47,497; A)  $^1\text{H}$  NMR, B)  $^{13}\text{C}$  NMR, C) Mass Parent Peak.

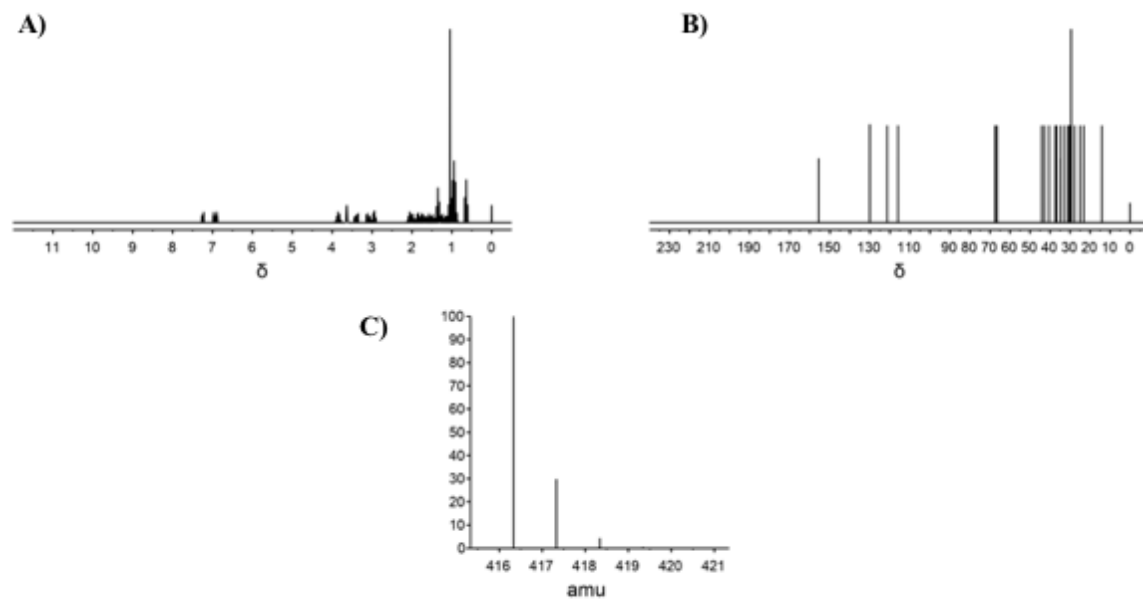


**Figure 65.** Spectral data for CP-55,244; A)  $^1\text{H}$  NMR, B)  $^{13}\text{C}$  NMR, C) Mass Parent Peak.

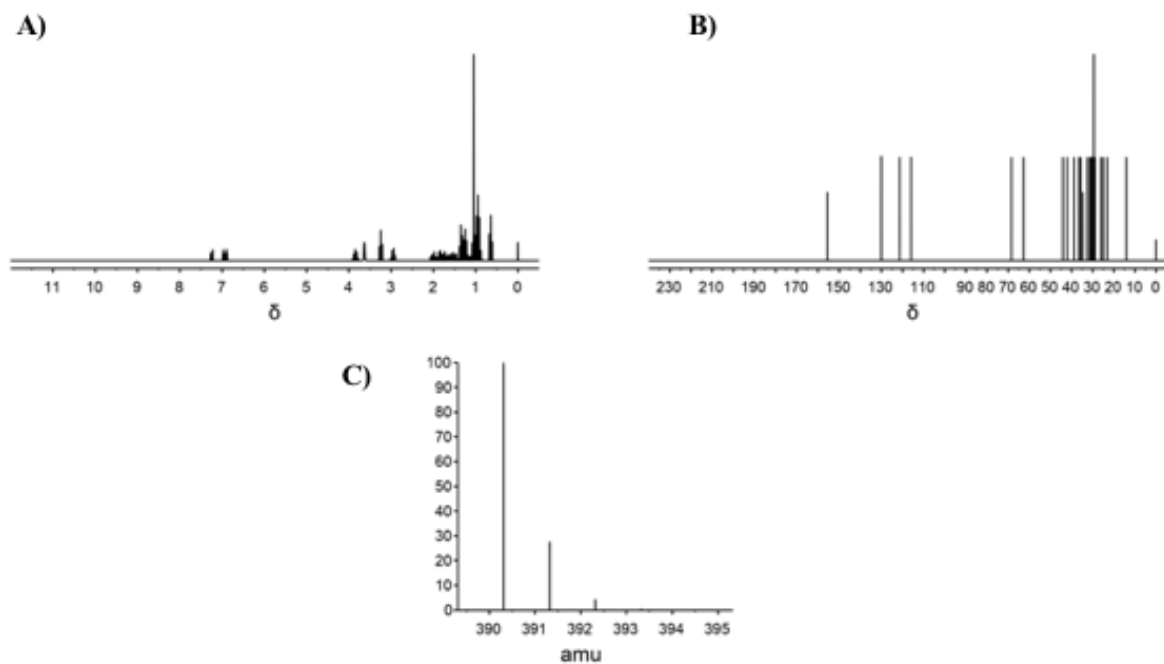


**Figure 66.** Spectral data for CP-55,490; A)  $^1\text{H}$  NMR, B)  $^{13}\text{C}$  NMR, C) Mass Parent Peak.

#### 4.4 Conclusions

This study examined the influence of alkyl chain length of known and novel homologs of the CP synthetic cannabinoids, CP-47,497, CP-55,244 and CP-55,490. Three known homologs of CP-47,497 exist; (C6), (C8) and (C9.) In this study each of the synthetic cannabinoids were examined with (C6), (C8) and (C9) alkyl chains. A previous study determined that the known (C8) homolog of CP-47,497 was several times more potent than the parent ligand. Melvin et al. determined that (C8) and (C7) ligands of CP-47,497 showed the most affinity for the CB1 receptor compared to the other homologs of CP-47,497.<sup>50</sup> The docking scores in this studied showed that each of the (C8) homologs had the best, most negative, docking score in each group. Based on the docking score (kcal/mol) it can be hypothesized that, like the (C8)-CP-47,497 homologs, the other (C8) homologs could be more potent than their parent structure. For the CP-47,497 group, the rank of docking scores was found to be (C9) > (C6) > (C7)\* > (C8). Based on rank of docking score, the results of this study support those found in the study by Melvin et al.<sup>59</sup> The rank of docking scores for CP-55,244 was determined to be (C7)\* > (C6) > (C9) > (C8) and for CP-55,490 the rank was (C6) > (C9) > (C7)\* > (C8). The binding energy estimations calculated in this study correlated to the experiment Ki values of the parent synthetic cannabinoids. The rank of binding energy estimations for the parent synthetic cannabinoids was determined to be CP-47,497 > CP-55,244 > CP-55,490. Based on this data it can be hypothesized that the binding affinity values of each of the homologs will be ranked as the following; for CP-47,497: (C9) > (C8) > (C7)\* > (C6) , for CP-55,244: (C9) > (C7)\* > (C8) > (C6) and for CP-55,490: (C8) > (C6) > (C7)\* > (C9). Interacting residues were examined and it was determined that  $\pi$ - $\pi$  stacking interactions and hydrogen bond interactions are essential to better docking of the ligands to the CB1 receptor. The position of each of the (C8) homologs

allowed for additional hydrogen bonding that was not observed in the parent ligand. The varying positions of the core structures of the ligands in the binding pocket of the CB1 receptor will be examined in future studies. More variation of the core structure was observed with the CP-47,497 group of homologs compared to the other groups examined in this study. Future studies will work to determine what is influencing the different positions in the binding pocket of the CB1 receptor observed in this study.



CHAPTER 5  
THE COMPUTATIONAL STUDY OF KNOWN AND NOVEL FENTANYL ANALOGS  
AND THE MU-OPIOID RECEPTOR

### 5.1 Introduction

Fentanyl was synthesized in 1960 by Dr. Paul Janssen of the Janssen Company to act as a rapid-acting analgesic. Unlike similar analgesics around that time, fentanyl did not have negative cardiovascular effects.<sup>53</sup> Fentanyl overdoses began to be reported around 1972, with the misuse being reported in increasing frequency as additional methods of administration became available.<sup>53</sup> From 1999 to 2011, the number of fatal opioid analgesic overdoses quadrupled and, for the year 2015, the death toll in the United States totaled 33,091.<sup>54</sup> One reason for this spike in overdose deaths is the now common practice by drug dealers of lacing heroin with fentanyl in order to increase their client's opioid high. In addition to the United States' regulation of fentanyl and various fentanyl derivatives, other countries are attempting to gain control of this epidemic as well. Unfortunately, as soon as a country has regulated a certain type of fentanyl, another comparable compound can be found on the market; causing fentanyl overdose deaths to likely be highly underreported.<sup>54</sup> Due to these factors, it is of utmost importance not only understand fentanyl itself, but to also understand several different fentanyl derivatives and how they interact with opioid receptors in the human body. Fentanyl and its derivatives are all agonists at the mu-opioid receptors. There are several physical effects of opioid binding at the mu-opioid receptor; including respiratory and central nervous system depression.<sup>54</sup> In fact, this respiratory depression

is what usually leads to fatality in a fentanyl overdose. Fentanyl related deaths are increasing, and more fentanyl derivatives are appearing in the drug market, some more potent than its predecessors. It is therefore imperative that the criminal justice community stay ahead of the illegal drug market. This can be accomplished by using computational methods to investigate ligand binding of illegal substances to their corresponding receptors before they make it into the market for recreational use.

The objectives of this study were to 1) analyze the binding of fentanyl and fentanyl analogs to the mu-opioid receptor through the use of molecular docking and 2) design and study potentially new fentanyl analogs and how various structural characteristics can influence binding. Once the newly designed analogs were analyzed, spectral data were calculated to begin compiling information for the development of a database.

## **5.2 Materials and Methods**

Schrödinger's molecular modeling software, Maestro, was used to examine the binding of select fentanyl analogs, and designed potential analogs, to the mu-opioid receptor. The mu-opioid receptor used in this study was prepared from the crystal structure, PDB:5C1M, developed by Huang et al.<sup>41</sup>

### **5.2.1 Ligand Selection and Design**

The focus of this study was to analyze known and novel fentanyl analogs. The novel fentanyl analogs were designed using the known analogs. Based on structural characteristics of the known analogs, new analogs were designed. The known analogs examined in this study included N-methyl fentanyl, fentanyl, and carfentanyl. The novel analogs were designed in two sets; 1) from the parent N-methyl fentanyl and fentanyl and 2) from the parent carfentanyl analog (Figure 67-68).

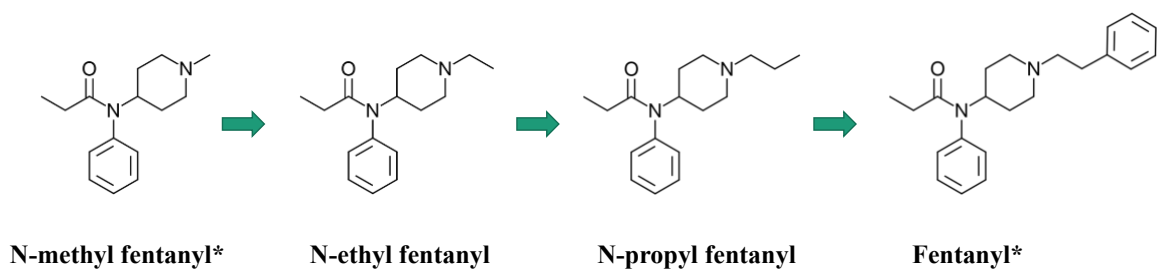


**Figure 67.** Structures of N-methyl fentanyl, N-ethyl fentanyl, N-propyl fentanyl, and fentanyl.

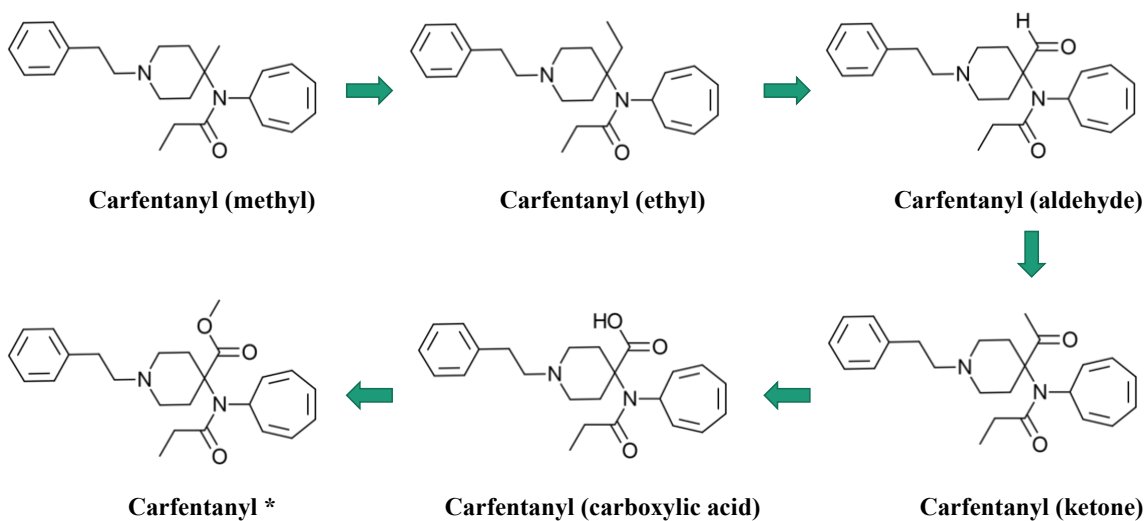


**Figure 68.** Structures of the designed carfetanyl analogs and the parent structure of carfetanyl.

### 5.2.2 Ligand Preparation

The *LigPrep* protocol is used to successfully convert ligands into three-dimensional structures. The preparation of the ligands involves generating possible states at a target pH of 7.0  $\pm$  2.0 using Epik. Epik is used to predict pKa values and determine all chemically sensible structures.<sup>18,42</sup>

### 5.2.3 Protein Preparation

The *Protein Preparation* application is used to convert the imported PDB file of 5C1M to a prepared model ready for docking. In order to prepare the mu-opioid receptor the following steps were taken. Once the PDB file “5C1M” was imported, the modified residue within the sequence was changed to its proper residue. This information was found within the Protein Data Bank. The modified residue present in 5C1M was YCM, S-(2-amino-2-oxoethyl)-L-cysteine, which was changed to the parent residue, cysteine (CYS). In the workspace the B chain and all the groups present, except 4VO, the co-crystallized ligand, were deleted. For preprocess all original hydrogens were removed, waters beyond 5 Å from co-crystallized ligand were deleted and protonation states were generated using Epik with a pH of 7.0  $\pm$  2.0. To refine the protein, the first step was optimization of H-bond assignment, which was done with sampling water orientations, using crystal symmetry and minimizing hydrogens of altered species. PROPKA was used at a pH of 7.0, PROPKA predicts Ka values of protein residues. Waters with less than 2 hydrogen bonds to non-waters were then removed. Minimization was performed converging heavy atoms to a distance of 0.30 Å with, hydrogens atoms minimized, using the force field OPLS3.

## 5.2.4 Receptor Grid Generation

The *Receptor Grid Generation* application is used to accurately place a grid around the binding pocket of the receptor. The structure present in the mu-opioid receptor model to generate the grid was 4VO. For this receptor there were no constraints but a rotatable group, TYR148 was selected for grid generation. The force field used was OPLS3. The grid created was used to accurately dock the ligands of interest to the receptor.

## 5.2.5 Ligand Docking

After the grid was generated and the desired ligands were prepared, the next step was *Glide Ligand Docking*. This step allowed for the prepared ligands to be docked into the receptor binding pocket selected during grid generation. Docking was completed using the standard precision (SP) method and force field OPLS3. Flexible ligand sampling was selected and Epik state penalties were added to the docking score. No constraints were selected to use in docking. The Glide program is able to produce potential ligand conformations. The program uses a set of ranked filters to find possible locations on the ligand in the binding pocket of the receptor. The filters include; 1) side-point search, 2a) diameter test, 2b) subset test, 2c) greedy score, 2d) refinement, 3) grid minimization, and 4) final scoring.<sup>43</sup> The *Glide Ligand Docking* process is described by Friesner et al. (2004).<sup>43</sup> For each ligand, up to five possible poses were generated and post-docking minimization was performed. The pose refers to the position and orientation of the ligand in relation to the receptor.<sup>43</sup> To determine the most accurate pose for each ligand, the docking scores and Glide Emodel scores were analyzed. Docking scores are an estimation of the binding free energy and are used to rank poses of different ligands.<sup>43,44</sup> The Glide Emodel was used to compare poses and determine the best, or most likely, pose for each ligand. Docking scores and Glide Emodel scores are negative. A more negative score means better docking. The

docking of each ligand, when using the same procedure, produces the same values. The algorithm used by Glide does not require docking multiple times and will produce the same values each time as long as the same procedure is used. The use of two and three decimal places is because differences in some of the values between ligands might not have been seen until the second or third decimal place. The software allows for more decimal places to be used, but it was decided to use two and three decimal places due to some of the small changes observed in the data.

### **5.2.6 Binding Energy Estimations: Prime MM-GBSA**

The relative binding free energy of each ligand was estimated using the *Prime MM-GBSA* application. These calculations are done following the equation:  $\Delta G_{\text{bind}} = E_{\text{complex}}(\text{minimized}) - (E_{\text{ligand}}(\text{minimized}) - E_{\text{receptor}}(\text{minimized}))$ .<sup>22</sup> The solvation model used was VSGB and calculations were done using OPLS3. Protein flexibility was applied within a distance of 5 Å from the ligand. The Prime MM-GBSA data values are not expected to be the same as the experimental binding affinities but are expected to give a ranking of the ligands that correlates with the experimental data of binding affinities ( $K_i$  values). A more negative binding free energy value correlates to a stronger binding of the ligand to the receptor.<sup>47</sup>

### **5.2.7 Spectral Simulation**

Following the analysis of the known and novel fentanyl analogs, spectral data were calculated for each of the new structures using spectral simulation software. The program ChemDoodle was able to produce <sup>1</sup>H NMR, <sup>13</sup>C NMR, and mass parent peak spectra of the novel compounds. The known synthetic cannabinoids were also analyzed by this method and compared to data from the NIST library to confirm accuracy.

### 5.3 Results and Discussion

In this study known and novel fentanyl analogs and their binding to the mu-opioid receptor were analyzed. Through molecular docking the ligands were virtually docked to the 3D model of the mu-opioid receptor. The mu opioid receptor was prepared from the crystal structure developed by Huang et al., PDB: 5C1M.<sup>55</sup> Once the ligands were docked their docking scores were analyzed. The docking scores are estimations of the binding free energy and were used to rank poses of different ligands. The lower, or more negative, the docking score is the stronger the binding is to the receptor. When docked, each ligand produced up to five possible poses. To determine the best pose of each ligand, the Glide Emodel value was used. The lowest, or most negative, value indicates the best pose for that ligand. Binding energy calculations were then done to determine the relative binding energy of the best pose of each ligand.

#### 5.3.1 Fentanyl Analogs

The first set of known and novel fentanyl analogs were N-methyl fentanyl, N-ethyl fentanyl, N-propyl fentanyl and fentanyl itself. The parent structures in this group are N-methyl fentanyl and fentanyl. N-ethyl and N-propyl fentanyl were designed to examine how the binding of the ligands changed as N-methyl fentanyl grew into fentanyl. (Figure 37)

The ligands were virtually docked into the prepared mu-opioid receptor using the molecular docking software Maestro. Once the ligands were docked their docking scores were analyzed. The docking scores are estimation of the binding free energy and was used to rank poses of different ligands. The lower, or more negative, the docking scores correlate to stronger binding of the ligand to the CB1 receptor. Once docked, each ligand produced up to five possible poses. To determine the best pose of each ligand, the Glide Emodel value was used. The lowest, or most

negative, value indicates the best pose for that ligand. Binding energy calculations were then done to determine the relative binding energy of the best pose of each ligand.

**Table 7.** Summary of experimental binding affinities, docking scores, glide Emodel values, and binding free energy estimations. The Ki values for N-methyl fentanyl and fentanyl are from experimental data from guinea pig brain membranes.<sup>56</sup>

| <b>Ligand</b>              | <b>Binding Affinity<br/>Ki (nM)<sup>(56)**</sup></b> | <b>Docking Score<br/>(kcal/mol)</b> | <b>Glide Emodel</b> | <b>Binding Energy<br/>(kcal/mol)</b> |
|----------------------------|--|-------------------------------------|---------------------|--------------------------------------|
| <b>N-methyl fentanyl *</b> | 18000 ± 3000   | -5.742                              | -50.799             | -41.971                              |
| <b>N-ethyl fentanyl</b>    | -  | -5.476                              | -49.824             | -45.155                              |
| <b>N-propyl fentanyl</b>   | -  | -5.333                              | -51.778             | -49.467                              |
| <b>Fentanyl*</b>           | 1.2 ± 0.2  | -6.870                              | -61.318             | -54.073                              |

\*parent structure

\*\*Inhibition of [<sup>3</sup>H]DAGO ( [D-Ala<sup>2</sup>, MePhe<sup>4</sup>, Gly<sup>5</sup>-ol]encephalin) was determined.<sup>56</sup>

The experimental Ki values used for comparison in this study were determined through competitive binding assays by Maguire et al.<sup>56</sup> The radioligand [D-Ala<sup>2</sup>, MePhe<sup>4</sup>, Gly<sup>5</sup>-ol]encephalin was used to measure displacement and determine the IC<sub>50</sub> value. IC<sub>50</sub> values determine the concentration of the ligand is required to inhibit half of the receptor's biological response. Maguire et al. used linear regression to calculate the IC<sub>50</sub> values. To determine the Ki values from the IC<sub>50</sub> values, the authors used a program known as LIGAND.<sup>57</sup> This computational program analyzed the competitive binding assay data to determine the Ki values.<sup>57</sup>

The parent compound fentanyl was found to have the best, most negative docking score (-6.870). Fentanyl also had the most negative binding affinity, -54. kcal/mol. The rank of



docking scores of these analogs was determined to be N-propyl fentanyl > N-ethyl fentanyl > N-methyl fentanyl > fentanyl. The rank of the binding affinities was determined to be N-methyl fentanyl > N-ethyl fentanyl > N-propyl fentanyl > fentanyl. The binding free energy estimations, while not identical to the  $K_i$  values, is expected to be similar in rank. Therefore, it can be assumed that the novel ligands N-ethyl fentanyl and N-propyl fentanyl will have larger  $K_i$  values than fentanyl but smaller than N-methyl fentanyl.

Using the *2D Ligand Interaction Diagram* application in Maestro, the residues interacting within a distance of 5 Å from the ligand were examined (Table 8). The types of interacting residues present within the binding pocket were labeled as hydrophobic, polar, negatively charged, and positively charged residues.

**Table 8.** Number and identification of interacting residues within 5 Å.

| Ligand                    | Docking score (kcal/mol) | Binding energy (kcal/mol) | Hydrophobic | Polar | Negatively Charged | Positively Charged |
|---------------------------|--------------------------|---------------------------|-------------|-------|--------------------|--------------------|
| <b>N-methyl fentanyl*</b> | -5.742                   | -41.971                   | 14          | 4     | 1                  | 0                  |
| <b>N-ethyl fentanyl</b>   | -5.476                   | -45.155                   | 16          | 5     | 1                  | 0                  |
| <b>N-propyl fentanyl</b>  | -5.333                   | -49.467                   | 20          | 5     | 1                  | 0                  |
| <b>Fentanyl*</b>          | -6.870                   | -54.073                   | 21          | 6     | 1                  | 1                  |

There were a few trends observed when analyzing the residues interacting within a distance of 5 Å. There was a correlation observed between the binding energy estimations and hydrophobic interactions, as well as the polar residue interactions. As N-methyl fentanyl transitioned into fentanyl, the binding energy estimations became more negative and the number

of hydrophobic and polar residue interactions increased. All the ligands contained 1 negatively charged residue, but fentanyl was the only ligand with a positively charged residue present in the binding pocket within 5 Å. The docking scores of N-ethyl and N-propyl fentanyl were more positive and they contained increased number of hydrophobic and polar residues compared to the parent analog N-methyl fentanyl. However, the transition from N-propyl fentanyl to fentanyl resulted in a large decrease, becoming more negative, docking score. This increase in docking can be contributed to the additional positively charged residue not seen in the other ligands. However, it is essential to analyze the direct interactions taking place as well. After examining the residues present within the binding pocket, the direct interactions between the analogs and the mu-opioid receptor were analyzed. Interactions can include  $\pi$ - $\pi$  stacking,  $\pi$ -cation, hydrogen bonding, and salt bridges.

**Table 9.** Residues interacting with the analogs within a distance of 5 Å.

| <b>Ligand</b>              | <b>Salt Bridge</b> | <b>Hydrogen Bond</b> | <b><math>\pi</math>-<math>\pi</math> Stacking</b> | <b><math>\pi</math>-Cation</b> |
|----------------------------|--------------------|----------------------|---|--------------------------------|
| <b>N-methyl fentanyl *</b> | ASP147             | ASP147               | TRP293  | -                              |
| <b>N-ethyl fentanyl</b>    | ASP147             | ASP147               | TRP293  | -                              |
| <b>N-propyl fentanyl</b>   | ASP147             | ASP147               | -   | -                              |
| <b>Fentanyl*</b>           | ASP147             | ASP147               | TRP293,<br>TYR326                                 | -                              |

Each analog ligand examined contained a salt bridge with ASP147 and a hydrogen bond ASP147. The interactions with ASP147 and each ligand was found to occur between the protonated nitrogen of the cyclohexane group and the residue.  $\pi$ - $\pi$  stacking interactions were

seen for every ligand except N-propyl fentanyl. N-propyl fentanyl also had the most positive docking score, indicating that  $\pi$ - $\pi$  stacking is essential to have better docking of the analogs to the mu-opioid receptor. Fentanyl was the only ligand in this group that contained two  $\pi$ - $\pi$  stacking interactions, one with TRP293 and an additional interaction with TYR326. Fentanyl also had the most negative docking score. Again, this indicated that  $\pi$ - $\pi$  stacking is essential to the strong binding of the analogs to the mu-opioid receptor. No  $\pi$ -cation interactions were seen in this group of ligands. 3D interaction diagrams were examined to gain of better understanding of the position of each ligand in the binding pocket.

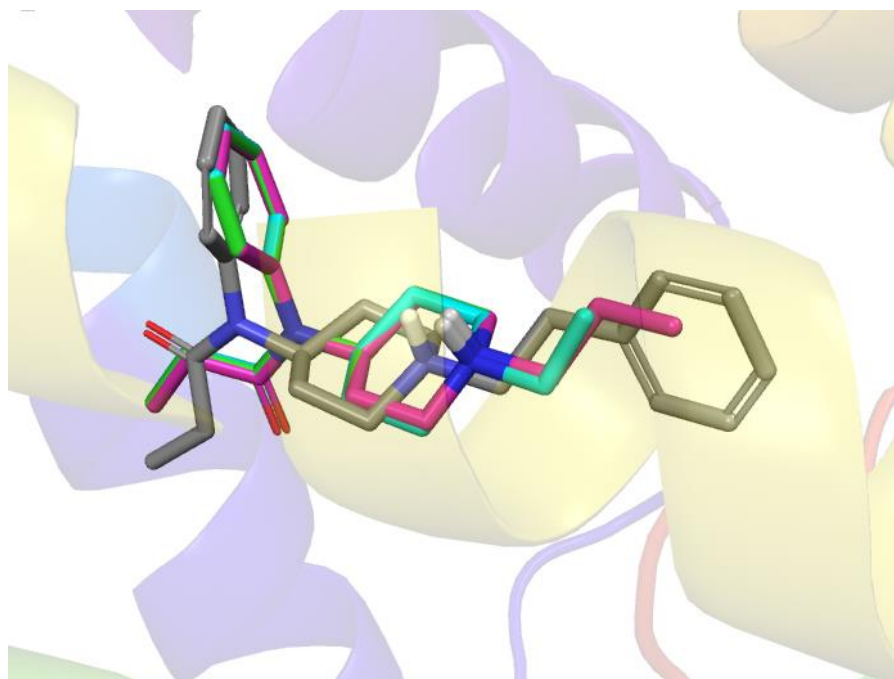


**Figure 69.** 3D interaction diagram of N-methyl fentanyl (green), N-ethyl fentanyl (cyan), N-propyl fentanyl (pink), and fentanyl (grey).

The N-methyl fentanyl, N-ethyl fentanyl, and N-propyl fentanyl ligands were all observed to be in similar positions. The position of the fentanyl was found to be the most different compared to the other ligands. The ligands with the best docking scores were N-methyl fentanyl and fentanyl (Figure 70).

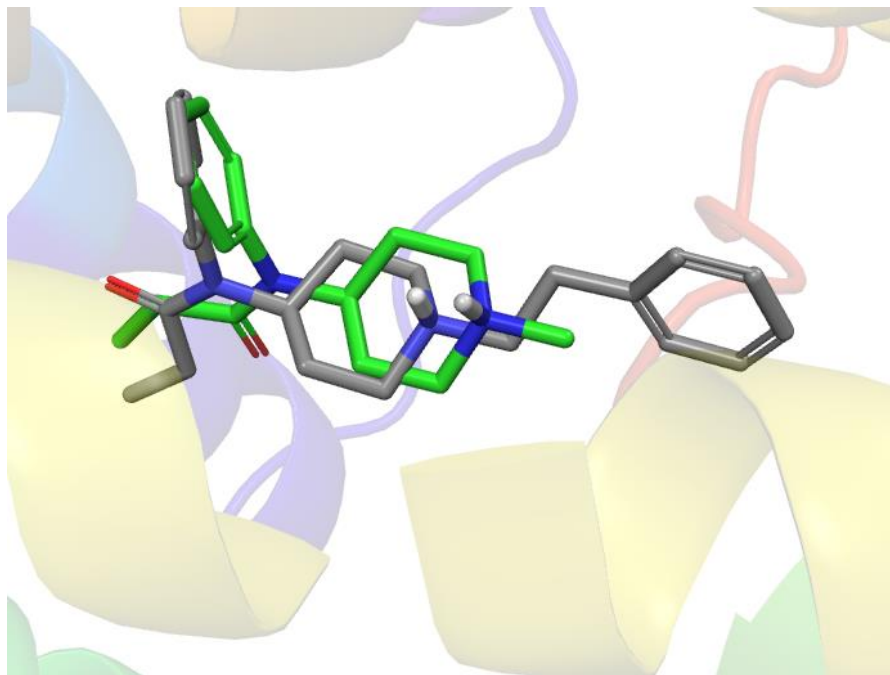


**Figure 70.** 3D interaction diagram of N-methyl fentanyl (green) and fentanyl (grey).

All ligands in this group were observed interacting with the ASP147 residue through both a salt bridge and a hydrogen bond ( Figure 71).

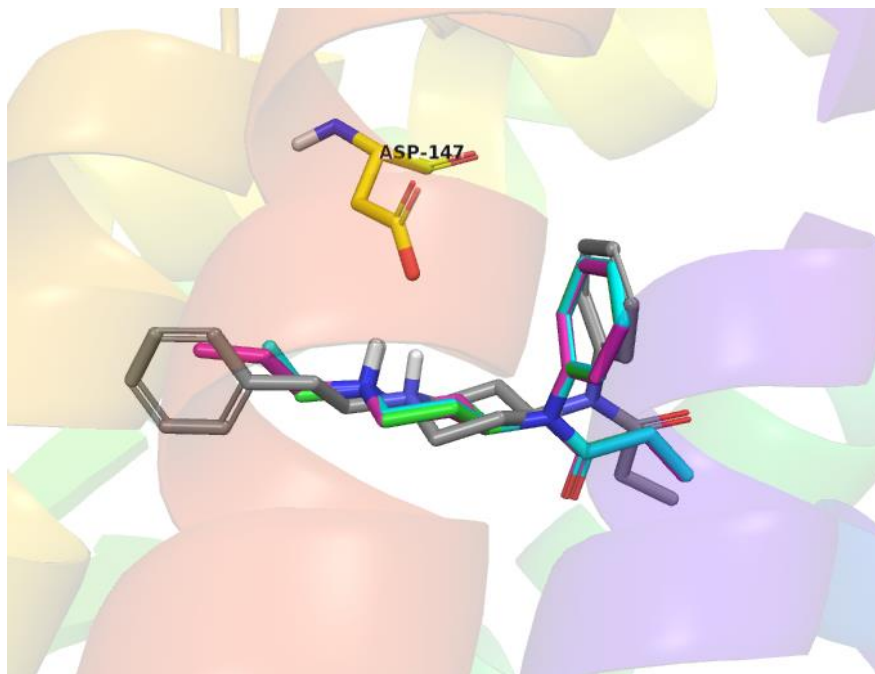


**Figure 71.** 3D interaction diagram of N-methyl fentanyl (green), N-ethyl fentanyl (cyan), N-propyl fentanyl (pink), and fentanyl (grey) with the ASP147 residue.

TRP 293 was only found to interact with three of the ligands in this group, N-methyl fentanyl, N-ethyl fentanyl, and fentanyl (Figure 72).

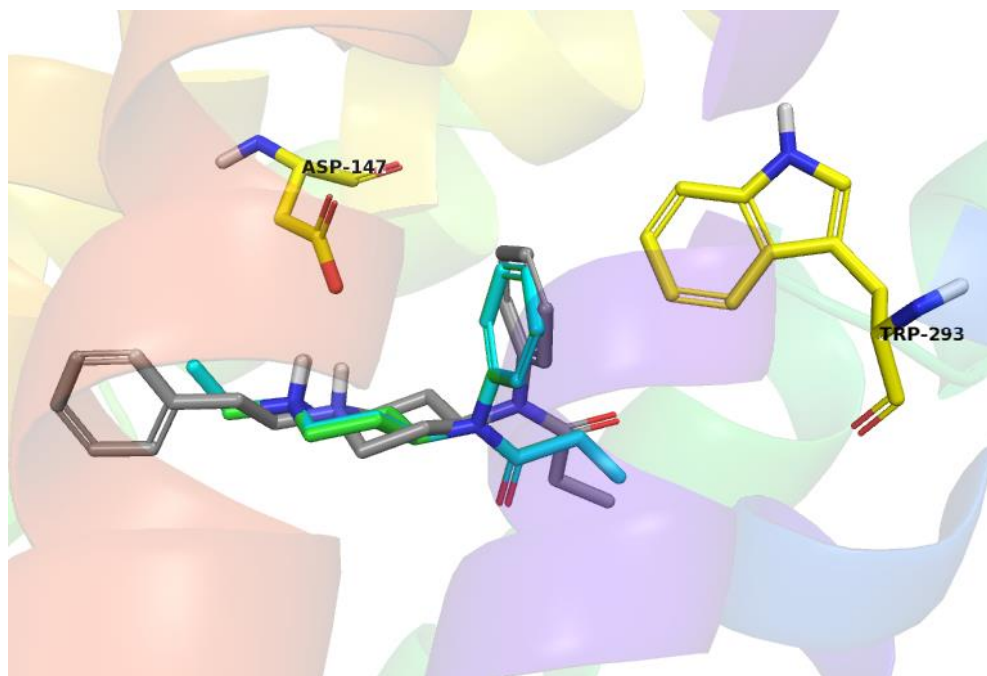


**Figure 72.** 3D interaction diagram of N-methyl fentanyl (green), N-ethyl fentanyl (cyan), and fentanyl (grey) with the ASP147 residue and the TRP293 residue.

N-methyl fentanyl, N-ethyl fentanyl and fentanyl displayed a salt bridge and hydrogen bonding with ASP147, as well as  $\pi$ - $\pi$  stacking with TRP293. The distance between the benzene group of the ligands and the TRP293 could be assumed to influence the over docking of the ligand. The benzene of the fentanyl interacting with the TRP293 residue was observed to be in closer proximity to the residue than the N-methyl and N-ethyl fentanyl ligands. Fentanyl was also observed to have an additional  $\pi$ - $\pi$  stacking interaction with TYR326 (Figure 73).

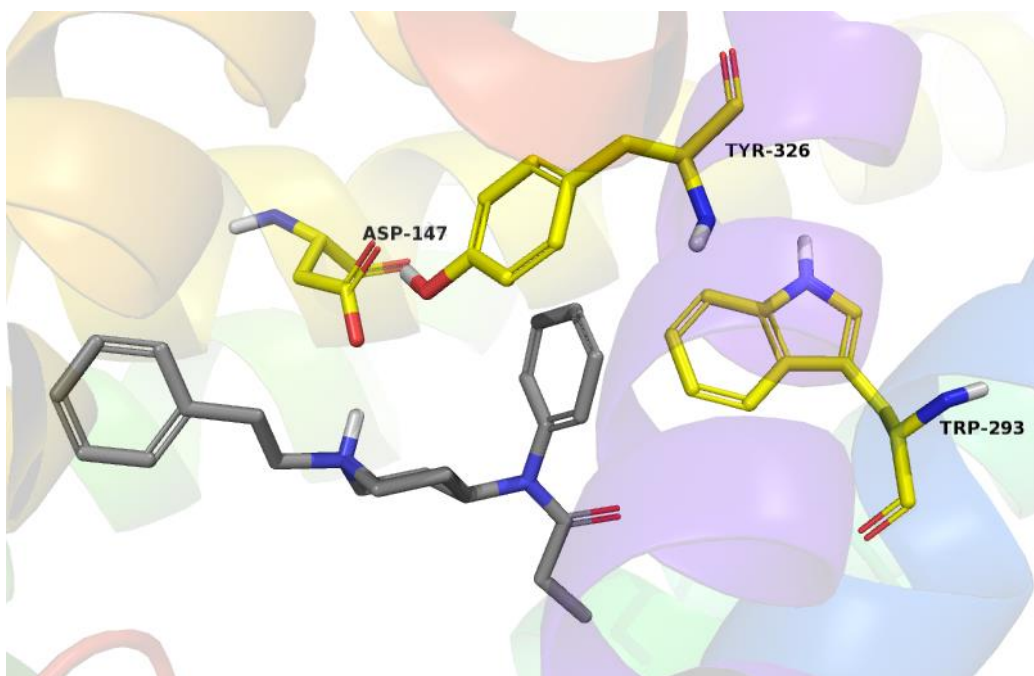


**Figure 73.** 3D interaction diagram of fentanyl (grey) with the residues TRP293, TYR326 and ASP147.

The fentanyl ligand was the only ligand in the group to have two  $\pi$ - $\pi$  stacking interactions, one with TRP293 and one with TYR326. The position of the fentanyl ligand in the binding pocket of the mu-opioid receptor allowed for the additional interaction to occur. Fentanyl was also determined to have the best docking score and the best binding energy estimation.

### 5.3.2 Carfentanyl Analogs

The second set of known and novel fentanyl analogs were designed from the parent analog. (Figure 38) The structural differences in the analogs took place at C4 of the piperidine ring, in the para position to the nitrogen. The analogs were virtually docked into the prepared mu-opioid receptor using the molecular docking software Maestro. Once the ligands were docked their docking scores were analyzed. The docking scores are estimation of the binding

free energy and was used to rank poses of different ligands. The lower, or more negative, the docking scores correlate to stronger binding of the ligand to the CB1 receptor. Once docked, each ligand produced up to five possible poses. To determine the best pose of each ligand, the Glide Emodel value was used. The lowest, or most negative, value indicates the best pose for that ligand. Binding energy calculations were then done to determine the relative binding energy of the best pose of each ligand.

**Table 10.** Summary of experimental binding affinities, docking scores, glide Emodel values, and binding free energy estimations. The Ki values provided for carfentanyl and lofentanyl are experimental data from guinea pig brain membranes.<sup>56</sup>

| <b>Ligand</b>                        | <b>Binding Affinity<br/>Ki(nM)<sup>(56)**</sup></b> | <b>Docking Score<br/>(kcal/mol)</b> | <b>Glide Emodel</b> | <b>Binding Energy<br/>(kcal/mol)</b> |
|--------------------------------------|---|-------------------------------------|---------------------|--------------------------------------|
| <b>Carfentanyl (methyl)</b>          | -   | -6.611                              | -63.161             | -52.512                              |
| <b>Carfentanyl (ethyl)</b>           | -   | -7.023                              | -63.890             | -61.265                              |
| <b>Carfentanyl (aldehyde)</b>        | -   | -6.937                              | -64.384             | -59.450                              |
| <b>Carfentanyl (ketone)</b>          | -   | -7.080                              | -59.307             | -59.104                              |
| <b>Carfentanyl (carboxylic acid)</b> | -   | -6.702                              | -58.704             | -42.687                              |
| <b>Carfentanyl*</b>                  | 0.024 ± 0.004                                       | -7.182                              | -68.850             | -60.126                              |

\*parent structure

\*\*Inhibition of [<sup>3</sup>H]DAGO ([D-Ala<sup>2</sup>, MePhe<sup>4</sup>, Gly<sup>5</sup>-ol]encephalin) was determined.<sup>56</sup>

The experimental Ki values used for comparison in this study were determined through competitive binding assays by Maguire et al.<sup>56</sup> The radioligand [D-Ala<sup>2</sup>, MePhe<sup>4</sup>, Gly<sup>5</sup>-ol]encephalin was used to measure displacement and determine the IC<sub>50</sub> value. IC<sub>50</sub> values determined the concentration of the ligand is required to inhibit half of the receptor's biological



response. Maguire et al used linear regression to calculate the IC<sub>50</sub> values. To determine the Ki values from the IC<sub>50</sub> values, the authors used a program known as LIGAND.<sup>57</sup> This computational program analyzed the competitive binding assay data to determine the Ki values.<sup>57</sup>

In this group of known and novel fentanyl analogs, carfentanyl was found to have the most negative docking score while the novel ligand carfentanyl (methyl) had the most positive docking score. The rank of docking scores was determined to be carfentanyl (methyl) > carfentanyl (carboxylic acid) > carfentanyl (aldehyde) > carfentanyl (ethyl) > carfentanyl (ketone) > carfentanyl. The most negative binding energy estimation was for the ligand carfentanyl (ethyl), which was only slightly more negative than the parent analog carfentanyl. The rank of binding free energy estimations was found to be carfentanyl (carboxylic acid) > carfentanyl (methyl) > carfentanyl (ketone) > carfentanyl (aldehyde) > carfentanyl > carfentanyl (ethyl). Therefore, it can be expected that carfentanyl (ethyl) would have a smaller binding affinity than carfentanyl, correlating to a stronger binding. The other novel analogs are expected to have a larger binding affinity for the mu-opioid receptor, weaker binding, compared to carfentanyl.

Using the *2D Ligand Interaction Diagram* application in Maestro, the residues interacting within a distance of 5 Å from the ligand were examined (Table 11). The types of interacting residues present within the binding pocket were labeled as hydrophobic, polar, negatively charged, and positively charged residues.

**Table 11.** Number and identification of interacting residues within 5 Å.

| <b>Ligand</b>                        | <b>Docking score (kcal/mol)</b> | <b>Binding energy (kcal/mol)</b> | <b>Hydrophobic</b> | <b>Polar</b> | <b>Negatively Charged</b> | <b>Positively Charged</b> |
|--------------------------------------|---------------------------------|----------------------------------|--------------------|--------------|---------------------------|---------------------------|
| <b>Carfentanyl (methyl)</b>          | -6.611                          | -52.512                          | 16                 | 6            | 1                         | 1                         |
| <b>Carfentanyl (ethyl)</b>           | -7.023                          | -61.265                          | 21                 | 6            | 1                         | 1                         |
| <b>Carfentanyl (aldehyde)</b>        | -6.937                          | -59.450                          | 17                 | 7            | 1                         | 2                         |
| <b>Carfentanyl (ketone)</b>          | -7.080                          | -59.104                          | 20                 | 5            | 1                         | 0                         |
| <b>Carfentanyl (carboxylic acid)</b> | -6.702                          | -42.687                          | 20                 | 6            | 1                         | 0                         |
| <b>Carfentanyl*</b>                  | -7.182                          | -60.126                          | 21                 | 6            | 1                         | 1                         |

The analogs carfentanyl and carfentanyl (ethyl) have the highest number of hydrophobic residue interactions (21) and also some of the more negative docking scores and the most negative binding energy estimations. These two ligands also had 6 polar residue interactions, 1 negatively charged and 1 positively charged residue. The highest number of polar residue interactions was observed in the analog carfentanyl (aldehyde). This was also the only analog with 2 positively charged residues present within a distance of 5 Å. The analog ligand with the most positive docking score, carfentanyl (methyl), also had the lowest number of hydrophobic interactions. To gain a better understanding of how the ligands interact with the mu-opioid receptor they direct interactions were analyzed. These interactions include  $\pi$ - $\pi$  stacking,  $\pi$ -cation, hydrogen bonding, and salt bridges.

**Table 12.** Residues interacting with the analogs within a distance of 5 Å.

| <b>Ligand</b>                        | <b>Salt Bridge</b> | <b>Hydrogen Bond</b> | <b><math>\pi</math>-<math>\pi</math> Stacking</b> | <b><math>\pi</math>-Cation</b> |
|--------------------------------------|--------------------|----------------------|---|--------------------------------|
| <b>Carfentanyl (methyl)</b>          | -                  | -                    | -   | -                              |
| <b>Carfentanyl (ethyl)</b>           | ASP147             | ASP147               | TRP293, TYR326                                    | -                              |
| <b>Carfentanyl (aldehyde)</b>        | ASP147             | ASP147               | HIS297  | HIS297                         |
| <b>Carfentanyl (ketone)</b>          | ASP147             | ASP147               | TRP293  | -                              |
| <b>Carfentanyl (carboxylic acid)</b> | ASP147             | ASP147               | TRP293  | -                              |
| <b>Carfentanyl*</b>                  | ASP147             | ASP147               | TRP293, TYR326                                    | -                              |

All analogs analyzed had salt bridge and hydrogen bond interactions with ASP147, with the exception of carfentanyl (methyl). The interactions with ASP147 were observed between the protonated nitrogen of the cyclohexane of the ligand and the ASP147 residue. Carfentanyl (methyl) had no direct interactions take place in the binding pocket. This ligand also had the most positive docking score. Therefore, it can be hypothesized that direct interactions are essential to better binding. All other ligands displayed  $\pi$ - $\pi$  stacking interactions, but the interacting residues varied with each ligand. The two analogs with the most negative binding energy estimations and some of the most negative docking score were carfentanyl and carfentanyl (ethyl). Both of these ligands had  $\pi$ - $\pi$  stacking with TRP293 and TYR326. It can be hypothesized that  $\pi$ - $\pi$  stacking is essential to have the strongest binding to the mu-opioid

receptor. Carfentanyl (aldehyde) was the only ligand that was observed to have a  $\pi$ -cation interaction, interacting with HIS297. 3D interaction diagrams were then used to better understand how the position of each ligand in the binding pocket of the receptor influenced the residue interactions and over docking of the ligand.

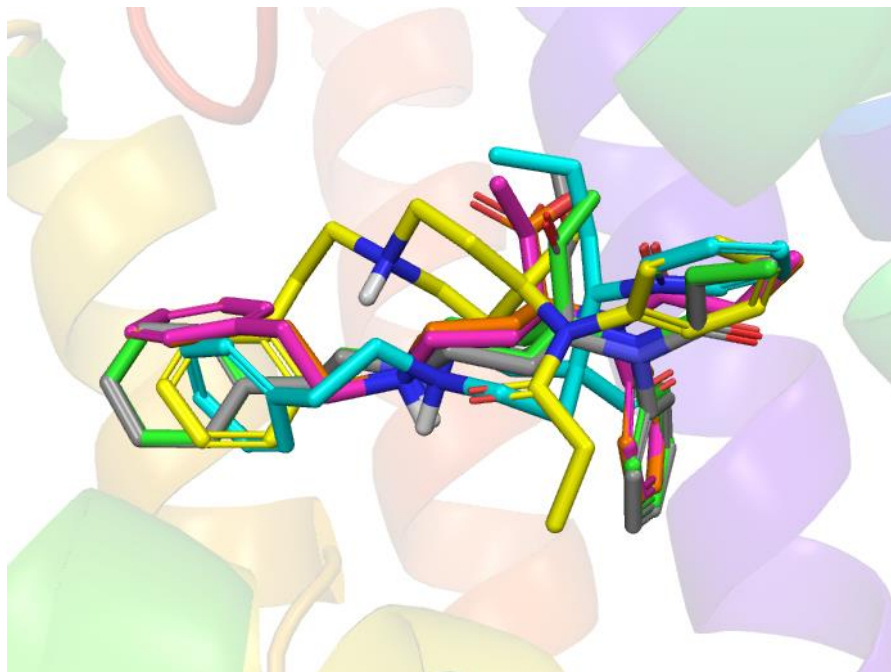


**Figure 74.** 3D diagram of the ligands carfentanyl (methyl) (yellow), carfentanyl (ethyl) (green), carfentanyl (aldehyde) (cyan), carfentanyl (ketone) (pink), carfentanyl (carboxylic acid) (orange), and carfentanyl (grey).

The 3D interaction diagram of all the carfentanyl ligands in this group showed the varying positions of the ligands in the binding pocket of the mu-opioid receptor. Carfentanyl and carfentanyl (ethyl) were found to have the best docking scores and binding energy estimations, as well as the same interacting residues. The 3D interaction diagram was used to better compare the ligands (Figure 75).

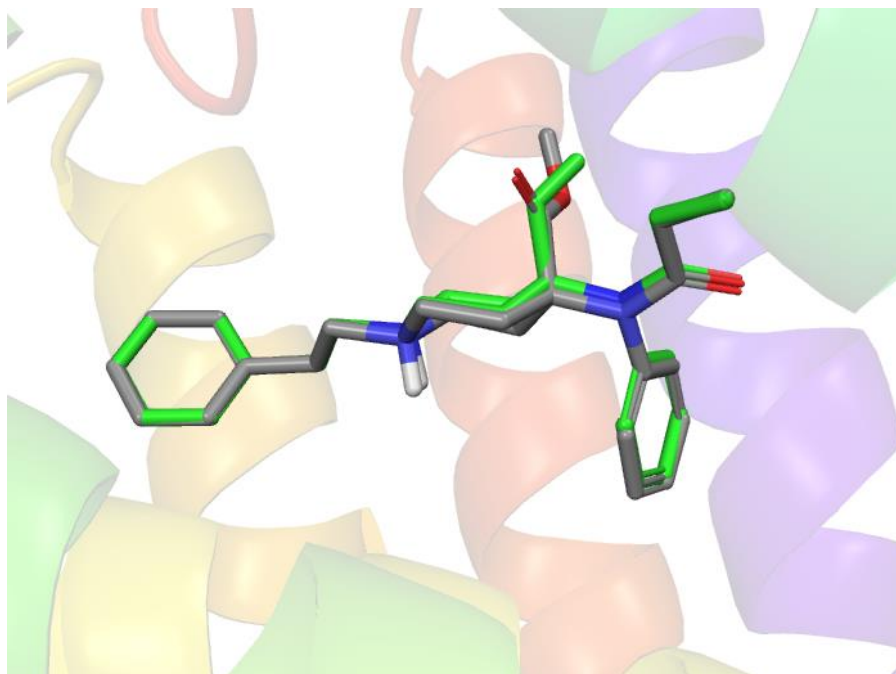


**Figure 75.** 3D interaction diagram of carfentanyl (grey) and carfentanyl (ethyl) (green).

Carfentanyl and carfentanyl (ethyl) were observed to be in very similar positions in the binding pocket of the mu-opioid receptor. The most notable difference in their positions was in the position and orientation of the ethyl group of the carfentanyl (ethyl) and the ester group of the carfentanyl. The ligands each had the same interacting residues; ASP147, TRP293, and TYR326 (Figure 76).

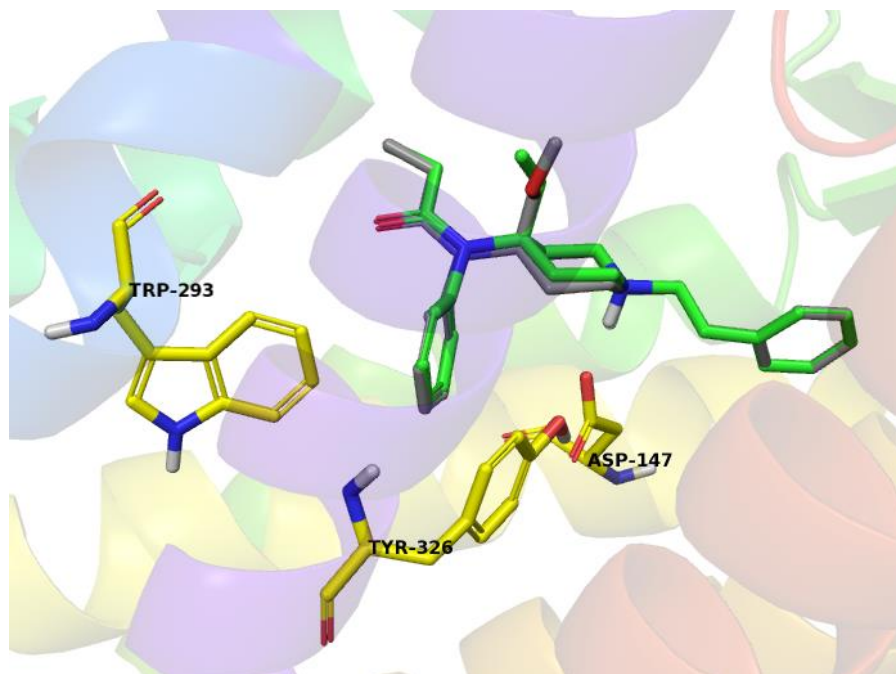


**Figure 76.** 3D interaction diagram of carfentanyl (grey) and carfentanyl (ethyl) (green) with interacting residues ASP147, TRP293, and TYR326.

Carfentanyl and carfentanyl (ethyl) displayed a salt bridge and hydrogen bond with the ASP147 residue and  $\pi$ - $\pi$  stacking with the TRP293 and TYR326 residues. Based on the 3D interaction diagram, it can be hypothesized that the distance of these interactions caused by the differences in positions is what influenced the docking scores and binding energy estimations of the two ligands. Carfentanyl (ethyl), carfentanyl (ketone), carfentanyl (carboxylic acid), and carfentanyl all had similar interacting residues (Figure 77).

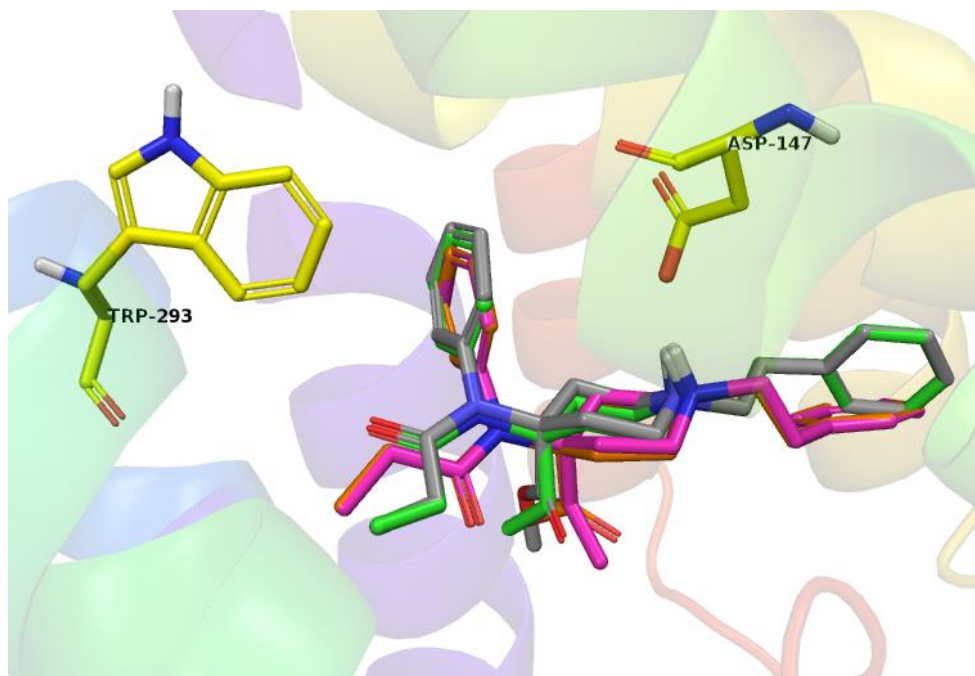


**Figure 77.** 3D interaction diagram of carfentanyl (ethyl) (green), carfentanyl (ketone) (pink), carfentanyl (carboxylic acid) (orange), and carfentanyl (grey) with interacting residues TRP293 and ASP147.

Carfentanyl (ethyl), carfentanyl (ketone), carfentanyl (carboxylic acid), and carfentanyl were all observed to have interactions with ASP147 and TRP293. Each ligand interacted with ASP147 through a salt bridge and hydrogen bond, and with TRP293 through  $\pi$ - $\pi$  stacking. The variations in positions of the ligands in the binding pocket can be assumed to be the cause of the differences observed in the docking scores and binding energy estimations. The carfentanyl (ethyl) and carfentanyl were also observed to have an additional  $\pi$ - $\pi$  stacking interaction that could be responsible for the better binding energy estimations compared to the other ligands. Carfentanyl (aldehyde) was the only ligand that was observed interacting with the HIS297 residue (Figure 78).

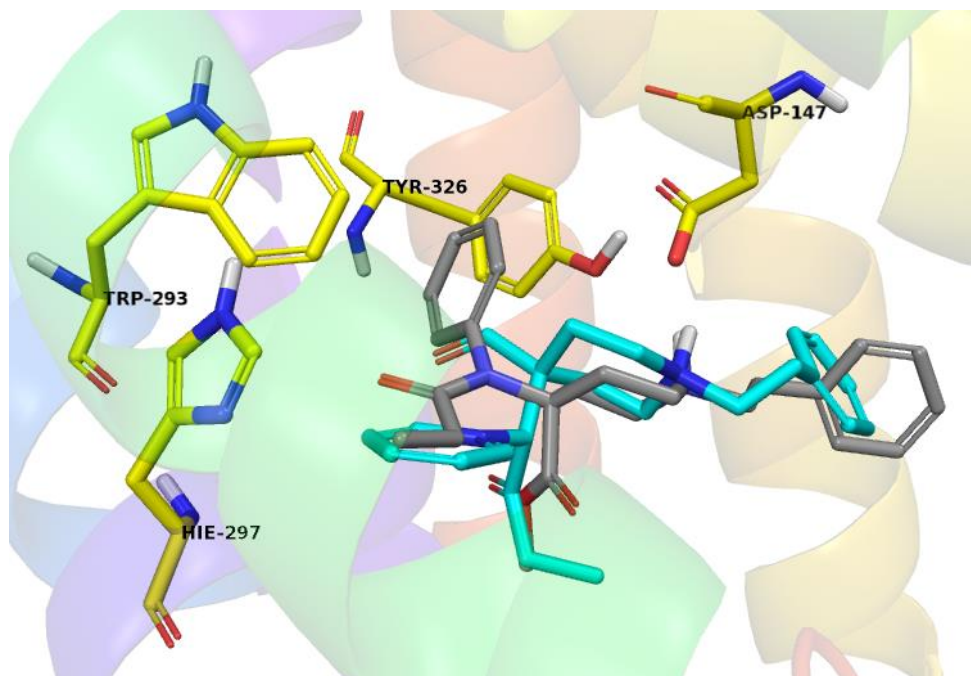


**Figure 78.** 3D diagram of carfentanyl (aldehyde) (cyan) and carfentanyl (grey) with the interacting residues ASP147, TRP293, TYR326 and HIS297. This HIS297 residue is labeled as HIE297 because the hydrogen is observed on the epsilon nitrogen. The HIE297 residue is only observed interacting with carfentanyl (aldehyde) through a  $\pi$ - $\pi$  stacking interaction and a  $\pi$ -cation interaction.

The carfentanyl (aldehyde) ligand displayed a salt bridge with ASP147 and a hydrogen bond with ASP147. Unlike the other ligands, it did not interact with TRP293 and TYR326. Instead, carfentanyl (aldehyde) was observed to have a  $\pi$ - $\pi$  stacking interaction and a  $\pi$ -cation interaction with HIS 297. The 3D interaction diagram displayed carfentanyl (aldehyde) in a very different position compared to carfentanyl. The position of the benzene ring in the carfentanyl (aldehyde) was too far from the TRP293 residue to interact but was in closer proximity to the HIS297 residue leading to that  $\pi$ - $\pi$  stacking interaction.



The software ChemDoodle was used to calculate spectral data of the novel analogs designed in this study. ChemDoodle is able to produce calculated  $^1\text{H}$  NMR and  $^{13}\text{C}$  NMR spectra of the analogs, as well as determine the mass parent peak. (Figure 79-80)

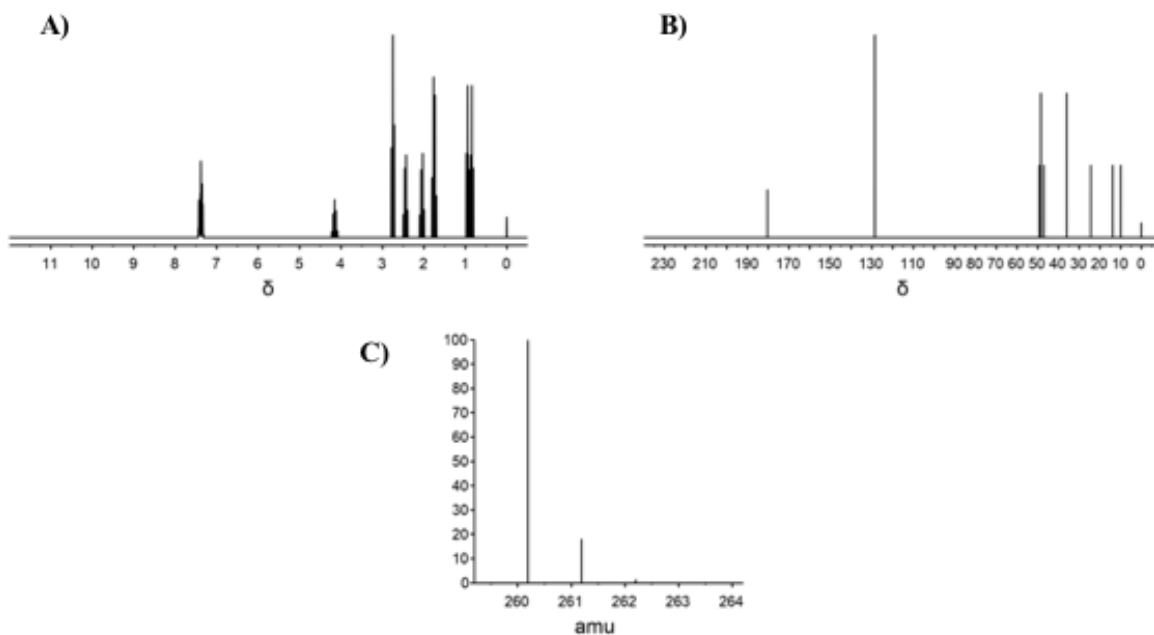


**Figure 79.** Spectral data for N-ethyl fentanyl; A)  $^1\text{H}$  NMR, B)  $^{13}\text{C}$  NMR, C) Mass Parent Peak.

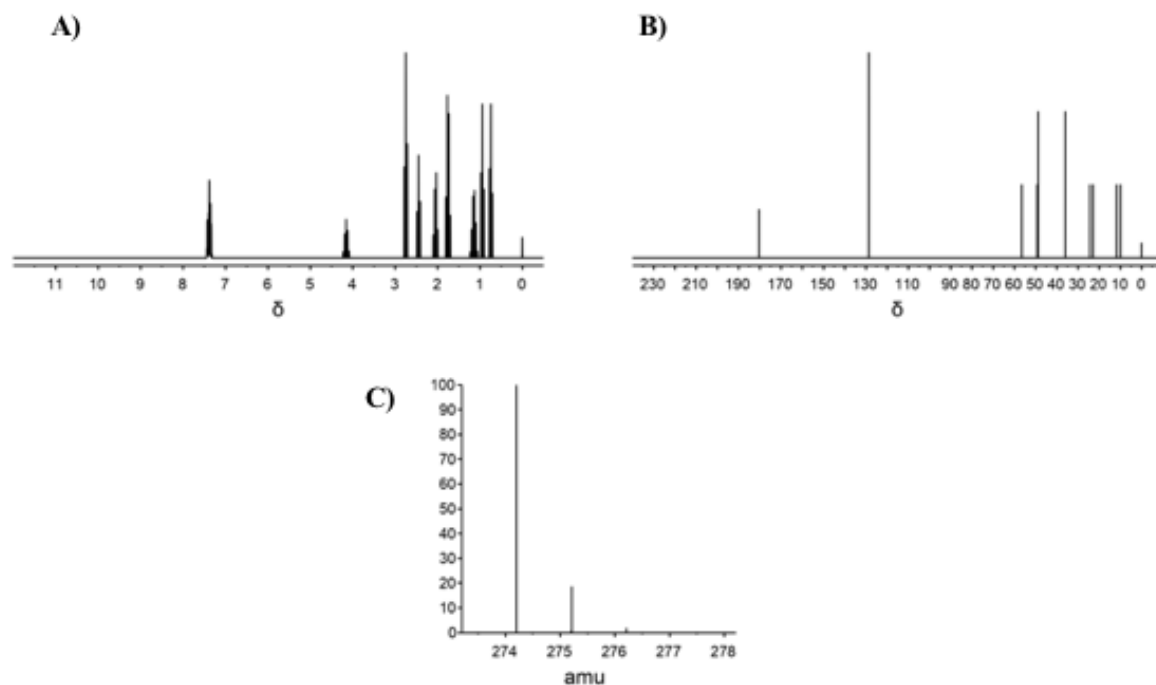


**Figure 80.** Spectral data for N-propyl fentanyl; A) <sup>1</sup>H NMR, B) <sup>13</sup>C NMR, C) Mass Parent Peak.

## 5.4 Conclusions

The objective of this study was to analyze the binding of fentanyl and fentanyl analogs to the mu-opioid receptor through the use of molecular docking and design and novel fentanyl analogs to study using the same methods. The first set of analogs examined in this study involved the parent analogs N-methyl fentanyl and fentanyl along with the novel analogs N-ethyl fentanyl and N-propyl fentanyl. The rank of docking scores of these analogs was determined to be N-propyl fentanyl > N-ethyl fentanyl > N-methyl fentanyl > fentanyl. The rank of the binding affinities was determined to be N-methyl fentanyl > N-ethyl fentanyl > N-propyl fentanyl > fentanyl. Therefore, it can be assumed that the novel ligands N-ethyl fentanyl and N-propyl fentanyl will have larger  $K_i$  values than fentanyl but smaller than N-methyl fentanyl. The  $\pi$ - $\pi$  stacking interactions were determined to be essential to better binding of these analogs to the

mu-opioid receptor. ASP147 was determined to be the most essential interacting residue for this group of ligands. Every ligand interacted with ASP147 through a salt bridge and hydrogen bonding.

The second set of novel analogs analyzed in this study were designed from the parent analog carfentanyl. The rank of docking scores was determined to be carfentanyl (methyl) > carfentanyl (carboxylic acid) > carfentanyl (aldehyde) > carfentanyl (ethyl) > carfentanyl (ketone) > carfentanyl. The most negative binding energy estimation was for the ligand carfentanyl (ethyl), which was only slightly more negative than the parent analog carfentanyl. The rank of binding free energy estimations was found to be carfentanyl (carboxylic acid) > carfentanyl (methyl) > carfentanyl (ketone) > carfentanyl (aldehyde) > carfentanyl > carfentanyl (ethyl). Therefore, it can be expected that carfentanyl (ethyl) would have a smaller binding affinity than carfentanyl, correlating to a stronger binding. The other novel analogs are expected to have a larger binding affinity for the mu-opioid receptor, weaker binding, compared to carfentanyl. It was determined in this study that the essential residues from strong docking were ASP147 and TRP293. The position and distance of the ligands from the residues were also impact the docking of the ligands to the mu-opioid receptor. Additional  $\pi$ - $\pi$  stacking with TYR326 was also found to lead to a better docking of the ligands to the receptor, as was observed in the carfentanyl and carfentanyl (ethyl) ligands. The 3D diagrams used to study the positions of the ligands in the binding pocket of the receptor displayed varying positions for some of the ligands with similar core structures. Future work will study what is influencing the different positions in the binding pocket observed between the ligands.

CHAPTER 6  
THE COMPUTATIONAL STUDY OF KRATOM ALKALOIDS AND THE MU-OPIOID  
RECEPTOR

### 6.1 Introduction

Kratom, or *Mitragyna speciosa*, is a tree found in Southeast Asia. It is the leaves of this tree that contain the compounds known for their psychoactive and therapeutic effects. These compounds are known as kratom alkaloids.<sup>58</sup> The leaves of the kratom tree were originally used in Southeast Asia by workers to keep them awake and alert for long periods of time. Smaller doses can give effects similar to stimulants, while higher doses produce opioid-like effects. Kratom has also been used for therapeutic purposes such as aiding in pain, fever, cough, diarrhea, diabetes and hypertension.<sup>59</sup> Popularity of this drug has increased because of its accessibility. Kratom is sold online, at gas stations and specialty stores and marketed as “not for human consumption”. It is also believed by some to help with opioid withdrawal, but there have been no studies to confirm it as a withdrawal aid. A study in 2019 examined the cases of kratom exposure from 2011-2017 that had been reported to Poison Control Centers. 1807 cases of kratom exposure were reported from 2011-2017, 11 of which resulted in death. Some of the reported cases involved only kratom, however a significant number of cases involved kratom and other drugs leading to the concern of the adverse effects caused by kratom used with other substances.<sup>60</sup>

Of the 1807 cases reported over those six years, two-thirds were seen from 2016-2017.<sup>60</sup> The popularity of kratom is increasing, but the DEA still only has it listed as a “Drug of Concern”. There have been around 44 alkaloids found in the leaves of the kratom plant. Up to 44 alkaloid compounds have been isolated from the leaves of the *mitragyna speciosa* plant; with two alkaloids, mitragynine and 7-hydroxymitragynine, being some of the most potent.<sup>61</sup> The potent alkaloids found in leaves are known to interact with the opioid receptors, specifically the mu-opioid receptor.

The objective of this study was to examine select kratom alkaloids and how they bind to the mu-opioid receptor through the use of molecular docking. This study will hopefully lead to a better understanding of how these alkaloids interact with the receptors and shed some light and if, and how, this substance can be used in positive ways, such as aiding in opioid withdrawal.

## **6.2 Materials and Methods**

Schrödinger’s molecular modeling software, Maestro, was used to examine the binding of select kratom alkaloids to the mu-opioid receptor. The mu-opioid receptor used in this study was prepared from the crystal structure, PDB:5C1M, developed by Huang et al.<sup>41</sup>

### **6.2.1 Ligand Selection and Preparation**

In this study, seven prominent kratom alkaloids were chosen to be analyzed. The alkaloids used in this study were mitragynine, 7-hydroxymitragynine, speciogynine, speciocilantine, corynantheidine, paynantheine, and mitragynine pseudindoxyl.

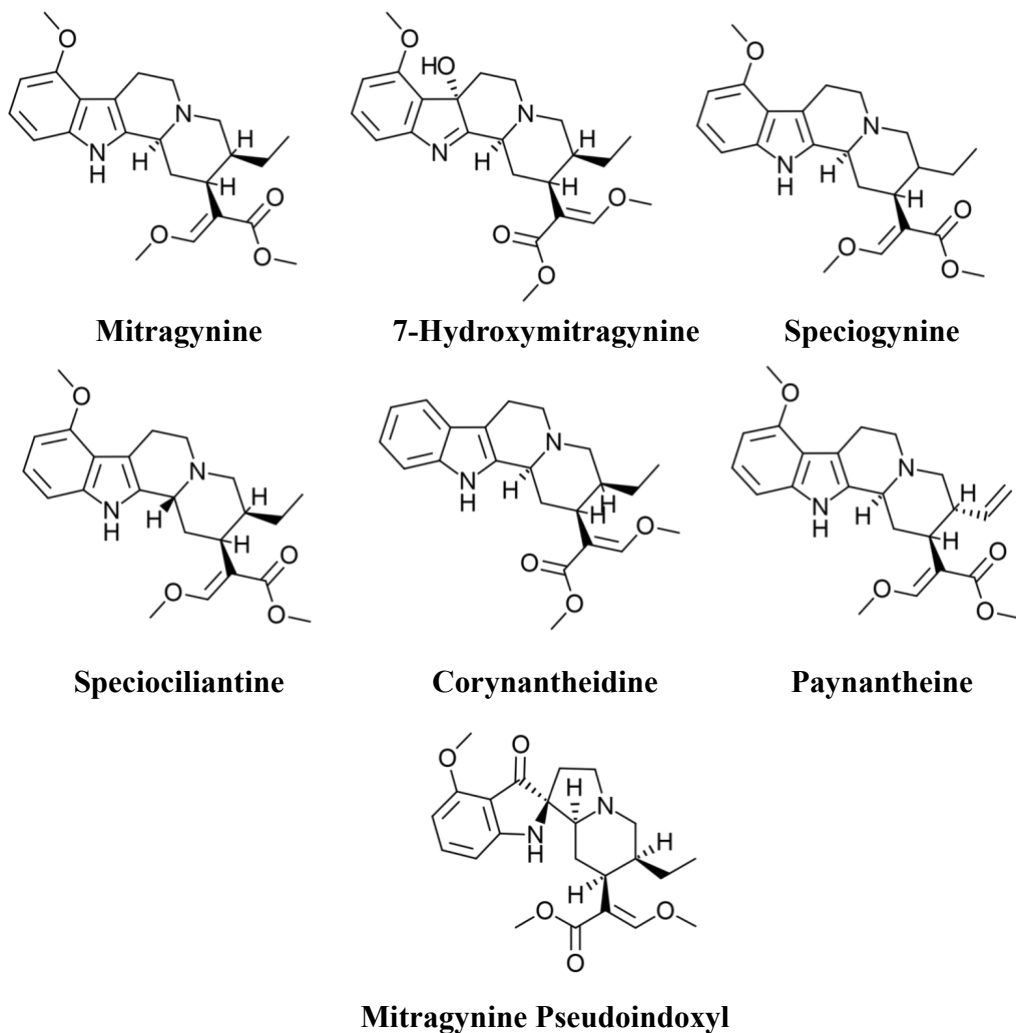


**Figure 81.** Structures of the kratom alkaloids.

The *LigPrep* protocol is used to successfully convert ligands into three-dimensional structures. The preparation of the ligands involves generating possible states at a target pH of 7.0 +/- 2.0 using Epik. Epik is used predict pKa values and determine all chemically sensible structures.<sup>18,42</sup>

### 6.2.2 Protein Preparation

The *Protein Preparation* application is used to convert the imported PDB file of 5C1M to a prepared model ready for docking.<sup>54</sup> In order to prepare the mu-opioid receptor the following steps were taken. Once the PDB file “5C1M” was imported, the modified residue within the sequence was changed to its proper residue. This information was found within the Protein Data Bank. The modified residue present in 5C1M was YCM which was changed to the correct residue, cysteine (CYS). In the workspace the B chain and all the groups present, except 4VO, were deleted. For preprocess all original hydrogens were removed, waters beyond 5 Å from het groups were deleted and het states were generated using Epik with a pH of 7.0 +/- 2.0. To refine the protein, the first step was optimization of H-bond assignment, which was done with sampling water orientations, using crystal symmetry and minimizing hydrogens of altered species. PROPKA was used at a pH of 7.0. Waters with less than 2 hydrogen bonds to non-waters were then removed. Minimization was performed converging heavy atoms to a distance of 0.30 Å with hydrogens only using the force field OPLS3.

### 6.2.3 Receptor Grid Generation

The *Receptor Grid Generation* application is used to accurately place a grid around the binding pocket of the receptor. The structure present in the mu-opioid receptor model to generate the grid was 4VO. For this receptor there were no constraints but a rotatable group, TYR 148 was selected for grid generation. The force field used was OPLS3. The grid created was used to accurately dock the ligands of interest to the receptor.

## 6.2.4 Ligand Docking

After the grid was generated and the desired ligands were prepared, the next step was *Glide Ligand Docking*. This step allowed for the prepared ligands to be docked into the receptor binding pocket selected during grid generation. Docking was completed using the standard precision (SP) method and force field OPLS3. Flexible ligand sampling was selected and Epik state penalties were added to the docking score. No constraints were selected to use in docking. The Glide program is able to produce potential ligand conformations. The program uses a set of ranked filters to find possible locations on the ligand in the binding pocket of the receptor. The filters include; 1) side-point search, 2a) diameter test, 2b) subset test, 2c) greedy score, 2d) refinement, 3) grid minimization, and 4) final scoring.<sup>43</sup> The *Glide Ligand Docking* process is explained by Friesner et al. (2004).<sup>43</sup> For each ligand, up to five possible poses were generated and post-docking minimization was performed. The pose refers to the position and orientation of the ligand in relation to the receptor.<sup>43</sup> To determine the most accurate pose for each ligand, the docking scores and Glide Emodel scores were analyzed. Docking scores are an estimation of the binding free energy and are used to rank poses of different ligands.<sup>43,44</sup> The Glide Emodel was used to compare poses and determine the best, or most likely, pose for each ligand. Docking scores and Glide Emodel scores are negative. A more negative score means better docking. The docking of each ligand, when using the same procedure, produces the same values. The algorithm used by Glide does not require docking multiple times and will produce the same values each time as long as the same procedure is used. The use of three decimal places is because differences in some of the values between ligands might not have been seen until the second or third decimal place. The software allows for more decimal places to be used, but it was decided to use three decimal places due to some of the small changes observed in the data.



### 6.2.5 Binding Energy Estimations: Prime MM-GBSA

The relative binding free energy of each ligand was estimated using the *Prime MM-GBSA* application. These calculations are done following the equation:  $\Delta G_{\text{bind}} = E_{\text{complex}} (\text{minimized}) - (E_{\text{ligand}} (\text{minimized}) + E_{\text{receptor}} (\text{minimized}))$ .<sup>22</sup> The solvation model used was VSGB and calculations were done using OPLS3. Protein flexibility was applied at a distance of 5 Å from the ligand. The Prime MM-GBSA data values are not expected to be the same as the experimental binding affinities but are expected to give a ranking of the ligands that correlates with the experimental data of binding affinities ( $K_i$  values). A more negative binding free energy value correlates to a stronger binding of the ligand to the receptor.<sup>47</sup>

## 6.3 Results and Discussion

In this study seven alkaloids found in the kratom leaf were analyzed through molecular docking. The alkaloids were virtually docked to the 3D model of the mu-opioid receptor. The mu-opioid receptor used in this study came from the crystal structure developed by Huang et al. Once the ligands were docked their docking scores were analyzed. The docking scores are estimation of the binding free energy and was used to rank poses of different ligands.<sup>43,44</sup> The lower, or more negative, the docking score is the stronger the binding is to the CB1 receptor. When docked, each ligand produced up to five possible poses. To determine the best pose of each ligand, the Glide Emodel value was used. The lowest, or most negative, value indicates the best pose for that ligand. Binding energy calculations were then done to determine the relative binding energy of the best pose of each ligand.

**Table 13.** Results from the docking of the alkaloids to the mu-opioid receptor.

| <b>Ligand</b>                    | <b>Ki (nM)<sup>(62)</sup></b> | <b>Docking Score (kcal/mol)</b> | <b>Glide Emodel</b> | <b>Binding energy (kcal/mol)</b> |
|----------------------------------|-------------------------------|---------------------------------|---------------------|----------------------------------|
| <b>Mitragynine</b>               | 233 ± 48                      | -7.109                          | -61.645             | -48.003                          |
| <b>7-OH-mitragynine</b>          | 47 ± 18                       | -4.743                          | -36.071             | -34.995                          |
| <b>Speciogynine</b>              | 728 ± 61                      | -7.126                          | -61.706             | -48.202                          |
| <b>Speciocilantine</b>           | 560 ± 168                     | -5.565                          | -46.101             | -36.603                          |
| <b>Corynantheidine</b>           | -                             | -6.398                          | -55.495             | -56.288                          |
| <b>Paynantheine</b>              | 410 ± 152                     | -5.405                          | -44.660             | -54.237                          |
| <b>Mitragynine Pseudoindoxyl</b> | -                             | -6.375                          | -51.821             | -53.665                          |

\*Ki was determined from inhibition of the activity of reference agonist U-50,488.<sup>62</sup>

The experimental Ki values used for comparison in this study were determined through radioligand binding assays by Kruegel et al.<sup>62</sup> The IC<sub>50</sub> values were determined from the inhibition of the agonist U-50,488. The IC<sub>50</sub> value expresses the concentration of the ligand required to inhibit half of the biological response. The IC<sub>50</sub> values were then used to determine the Ki values using the Cheng and Prusoff equation;  $K_i = IC_{50}/(1+[C^*]/K_D^*)$ <sup>62</sup> The alkaloid speciogynine was found to have the most negative docking score and 7-hydroxymitragynine had the most positive docking score. The rank of docking scores was determined to be 7-hydroxymitragynine > paynantheine > speciocilantine > mitragynine pseudoindoxyl > corynantheidine > mitragynine > speciogynine. Binding energy estimations were also completed within the Maestro software. These values are not expected to be the same as the experimental binding affinities but are expected to give a ranking of the ligands similar to the experimental data. A more negative binding free energy value correlates to a stronger binding of

the ligand to the receptor. From this data it was determined that the rank of binding energy estimations is 7-hydroxymitragynine > speciociliantine > mitragynine > speciogynine > mitragynine pseudoindoxyl > paynantheine > corynantheindine. The estimated binding free energies calculated in this study were not consistent with the experimental binding affinities. Kratom, and its alkaloids, has been noted as an emerging drug on the market and research on this drug is still being done. For that reason, there was very little experimental binding affinity data to be found on kratom and its alkaloids in the current literature. It can be expected that as more information becomes available of these alkaloids more computational studies will need to be performed to better understand their interactions with the opioid receptors.

Using the 2D Ligand Interaction Diagram application in Maestro, the residues interacting within a distance of 5 Å from the ligand were examined. (Table 14) The types of interacting residues present within the binding pocket were labeled as hydrophobic, polar, negatively charged or positively charged residues.

**Table 14.** Number and identification of interacting residues within 5 Å for the kratom alkaloids.

| <b>Ligand</b>                    | <b>Docking Score (kcal/mol)</b> | <b>Binding Energy (kcal/mol)</b> | <b>Hydrophobic</b> | <b>Polar</b> | <b>Negative Charged</b> | <b>Positive Charged</b> |
|----------------------------------|---------------------------------|----------------------------------|--------------------|--------------|-------------------------|-------------------------|
| <b>Mitragynine</b>               | -7.109                          | -48.003                          | 20                 | 8            | 1                       | 2                       |
| <b>7-OH-mitragynine</b>          | -4.743                          | -34.995                          | 17                 | 7            | 1                       | 2                       |
| <b>Speciogynine</b>              | -7.126                          | -48.202                          | 20                 | 8            | 1                       | 2                       |
| <b>Speciocilantine</b>           | -5.565                          | -36.603                          | 19                 | 6            | 1                       | 1                       |
| <b>Corynantheidine</b>           | -6.398                          | -56.288                          | 19                 | 6            | 1                       | 2                       |
| <b>Paynantheine</b>              | -5.405                          | -54.237                          | 23                 | 7            | 1                       | -                       |
| <b>Mitragynine Pseudoindoxyl</b> | -6.375                          | -53.665                          | 22                 | 7            | 1                       | 2                       |

It was observed that speciogynine and mitragynine, with the most negative docking scores, had the same number of interacting residues. Each ligand had 20 hydrophobic, 8 polar, 1 negative and 2 positive residues. Speciogynine and mitragynine also had the highest number of polar residue interactions of all the alkaloids. 7-hydroxymitragynine was found to have the most positive docking score. It also had the lowest number of hydrophobic interacting residues present within 5 Å. Paynantheine, with a docking score only slightly more negative than 7-hydroxymitragynine, had the most hydrophobic residues (23). However, it was the only alkaloid that did not have any positively charged interacting residues within 5 Å. The positively charged residues were observed when the distance was increased to 6 Å. Speciocilantine had a docking score that was slight more negative than paynantheine. This alkaloid was the only ligand with 1 positively charged residue. Corynantheidine and speciocilantine had the same number of interacting residues except for the additional positively charged residue interacting with

corynantheidine. After examining the number of interacting residues present within the binding pocket, it was necessary to analyze the direct interacting residues between the alkaloids and the mu-opioid receptor. These interactions can include  $\pi$ - $\pi$  stacking,  $\pi$ -cation, hydrogen bonding and salt bridge interactions. (Table 15)

**Table 15.** Residues interacting with the kratom alkaloids within a distance of 5 Å.

| <b>Ligand</b>                        | <b><math>\pi</math>-<math>\pi</math><br/>Stacking</b> | <b><math>\pi</math>-cation</b> | <b>Hydrogen Bond</b> | <b>Salt<br/>Bridge</b> |
|--------------------------------------|---|--------------------------------|----------------------|------------------------|
| <b>Mitragynine</b>                   | -   | -                              | ASP147               | -                      |
| <b>7-OH-mitragynine</b>              | -   | HIS54                          | -                    | -                      |
| <b>Speciogynine</b>                  | -   | -                              | ASP147               | -                      |
| <b>Speciocilantine</b>               | -   | -                              | ASP147               | -                      |
| <b>Corynantheidine</b>               | -   | HIS54                          | ASP147               | -                      |
| <b>Paynantheine</b>                  | HIS54   | -                              | ASP147               | ASP147                 |
| <b>Mitragynine<br/>Pseudoindoxyl</b> | -   | HIS54                          | HIS54                | -                      |

Only two residues were seen to have direct interactions with the kratom alkaloids. These residues were HIS54 and ASP147.  $\pi$ - $\pi$  stacking was only observed with one alkaloid, paynantheine, and the residue HIS54. Paynantheine had one of the more positive docking scores, but one of the more negative binding energy estimations.  $\pi$ -cation interactions were observed between three of the alkaloids and the HIS54 residue. The  $\pi$ -cation interactions were observed between the protonated nitrogen on the cyclohexane ring and the HIS54 residue. The three alkaloids were 7-hydroxymitragynine, corynantheidine, and mitragynine pseudoindoxyl. Hydrogen bonding was observed with all but one of the ligands, 7-hydroxymitragynine. 7-

Hydroxymitragynine was also the ligand with the most positive docking score and most positive binding energy estimation. It can be assumed that hydrogen bonding between alkaloids and the mu-opioid receptor is essential for stronger binding. Mitragynine pseudoindoxyl was the only alkaloid that had hydrogen bonding with HIS54, while the remaining alkaloids interacted with ASP147 through hydrogen bonding. The hydrogen bond between HIS54 and the mitragynine pseudoindoxyl ligand was observed between the -NH group of the cyclopentanone and he residue. The paynantheine alkaloid was the only alkaloid observed to have a salt bridge interaction. This salt bridge interaction was with the ASP147 residue. The salt bridge was observed between the protonated nitrogen of the cyclohexane and the ASP147 residue. Based on this data it can be hypothesized that the HIS54 and ASP147 residues are essential to the binding of alkaloids to the mu-opioid receptor.

## 6.4 Conclusions

The objective of this study was to examine select kratom alkaloids and how they bind to the mu-opioid receptor through the use of molecular docking. The rank of docking scores was determined to be 7-hydroxymitragynine > paynantheine > speciociliantine > mitragynine pseudoindoxyl > corynantheindine > mitragynine > speciogynine. Binding energy estimations were also completed within the Maestro software. From this data it was determined that the rank of binding energy estimations was determined to be 7-hydroxymitragynine > speciociliantine > mitragynine > speciogynine > mitragynine pseudoindoxyl > paynantheine > corynantheindine. The estimated binding free energies calculated in this study were not consistent with the experimental binding affinities. Very little experimental binding affinity data is available for kratom and its alkaloids in the literature. As more data becomes available, the binding free

energies of these alkaloids will need to be examined further. Essential residues were determined to be HIS54 and ASP147. Hydrogen bonding was also found to be a crucial interaction for better docking of the alkaloids to the receptor.

Future studies of the kratom alkaloids through the use of molecular docking will include the docking of the kratom alkaloids to the other opioid receptors. Some of the kratom alkaloids have a higher affinity for the delta or kappa-opioid receptor and it will be essential to study the docking of the alkaloids to each receptor. Other kratom alkaloids, besides the seven mentioned in this study, will also need to be examined to get a bigger picture of how the kratom alkaloids interact with the opioid receptors.

## CHAPTER 7

### CONCLUSIONS AND FUTURE WORK

The objective of this dissertation was to use a computational approach to predict and understand new psychoactive substances (NPS). In chapter 2, known and novel synthetic cannabinoids from the JWH family and how structural characteristics can influence docking and residue interactions between the synthetic cannabinoids and the CB1 receptor were examined. In this study the length of the alkyl chain on the naphthalene group of each ligand was analyzed. The ligands in this study were examined in two phases, each phase consisting of two groups of ligands. This was done to better understand the influence certain structural characteristics have on the binding of the ligand to the CB1 receptor and what specific residues interactions are taking place. It was determined that two structural characteristics were influential on the docking of the ligands to the CB1 receptor, the carbonyl group between the naphthalene and the indole and the length of the N-linked alkyl chain. 3D interaction diagrams were utilized to better understand the influence of the structural characteristics on the position of the ligand in the binding pocket of the CB1 receptor. Through the 3D interaction diagrams, it was determined that the presence of a carbonyl group greatly impacts the positions of the ligands. When there was not a carbonyl present (MGCS-175-073 and JWH-175), the ligands were found to be in very similar in their positions. The length of alkyl chain on the naphthalene was determined to influence the position of the alkyl chain; however, it did not appear to influence the overall position of the ligand in the CB1 receptor.



In chapter 3, known and novel halogenated derivatives of the synthetic cannabinoids JWH-018 were studied. This study confirmed the rank of potency determined by Vigolo et al., JWH-018 > JWH-018 Cl > JWH-018 Br through the docking scores of these structures. The novel halogenated derivatives of JWH-018, JWH-018 F and JWH-018 I, were also examined in this study. The rank of potency when compare to JWH-018 and its known halogenated derivatives was determined to be JWH-018 > JWH-018 I > JWH-018 Cl > JWH-018 Br > JWH 018 F, based on docking scores. Based on the binding energy estimations, it can be hypothesized that JWH-018 F would have a smaller  $K_i$  value than JWH-018 but a larger, or weaker binding affinity, compared to the other halogenated derivatives. JWH-018 I can be hypothesized to have the lowest, strongest binding,  $K_i$  value compared to all other ligands in this study. Through 3D interaction diagrams it was observed that the position of JWH-018 inside the binding pocket of the CB1 receptor differed greatly from its halogenated derivations which can explain the differences in interacting residues and the differences in docking scores and binding energy estimations. JWH-018 F and JWH-018 Cl where observed to be in similar positions in the binding pocket, which correlates to the similarities seen in their interacting residues. JWH-018 Br and JWH-018 I were observed in opposite positions, compared to JWH-018 F and JWH-018 C, which is correlated to the differences in residue interactions.

In chapter 4, the influence of alkyl chain length of known and novel homologs of the CP synthetic cannabinoids, CP-47,497, CP-55,244 and CP-55,490 was studied. Three known homologs of CP-47,497 exist; (C6), (C8) and (C9). In this study each of the synthetic cannabinoids were examined with (C6), (C8) and (C9) alkyl chains. The docking scores in this studied showed that each of the (C8) homologs had the best, most negative, docking score in each group. For the CP-47,497 group, the rank of docking scores was found to be (C9) > (C6) >

(C7)\* > (C8). Based on rank of docking score, the results of this study support those found in the study by Melvin et al.<sup>50</sup> The rank of docking scores for CP-55,244 was determined to be (C7)\* > (C6) > (C9) > (C8) and for CP-55,490 the rank was (C6) > (C9) > (C7)\* > (C8). Based on the data it was hypothesized that the binding affinity values of each of the homologs will be ranked as the following; for CP-47,497: (C9) > (C8) > (C7)\* > (C6) , for CP-55,244: (C9) > (C7)\* > (C8) > (C6) and for CP-55,490: (C8) > (C6) > (C7)\* > (C9). Interacting residues were examined and it was determined that  $\pi$ - $\pi$  stacking interactions and hydrogen bond interactions are essential to better docking of the ligands to the CB1 receptor. The position of each of the (C8) homologs allowed for additional hydrogen bonding that was not observed in the parent ligand. It can be concluded that the hydrogen bonding is also essential to better docking and binding of the CP ligands to the CB1 receptor.

The objective of chapter 5 was to analyze the binding of fentanyl and fentanyl analogs to the mu-opioid receptor and design and novel fentanyl analogs to study using the same methods. The rank of docking scores of these analogs was determined to be N-propyl fentanyl > N-ethyl fentanyl > N-methyl fentanyl > fentanyl. The rank of the binding affinities was determined to be N-methyl fentanyl > N-ethyl fentanyl > N-propyl fentanyl > fentanyl. Therefore, it can be assumed that the novel ligands N-ethyl fentanyl and N-propyl fentanyl will have larger  $K_i$  values than fentanyl but smaller than N-methyl fentanyl. The  $\pi$ - $\pi$  stacking interactions were determined to be essential for better binding of these analogs to the mu-opioid receptor. ASP147 was determined to be the most essential interacting residue for this group of ligands. The second set of novel analogs analyzed in this study were designed from the parent analog carfentanyl. The rank of docking scores was determined to be carfentanyl (methyl) > carfentanyl (carboxylic acid) > carfentanyl (aldehyde) > carfentanyl (ethyl) > carfentanyl (ketone) > carfentanyl. The rank of

binding free energy estimations was found to be carfentanyl (carboxylic acid) > carfentanyl (methyl) > carfentanyl (ketone) > carfentanyl (aldehyde) > carfentanyl > carfentanyl (ethyl). Therefore, it can be expected that carfentanyl (ethyl) would have a smaller binding affinity than carfentanyl, correlating to a stronger binding. The other novel analogs are expected to have a larger binding affinity for the mu-opioid receptor, weaker binding, compared to carfentanyl. It was determined in this study that the essential residues from strong docking were ASP147 and TRP293. The position and distance of the ligands from the residues were also impact the docking of the ligands to the mu-opioid receptor. Additional  $\pi$ - $\pi$  stacking with TYR326 was also found to lead to a better docking of the ligands to the receptor, as it was observed in the carfentanyl and carfentanyl (ethyl) ligands.

In chapter 6 select kratom alkaloids and how they bind to the mu-opioid receptor were studied through the use of molecular docking . The rank of docking scores was determined to be 7-hydroxymitragynine > paynantheine > speciociliantine > mitragynine pseudoindoxyl > corynantheindine > mitragynine > speciogynine. From this data it was determined that the rank of binding energy estimations is be 7-hydroxymitragynine > speciociliantine > mitragynine > speciogynine > mitragynine pseudoindoxyl > paynantheine > corynantheindine. The estimated binding free energies calculated in this study were not consistent with the experimental binding affinities. Interacting residues between the alkaloids and the mu-opioid receptor were also examined. Essential interacting residues HIS54 and ASP147 were observed for each of the alkaloids. Hydrogen bonding was observed with all but one of the ligands, 7-hydroxymitragynine. Hydrogen bonding was determined to be essential for stronger docking to the mu-opioid receptor.

New psychoactive substances (NPS) pose many issues within the criminal justice field. One of the main issues is the inability of agencies, like the Drug Enforcement Administration (DEA), to keep up with the increasing number of NPS that appear on the streets, used recreationally, and have a high potential of abuse. When a new compound appears, it can take analysts a significant amount of time to identify the compound and understand its properties. The work in this dissertation is the foundation of a larger project. The success of this larger project would lead to a database, that will be made available to all state and federal crime laboratories, containing potential NPS that could aid in the rapid identification and pharmacological understanding of new compounds. Rapid identification is essential in the ability of agencies to schedule the compounds as drugs of abuse and help remove them from the drug market.

## REFERENCES

1. UNODC Early Warning Advisory on New Psychoactive Substances.(2019). *What Are NPS?*, UNODC, 2019, [www.unodc.org/LSS/Page/NPS](http://www.unodc.org/LSS/Page/NPS).
2. New Psychoactive Substances. (2019). Retrieved from [https:// adf.org/au/drug-facts/new psychoactive-substances/](https://adf.org/au/drug-facts/new-psychoactive-substances/)
3. Vardakou, I., Pistos, C., & Spiliopoulou, C. (2010). Spice drugs as a new trend: Mode of action, identification and legislation. *Toxicology Letters*, 197(3), 157-162. doi:10.1016/j.toxlet.2010.06.002
4. Tai, S, and W E Fantegrossi. "Synthetic Cannabinoids: Pharmacology, Behavioral Effects, and Abuse Potential." *Current Addiction Reports.*, U.S. National Library of Medicine, 1 June 2014, [www.ncbi.nlm.nih.gov/pubmed/26413452](http://www.ncbi.nlm.nih.gov/pubmed/26413452).
5. Human Endocannabinoid System. (n.d.) Retrieved 2019, from <https://www.uclahealth.org/cannabis/human-endocannabinoid-system>
6. Li, J., Ning, Y., Hedley, W., Saunders, B., Chen, Y., Tindill, N.,....Subramaniam, S. (2002). *The Molecule Pages database. Nature*, 420(6916), 716-717. doi:10.1038/nature01307
7. G Proteins. European Bioinformatics Institute. (n.d.) Retrieved from [https://www.ebi.ac.uk/interpro/potm/2004\\_10/Page2.htm](https://www.ebi.ac.uk/interpro/potm/2004_10/Page2.htm)
8. Zou, S. and Kumar, U. (2018). Cannabinoid Receptors and the Endocannabinoid System: Signaling and Function in the Central Nervous System. *International Journal of Molecular Sciences*, 19(3), 833. doi:10.3390/ijms19030833
9. *Textbook of Structural Biology* (2<sup>nd</sup> ed.) Chapter 2. (2009). New Jersey: World Scientific. Doi:99.118.72.75
10. NIH. (n.d.). Protein. Retrieved from <https://www.genome.gov/genetics-glossary/Protein?id=169>
11. Stanley, T. H. (2014). The Fentanyl Story. *The Journal of Pain*, 15(12), 1215-1226.
12. Fentanyl. DEA. Retrieved 2019, from <https://www.dea.gov/factsheets/fentanyl>
13. Armenian, P., Vo, K. T., Barr-Walker, J., & Lynch, K. L. (2017). Fentanyl, fentanyl analogs and novel synthetic opioids: A comprehensive review. *Neuropharmacology*.
14. Pizarro-Osilla, C. (2017). Introducing... Kratom. *Journal of Emergency Nursing*, 43(4), 373-374. doi:10.1016/j.jen.2017.03.016
15. Kruegel, A. C., Gassaway, M. M., Kapoor, A., Váradi, A., Majumdar, S., Filizola, M., Sames, D. (2016). Synthetic and Receptor Signaling Explorations of the Mitragyna Alkaloids: Mitragynine as an Atypical Molecular Framework for Opioid Receptor Modulators. *Journal of the American Chemical Society*, 138(21), 6754-6764. doi:10.1021/jacs.6b00360
16. Singh, D., Narayanan, S., & Vicknasingam, B. (2016). Traditional and non-traditional uses of Mitragynine (Kratom): A survey of the literature. *Brain Research Bulletin*, 126, 41-46. doi:10.1016/j.brainresbull.2016.05.004
17. Al-Hasani, R. and Bruchas, M. R. (2011)Molecular Mechanisms of Opioid Receptor-Dependent Signaling and Behavior. *Anesthesiology*, 1. doi:10.1097/aln.0b013e318238bba6

18. Schrödinger. (n.d.). LigPrep. Retrieved 2019, from <https://www.schrodinger.com/ligprep>
19. pH and pOH. (2019). Chemistry Libre Texts (14.2). Retrieved 2019, from [https://chemlibretexts.org/Bookshelves/General\\_Chemistry/Book3%20A\\_Chemistry\\_\(OpenSTAX\)/14%20Acid-Base\\_Equilibrium/14.2%20pH\\_and\\_pOH](https://chemlibretexts.org/Bookshelves/General_Chemistry/Book3%20A_Chemistry_(OpenSTAX)/14%20Acid-Base_Equilibrium/14.2%20pH_and_pOH)
20. Libretexts. (2019). 5.3: Acid Strength and pKa. Retrieved from [https://chem.libretexts.org/Courses/University\\_of\\_Illinois,\\_Springfield/UIS:\\_CHE\\_267\\_-\\_Organic\\_Chemistry\\_I\\_\(Morsch\)/Chapters/Chapter\\_02:\\_Acids\\_and\\_Bases/5.3:\\_Acid\\_strength\\_and\\_pKa](https://chem.libretexts.org/Courses/University_of_Illinois,_Springfield/UIS:_CHE_267_-_Organic_Chemistry_I_(Morsch)/Chapters/Chapter_02:_Acids_and_Bases/5.3:_Acid_strength_and_pKa)
21. Cockcroft, L., & Graham. (2009, July 01). What is entropy? Retrieved 2019, from <https://eic.rsc.org/feature/what-is-entropy/2020274.article>
22. Knowledge Base. (2015, February 10). Retrieved 2019, from <https://www.schrodinger.com/kb/1635>
23. Binding Affinity | Dissociation Constant. (2019). Retrieved from <https://www.malvernpanalytical.com/en/products/measurement-type/binding-affinity>
24. Libretexts. (2019, June 05). Hydrophobic Interactions. Retrieved from [https://chem.libretexts.org/Bookshelves/Physical\\_and\\_Theoretical\\_Chemistry\\_Textbook\\_Maps/Supplemental\\_Modules\\_\(Physical\\_and\\_Theoretical\\_Chemistry\)/Physical\\_Properties\\_of\\_Matter/Atomic\\_and\\_Molecular\\_Properties/Intermolecular\\_Forces/Hydrophobic\\_Interactions](https://chem.libretexts.org/Bookshelves/Physical_and_Theoretical_Chemistry_Textbook_Maps/Supplemental_Modules_(Physical_and_Theoretical_Chemistry)/Physical_Properties_of_Matter/Atomic_and_Molecular_Properties/Intermolecular_Forces/Hydrophobic_Interactions)
25. Biomolecules: Protein 1. (n.d.). Retrieved 2019, from <https://www.chem.wisc.edu/deptfiles/genchem/netorial/modules/biomolecules/modules/protein1/prot13.htm>
26. Libretexts. (2019, June 05). 4.4: Polar and Non-polar Covalent Bonds. Retrieved from [https://chem.libretexts.org/Courses/Eastern\\_Mennonite\\_University/EMU:\\_Chemistry\\_for\\_the\\_Life\\_Sciences\\_\(Cessna\)/4:\\_Covalent\\_Bonding\\_and\\_Simple\\_Molecular\\_Compounds/4.4:\\_Polar\\_and\\_Non-polar\\_Covalent\\_Bonds](https://chem.libretexts.org/Courses/Eastern_Mennonite_University/EMU:_Chemistry_for_the_Life_Sciences_(Cessna)/4:_Covalent_Bonding_and_Simple_Molecular_Compounds/4.4:_Polar_and_Non-polar_Covalent_Bonds)
27. Rahman, M., Muhseen, Z., Junaid, M., & Zhang, H. (2015). The Aromatic Stacking Interactions Between Proteins and their Macromolecular Ligands. *Current Protein & Peptide Science*, 16(6), 502-512. doi:10.2174/138920371606150702131516
28. Boudreaux, K. A. (n.d.). Aromatic Rings. Retrieved from [https://www.angelo.edu/faculty/kboudrea/molecule\\_gallery/04\\_aromatics/00\\_aromatics.htm](https://www.angelo.edu/faculty/kboudrea/molecule_gallery/04_aromatics/00_aromatics.htm)
29. Knowles, R. (2005, February 9). Aromatic Interactions. Retrieved from [https://www.princeton.edu/chemistry/macmillan/group-meetings/cation\\_pi.pdf](https://www.princeton.edu/chemistry/macmillan/group-meetings/cation_pi.pdf)
30. Hydrogen Bonding. (n.d.). Retrieved 2019, from <https://www.chem.purdue.edu/gchelp/liquids/hbond.html>
31. Salt Bridges. (n.d.). Retrieved 2019, from [http://openmopac.net/manual/salt\\_bridges.html](http://openmopac.net/manual/salt_bridges.html)

32. Rizzo. (n.d.). Chapter 13. Nuclear Magnetic Resonance (NMR) Spectroscopy. Retrieved 2019, from <https://www.vanderbilt.edu/AnS/Chemistry/Rizzo/chem220a/Ch13slides.pdf>
33. Chemical Shifts in NMR Spectra. (n.d.). Retrieved 2019, from <http://hyperphysics.phy-astr.gsu.edu/hbase/Nuclear/nmrsh.html>
34. Libretexts. (2019, June 05). NMR: Theory. Retrieved from [https://chem.libretexts.org/Bookshelves/Physical\\_and\\_Theoretical\\_Chemistry\\_Textbook](https://chem.libretexts.org/Bookshelves/Physical_and_Theoretical_Chemistry_Textbook)
35. IChemLabs. (2019, April 29). ChemDoodle® v9.1 User Guide. Retrieved from <https://www.chemdoodle.com/downloads/ChemDoodleUserGuide.pdf>
36. What is Mass Spectrometry? (2016, June 24). Retrieved from <https://www.broadinstitute.org/proteomics/what-mass-spectrometry>
37. Libretexts, & Soderberg, T. (2019, June 05). 4.1: Mass Spectrometry. Retrieved from [https://chem.libretexts.org/Bookshelves/Organic\\_Chemistry/Book:\\_Organic\\_Chemistry\\_with\\_a\\_Biological\\_Emphasis\\_\(Soderberg\)/Chapter\\_04:\\_Structure\\_Determination\\_I/4.1:\\_Mass\\_Spectrometry](https://chem.libretexts.org/Bookshelves/Organic_Chemistry/Book:_Organic_Chemistry_with_a_Biological_Emphasis_(Soderberg)/Chapter_04:_Structure_Determination_I/4.1:_Mass_Spectrometry)
38. National Institute on Drug Abuse. (2018, February). Synthetic Cannabinoids (K2/Spice). Retrieved 2019, from <https://www.drugabuse.gov/publications/drugfacts/synthetic-cannabinoids-k2spice>
39. McCoy, T. (2015, August 09). How this chemist unwittingly helped spawn the synthetic drug industry. Retrieved 2019, from [https://www.washingtonpost.com/local/social-issues/how-a-chemist-unwittingly-helped-spawn-the-synthetic-drug-epidemic/2015/08/09/94454824-3633-11e5-9739-170df8af8eb9\\_story.html?noredirect=on&utm\\_term=.b59032bf0ed7](https://www.washingtonpost.com/local/social-issues/how-a-chemist-unwittingly-helped-spawn-the-synthetic-drug-epidemic/2015/08/09/94454824-3633-11e5-9739-170df8af8eb9_story.html?noredirect=on&utm_term=.b59032bf0ed7)
40. Huffman, J. W., Mabon, R., Wu, M., Lu, J., Hart, R., Hurst, D. P., . . . Martin, B. R. (2003). 3-Indolyl-1-naphthylmethanes: New cannabimimetic indoles provide evidence for aromatic stacking interactions with the CB1 cannabinoid receptor. *Bioorganic & Medicinal Chemistry*, *11*(4), 539-549. doi:10.1016/s0968-0896(02)00451-0
41. Hua, T., Vemuri, K., Nikas, P., Laprairie, R., Wu, Y., Qu, L., . . . Liu, Z. (2017). Crystal structure of the human CB1 in complex with agonist AM841. *Cell*. doi:10.2210/pdb5xr8/pdb
42. Shelley, J. C., Cholleti, A., Frye, L. L., Greenwood, J. R., Timlin, M. R., & Uchimaya, M. (2007). Epik: A software program for pK<sub>a</sub> prediction and protonation state generation for drug-like molecules. *Journal of Computer-Aided Molecular Design*, *21*(12), 681-691. doi:10.1007/s10822-007-9133-z
43. Friesner, R. A.; Banks, J. L.; Murphy, R. B.; Halgren, T. A.; Klicic, J. J.; Mainz, D. T.; Repasky, M. P.; Knoll, E. H.; Shaw, D. E.; Shelley, M.; Perry, J. K.; Francis, P.; Shenkin, P. S, "Glide: A New Approach for Rapid, Accurate Docking and Scoring. 1. Method and Assessment of Docking Accuracy", *J. Med. Chem.* **2004**, *47*, 1739-1749
44. Friesner, R. A.; Murphy, R. B.; Repasky, M. P.; Frye, L. L.; Greenwood, J. R.; Halgren, T. A.; Sanschagrin, P. C.; Mainz, D. T., "Extra Precision Glide: Docking and Scoring Incorporating a Model of Hydrophobic Enclosure for Protein-Ligand Complexes", *J. Med. Chem.* **2006**, *49*, 6177-6196.



45. World Health Organization. (2014). JWH-018 Critical Review Report. Retrieved 2019, from [https://www.who.int/medicines/access/controlled-substances/4.11\\_JWH-073\\_CritReview.pdf?ua=1](https://www.who.int/medicines/access/controlled-substances/4.11_JWH-073_CritReview.pdf?ua=1)
46. Vigolo, A., Ossato, A., Trapella, C., Vincenzi, F., Rimondo, C., Seri, C., Varnani, K., Serpelloni, G., Marti, M. (2015). Novel Halogenated Derivatives of JWH-018: Behavioral and Binding Studies in Mice. *Neuropharmacology*, *95*, 68-82. doi:2015.02.008.0028.3908
47. Schrodinger. (2015, November 10). Knowledge Base. Article ID: 1647. Retrieved 2019, from <https://www.schrodinger.com/kb/1647>
48. Clark, J. (2013). Electronegativity. Retrieved 2019, from <https://www.chemguide.co.uk/atoms/bonding/electroneg.html>
49. Leishman, E., Murphy, M. N., Murphy, M. I., Mackie, K., & Bradshaw, H. B. (2018). Broad and Region-Specific Impacts of the Synthetic Cannabinoid CP 55,940 in Adolescent and Adult Female Mouse Brains. *Frontiers in Molecular Neuroscience*, *11*. doi:10.3389/fnmol.2018.00436
50. Melvin, L., Milne, G., Johnson, M., Subramaniam, B., Wilken, G., & Howlett, A. (1993). Structure-activity relationships for cannabinoid receptor-binding and analgesic activity: studies of bicyclic cannabinoid analogs. *Molecular Pharmacology*. *44*, 1008-1015.
51. Ellis, C. R., Kruhlak, N. L., Kim, M. T., Hawkins, E. G., & Stavitskaya, L. (2018). Predicting opioid receptor binding affinity of pharmacologically unclassified designer substances using molecular docking. *Plos One*, *13*(5). doi:10.1371/journal.pone.0197734
52. Griffin, G., Wray, E. J., Martin, B. R., & Abood, M. E. (1999). Cannabinoid agonists and antagonists discriminated by receptor binding in rat cerebellum. *British Journal of Pharmacology*, *128*(3), 684-688. doi:10.1038/sj.bjp.0702806
53. Stanley, T. H. (2014). The Fentanyl Story. *The Journal of Pain*, *15*(12), 1215-1226.
54. Armenian, P., Vo, K. T., Barr-Walker, J., & Lynch, K. L. (2017). Fentanyl, fentanyl analogs and novel synthetic opioids: A comprehensive review. *Neuropharmacology*.
55. Huang, W., Manglik, A., Venkatakrisnan, A. J., Laeremans, T., Feinberg, E. N., Sanborn, A. L., . . . Kobilka, B. K. (2015). Structural insights into [mu]-opioid receptor activation. *Nature*, *524*(7565), 315. doi:10.1038/nature14886
56. Maguire P, Tsai N, Kamal J, Cometta-Morini C, Upton C, Loew G. Pharmacological profiles of fentanyl analogs at mu, delta and kappa opiate receptors. *Eur J Pharmacol*. 1992;213(2):219–25. pmid:1355735.
57. Munson, P.J. and D. Rodbard, 1980, LIGAND: A versatile computerized approach for characterization of ligand-binding systems, *Analytical Biochemistry*, *107*(1),220-239.doi:10.1016/0003-2697(80)90515-1.
58. National Institute on Drug Abuse. (n.d.). Kratom. Retrieved 2019, from <https://www.drugabuse.gov/publications/drugfacts/kratom>
59. Singh, D., Narayanan, S., & Vicknasingam, B. (2016). Traditional and non-traditional uses of Mitragynine (Kratom): A survey of the literature. *Brain Research Bulletin*, *126*, 41-46. doi:10.1016/j.brainresbull.2016.05.004

60. Post, S., Spiller, H. A., Chounthirath, T., & Smith, G. A. (2019). Kratom exposures reported to United States poison control centers: 2011–2017. *Clinical Toxicology*, 1-8. doi:10.1080/15563650.2019.1569236
61. Pizarro-Osilla, C. (2017). Introducing... Kratom. *Journal of Emergency Nursing*, 43(4), 373-374. doi:10.1016/j.jen.2017.03.016
62. Kruegel, A. C., Gassaway, M. M., Kapoor, A., Váradi, A., Majumdar, S., Filizola, M., . Sames, D. (2016). Synthetic and receptor signaling explorations of the mitragyna alkaloids: Mitragynine as an atypical molecular framework for opioid receptor modulators. *Journal of the American Chemical Society*, 138(21), 6754-6764. doi:10.1021/jacs.6b00360

## CURRICULUM VITAE

---

### EDUCATION

---

- Ph.D. in Chemistry, University of Mississippi, University, MS** August 2019  
Current GPA: 3.56/4.00  
Advisor: Dr. Murrell Godfrey
- B.S. in Forensic Chemistry, University of Mississippi, University, MS** May 2014  
GPA: 3.43/4.00
- 

### AWARDS

---

- UM Study Abroad and Forensic Chemistry CSI:Leicester Award 2013
- Outstanding Forensic Chemistry Student 2014
- GAANN Fellow 2014-2017
- ACS Outstanding Leadership in Laboratory Teaching 2015
- ACS Outstanding Analytical Graduate Student 2018
- AAFS Student Scholarship 2019
- 

### PUBLICATIONS

---

1. **Spencer, Caroline A.**, Bond, John W. OBE D.Phil., “A Calibration Test for Latent Fingerprint Development on Thermal Paper”, *Journal of Forensic Sciences*, vol.59, no.6, **2014**, pp.1635-1637.
2. **Spencer, Caroline**, Robert, Ann-Elodie, Black, Oscar, Roy, Shannon, Cizdziel, James, Godfrey, Murrell, “Evaluation of Fingerprint Development Techniques on 3D-Printed Firearms”, *Forensic Analysis of Gunshot Residue, 3D-Printed Firearms, and Gunshot Injuries: Current Research and Future Perspectives*. Hauppauge, NY: Nova Science Publishers, Inc., **2019**.

---

## PRESENTATIONS

---

1. **Spencer, Caroline**, Pettus, Kelsey, Pandey, Pankaj, Doerksen, Robert J., Godfrey, Murrell. “Study of an Active-State CB1 Receptor Model and Synthetic Cannabinoid Interactions”. American Academy of Forensic Sciences Annual Meeting, New Orleans, LA, February **2017**. (Poster presentation)
2. Boone, Rachel, Hawkins, Nena, **Spencer, Caroline**, Robert, Ann-Elodie, Godfrey, Murrell. “Mitochondrial DNA Extraction from Modern Teeth Using Commercially Available DNA Extraction Kits Designed for Buccal Samples”. National Organization for the Professional Advancement of Black Chemists and Chemical Engineers Conference, Minneapolis, MN, November **2017**. (Poster presentation)
3. Hawkins, Nena, Robert, Ann-Elodie, **Spencer, Caroline**, Boone, Rachel, Godfrey, Murrell. “The Applications and Comparison of Two Commercially Available DNA Extraction Kits to Mitochondrial DNA Extraction from Modern Teeth”. New England Science Symposium, Harvard Medical School, Boston, MA, April **2018**. (Poster presentation)
4. Hawkins, Nena, Robert, Ann-Elodie, **Spencer, Caroline**, Boone, Rachel, Godfrey, Murrell. “Comparison of Two Commercially Available DNA Extraction Kits to Mitochondrial DNA from Modern Teeth”. Emerging Researchers National Conference in STEM, Washington, D.C., February **2018**. (Poster presentation)
5. Spencer, Caroline, Pandey, Pankaj, Doerksen, Robert J., Godfrey, Murrell. “A Study of an Active-State CB1 Receptor Model and JWH Synthetic Cannabinoids”. American Academy of Forensic Sciences Annual Meeting, Seattle, WA, February **2018**. (Oral presentation)
6. Robert, Ann-Elodie, **Spencer, Caroline**, Hughes, Deedra, Dawson-Cruz, Tracey, Godfrey, Murrell. “DNA Extraction from Modern Teeth Using Commercially Available DNA Extraction Kits Designed for Buccal Samples”. National Organization for the Professional Advancement of Black Chemists and Chemical Engineers Conference, Orlando, FL, September **2018**. (Oral presentation)
7. Robert, Ann-Elodie, **Spencer, Caroline**, Hughes, Deedra, Dawson-Cruz, Tracey, Godfrey, Murrell. “Modification of Commercially Available Kits to Extract DNA from Teeth Samples”.

Emerging Researchers National Conference in STEM, Washington, D.C., February **2019**.  
(Oral presentation)

8. Chamblee, Reba, **Spencer, Caroline**, Pandey, Pankaj, Doerksen, Robert J., Godfrey, Murrell. “Study of the Mu-, Kappa-, and Delta- Opioid Receptor Models and the Kratom Alkaloids”. American Academy of Forensic Sciences Annual Meeting, Baltimore, MD, February **2019**. (Poster presentation)

9. Teske, Marissa, **Spencer, Caroline**, Pandey, Pankaj, Doerksen, Robert J., Godfrey, Murrell. “Investigating the Binding of Fentanyl and Fentanyl Analogs to the Opioid Receptors”. American Academy of Forensic Sciences Annual Meeting, Baltimore, MD, February **2019**. (Poster presentation)

10. **Spencer, Caroline**, Pandey, Pankaj, Doerksen, Robert J. , Godfrey, Murrell. “The Use of Molecular Modeling to Investigate the Influence of Structural Characteristics on the Binding of Synthetic Cannabinoids to the CB1 Receptor”. American Academy of Forensic Sciences Annual Meeting, Baltimore, MD, February **2019**. (Oral presentation)

---

## RESEARCH EXPERIENCE

---

**Summer Research Internship, University of Leicester, Leicester, UK** **2013**  
Developed a calibration test for latent fingerprint development of thermal paper under the advisement of Dr. John W. Bond OBE, D. Phil.

**Graduate Research Associate, University of Mississippi** **2014-2019**  
Dedicated to investigating various research topics with forensic science applications.

- (a) Studied new psychoactive substances (NPS) and their interactions with corresponding receptors through the use of molecular modeling, including: synthetic cannabinoids, synthetic opioids, and plant-based psychoactive substances. Designed and studied potential new structures of NPS to gain a better understanding of their possible binding properties and pharmacological characteristics.
- (b) Optimized DNA extraction methods applicable to teeth and bone samples. Modified commercially available nuclear and mitochondrial DNA extraction kits designed for buccal samples to work for teeth samples. Amplified nuclear and mitochondrial DNA through the use of polymerase chain reaction (PCR) and analyzed autosomal DNA profiles.

---

## TEACHING EXPERIENCE

---

|  |           |
|--|-----------|
| Organic Chemistry Lab Teaching Assistant, University of Mississippi              | 2014      |
| Forensic DNA Lab Graduate Teaching Assistant, University of Mississippi          | 2014-2018 |
| Biochemistry Lab Graduate Teaching Assistant, University of Mississippi          | 2015-2017 |
| Instrumental Analysis Lab Graduate Teaching Assistant, University of Mississippi | 2017-2019 |

---

## PROFESSIONAL DEVELOPMENT

---

**Undergraduate Mentor, University of Mississippi** 2014-2019

Mentored, on average, 5 undergraduate students each semester. Designed research projects, instructed students in the lab on skills ranging from proper lab safety to use of analytical techniques. Taught students how to analyze results, identify issues within the research, and determine solutions. Instructed students how to properly write research papers.

**Graduate Mentor, University of Mississippi** 2017-2019

Mentored new graduate students in Dr. Murrell Godfrey's group. Helped design projects, instructed new graduate students on experimental methods, analysis of research results, identifying scientific problems, and developing solutions.

---

## PROFESSIONAL ASSOCIATIONS

---

|   |              |
|---|--------------|
| Member of Graduate Women in Science (GWS)                             | 2015-Present |
| Student Affiliate of the American Academy of Forensic Sciences (AAFS) | 2016-Present |
| Member of American Chemical Society (ACS)                             | 2019-Present |

---

## COLLABORATORS

---

**Dr. Robert Doerkson**, Department of BioMolecular Sciences, University of Mississippi

**Dr. Pankaj Pandey**, Postdoc, Department of BioMolecular Sciences, University of Mississippi

**Dr. Carolyn Freiwald**, Department of Sociology and Anthropology, University of Mississippi

**Deedra Jordan-Hughes**, Assistant Director, DNA Technical Leader, Mississippi Forensic Laboratory

**Dr. Tracey Dawson-Cruz**, Chair of Forensic Science, Virginia Commonwealth University

**Shannon Roy**, Latent Print Examiner, Mississippi Forensics Laboratory

**Dr. James Cizdziel**, Department of Chemistry and Biochemistry, University of Mississippi

**Dr. Oscar Black**, Postdoc, Research Institute of Pharmaceutical Sciences, University of Mississippi

---

## ACADEMIC AND COMMUNITY SERVICE

---

### Manuscript Peer Review

Journal of Forensic Sciences

**2018**

### Educational Outreach

AAFS CSI Camp Coordinator, University of Mississippi

**2015-2019**

Organized forensic science camp for around 40 high school students each summer. Lectured on forensic topics and led hands-on laboratory exercises.

Forensic Chemistry Representative, University of Mississippi

**2015-2017**

Demonstrated and led forensic laboratory experiments for local middle and high school students.

Forensic Chemistry Representative, Girl Scouts STEM Day, Oxford, MS

**2017**

Demonstrated forensic techniques to local girl scout troops, teaching them about the field of forensic science.